

Copyright
by
HyeongUk Lim
2019

The Dissertation Committee for HyeongUk Lim
certifies that this is the approved version of the following dissertation:

**Uncertainty Quantification in the
Dynamic Analysis of Offshore Structures**

Committee:

Lance Manuel, Supervisor

Loukas F. Kallivokas

Spyros A. Kinnas

Gyorzy Zoltan Nagy

Michael R. Haberman

**Uncertainty Quantification in the
Dynamic Analysis of Offshore Structures**

by

HyeongUk Lim

DISSERTATION

Presented to the Faculty of the Graduate School of
The University of Texas at Austin
in Partial Fulfillment
of the Requirements
for the Degree of

DOCTOR OF PHILOSOPHY

THE UNIVERSITY OF TEXAS AT AUSTIN

December 2019

Dedicated to my family.

Acknowledgments

I would like to express my deepest appreciation to my doctoral advisor Professor Lance Manuel for profound belief in my abilities and invaluable insight into uncertainty quantification, structural dynamics, and reliability analysis. The completion of my dissertation would not have been possible without the support and nurturing of him.

I would also like to extend my deepest gratitude to each of my dissertation committee members. Professor Loukas F. Kallivokas guided me with his extensive knowledge in wave mechanics. Professor Spyros A. Kinnas provided valuable advice on vortex-induced vibration. Professor Zoltan Nagy gave insightful suggestions regarding machine learning. Professor Michael R. Haberman provided practical suggestions on data-driven modeling. Their guidance helped me complete a successful doctoral degree.

I am extremely grateful to the department's staff members, Leslie McCroddan, Velma Vela, Danny Quiroz, Chris Trevino, and Kathryn McWilliams, for their outstanding dedication to students.

I also wish to thank the former and current group members who enjoy office life together: Jae Sang Moon, Seungbum Koo, Hamidreza Mashayekh, Ying-Chuan Chen, Nan-You Lu, Heedong Goh, Jinsong Liu, Sedef Kocakaplan, Phong Nguyen, Taemin Heo, Bushra Islam, and Chi-Hsiang Huang.

I cannot begin to express my thanks to my father, mother, and sister, who never wavered in their support.

Finally, I am deeply indebted to my wife, Elaine Park, who never let me down throughout the duration of my study. I am truly blessed to have such wonderful family and friends.

Uncertainty Quantification in the Dynamic Analysis of Offshore Structures

HyeongUk Lim, Ph.D.

The University of Texas at Austin, 2019

Supervisor: Lance Manuel

Consideration for uncertainty is critical in problems associated with structural dynamics, especially in the offshore environment. Deterministic solutions are often insufficient to achieve confidence in computational results and for use in design. In uncertainty quantification (UQ) for problems dealing with many random or stochastic sources, surrogate models are often developed to reduce costs associated with running a “truth” model to verify response levels associated with low probability. Polynomial chaos expansion (PCE) is one approach used in developing such surrogate models. However, conventional PCE relies on parametric families to define the polynomials for expansion. Also, for high-dimensional problems, PCE can be inefficient if appropriate dimension reduction is not employed. Arbitrary PCE (aPCE) approaches, based on Gram-Schmidt orthogonalization, can be used to define polynomials in terms of the uncertain variables and offers a non-parametric option for UQ. An aPCE approach that can systematically account for multivariate stochasticity is developed in this study. Dimension reduction can aid in developing computationally efficient surrogate models; in this study, a gradient-based active subspace

approach that identifies dominant influences on a model output's variability is employed for dimension reduction. Both aPCE and active-subspace dimension reduction are employed in studies that are focused on the dynamics of offshore structures and on low-probability events of interest.

This dissertation represents a collection of four papers that deal with PCE surrogate modeling and dimension reduction. Each paper, representing a separate chapter, contributes to the development of accurate and efficient UQ approaches for offshore structure dynamics problems involving various sources of uncertainty. We demonstrate the proposed approaches in different applications: I. estimation of fatigue damage in a marine riser due to vortex-induced vibration; II. prediction of the long-term extreme response of a moored floating structure; III. surrogate model development for structural reliability analysis; and IV. dimension reduction in the extreme response prediction of offshore structures.

Table of Contents

Acknowledgments	v
Abstract	vii
List of Tables	xiii
List of Figures	xiv
Chapter 1. Introduction	1
1.1 Dissertation Structure	1
1.2 Background and Motivation	1
1.3 Objectives and Scope	2
1.4 Preliminary Knowledge	3
1.4.1 Need for Quantifying Uncertainty	3
1.4.2 Sources of Uncertainty	3
1.4.3 Computational Model	4
1.4.4 Uncertainty Quantification (UQ)	4
1.4.5 UQ Methods	5
1.4.6 Surrogate Model Development	6
1.5 List of Papers Based on this Study	6
1.6 Summary of Papers	7
1.7 Summary	9
Paper I:	10
Chapter 2. Efficient Surrogate Model Development for Riser Fatigue Damage Estimation	11
2.1 Introduction	12
2.2 Fluid-Structure Interaction Model for Riser VIV	15

2.3	Fatigue Damage Estimation	19
2.3.1	Rainflow Cycle-Counting and MCS	19
2.3.2	PCE-based Fatigue Analysis	25
2.4	Numerical Studies	29
2.4.1	Example with 3 Variables	29
2.4.2	Uncertainties of PCE Surrogate Models for Various Choices of Input Parameters	34
2.4.3	Different Locations of Interest Along the Riser	35
2.4.4	Influence of S-N Parameters: $m = 5$	38
2.5	Refined PCE Analysis	40
2.6	Conclusions	44
	Bibliography	46
Paper II:		50
Chapter 3.	On Efficient Surrogate Model Development for Pre- diction of the Long-Term Extreme Response of a Moored Floating Structure	51
3.1	Introduction	52
3.2	Problem Formulation	55
3.3	Environmental Conditions	56
3.4	Short-Term Extreme Response and QoI	57
3.5	Long-Term Extreme Response	58
3.6	Polynomial Chaos Expansion	59
3.7	Monte Carlo Simulations and PCE-based Surrogate Models . .	63
3.8	MCS and PCE with Important Sampling	72
3.9	Conclusions	78
	Bibliography	80
Paper III:		84

Chapter 4. Distribution-Free Polynomial Chaos Expansion Surrogate Models for Efficient Structural Reliability Analysis	85
4.1 Introduction	86
4.2 Polynomial Chaos Expansion	88
4.2.1 Underlying Assumptions	88
4.2.2 Traditional PCE Formulation	89
4.2.3 PCE Coefficient Estimation	90
4.3 Distribution-Free Polynomial Chaos Expansion	91
4.3.1 Univariate Basis Polynomial Functions Using Gram-Schmidt Orthogonalization	91
4.3.2 Distribution-Free Multivariate Basis Polynomial Functions	92
4.4 Numerical Examples	94
4.4.1 Example 1: Noisy Limit State Function	96
4.4.2 Example 2: Quadratic Function	97
4.4.3 Example 3: Correlated Non-Normal Variables	98
4.4.4 Example 4: Multimodal Random Variables	101
4.4.5 Example 5: Mixed Discrete-Continuous Support	103
4.4.6 Example 6: Computational Time-Domain Solver for Performance Function	105
4.5 Conclusions	107
Bibliography	109
Paper IV:	114
Chapter 5. Dimension Reduction in Extreme Response Prediction for Offshore Structures	115
5.1 Introduction	116
5.2 Problem Formulation	118
5.3 Metocean Conditions	118
5.4 Uncertainties in Extreme Response	119
5.4.1 Short-Term Extreme Response and QoI	119
5.4.2 Long-Term Extreme Response	120
5.5 Monte Carlo Simulations	121

5.6	Dimension Reduction	121
5.6.1	Model Order Reduction	121
5.6.2	Construction of Active Subspace	124
5.6.3	Gradient Vector and Covariance Matrix Approximation	125
5.6.4	Polynomial Chaos Expansion in a Reduced Dimension Space	127
5.7	Numerical Examples	129
5.7.1	Simple Quadratic Model	130
5.7.2	Quadratic Model with a Non-Polynomial Term	133
5.7.3	High-Dimensional Linear Limit State Function	136
5.7.4	High-Dimensional Nonlinear Limit State Function	138
5.7.5	Extreme Wave Elevations at Different Sites of Interest .	140
5.7.5.1	Site I: North Sea	140
5.7.5.2	Site II: National Data Buoy Center Station 46022	145
5.7.5.3	Site III: Barent Sea	147
5.7.6	Extreme Response of Various Offshore Structures	149
5.7.6.1	Type I: Long Natural Period	149
5.7.6.2	Type II: Short Natural Period	153
5.8	Conclusions	155
	Bibliography	156
	Bibliography	160
	Vita	170

List of Tables

2.1	Tabulated multi-index for $N_X = 3$ and $p = 2$	27
2.2	Properties of the selected TTR	30
3.1	Comparisons of short-term Z values in meters, predicted by the truth system (MCS) and by using 10 PCE surrogate models ($p = 3, N_E = 100$) for selected H_s - T_p pairs	71
4.1	Random variables in Example 1	97
4.2	Comparison of statistics based on APCE and HPCE for Example 1	97
4.3	Random variables in Example 2	98
4.4	Comparison of statistics based on APCE and HPCE for Example 2	98
4.5	Random variables in Example 3	99
5.1	Three cases of different $\{c_i\}_{i=1,\dots,4}$ values in the simple quadratic model	131
5.2	Three cases of different $\{c_i\}_{i=1,\dots,4}$ values in the simple quadratic model with a non-polynomial term	133
5.3	Joint PDFs of H_s and T_p at selected sites of interest	140

List of Figures

1.1	Two considerations in computational modeling: (1) mathematical idealization of the physical phenomenon; and (2) computational implementation of numerical solution of the math model.	4
1.2	The use of “surrogate” models that serve as approximations for the “truth” models	6
2.1	Schematic diagram of the selected top-tensioned riser in uniform current flow	15
2.2	Measurement data and the empirical curves (Eqs. 2.15 and 2.16) against S_G : A_{\max} (top) and $\omega_{s,A}/\omega_n$ (bottom)	21
2.3	Fitted distributions of the residuals (Eqs. 2.13 and 2.14) of the measurement data by SGLD: ΔA_{\max} (top) and $\Delta \omega$ (bottom) .	22
2.4	Scatter plots of the relationships between three variables (ΔA_{\max} , $\Delta \omega$, and V): uncorrelated (left column) and correlated (right column), using 1000 MCS in the truth model— $\rho_{\Delta A_{\max}, \Delta \omega} = \rho_{X_1 X_2} = 0.3607$	31
2.5	Comparisons of pdf’s (top), Q-Q plots (middle), and exceedance probability (bottom) plots for a polynomial order-5 PCE model—10 sets with three uncertain variables	33
2.6	Comparisons of the mean exceedance probabilities for each PCE model of various model input selections: one variable (ΔA_{\max} or $\Delta \omega$), two variable (ΔA_{\max} and $\Delta \omega$), and three variables (ΔA_{\max} , $\Delta \omega$, and V)	35
2.7	Stress range histograms obtained by rainflow cycle-counting at three different locations along the riser ($x = L/4$, $L/2$, and $3L/4$ —from the top) under $V = 0.4$ m/s	36
2.8	Cross flow motion time history $v(x, t)$ at different locations ($x = L/4$, $L/2$, $3L/4$ —from the top in the riser) under $V = 0.4$. .	37
2.9	Order-5 PCE-based fatigue damage exceedance probability curves at three locations along the riser ($x = L/4$, $L/2$, and $3L/4$ —from the top) arising from consideration of three uncertain variables (ΔA_{\max} , $\Delta \omega$, and V).	38

2.10	Comparisons of 10 sets of order-5 (top) and order-7 (bottom) PCE-based exceedance probability curves for $m = 5$ against the MCS-based curve with 99% confidence intervals	40
2.11	Estimations of exceedance probabilities for the cases two (top) and three (bottom) variables involved, by PEM and rPEM; comparisons are made against MCS of 99% confidence intervals	42
2.12	Improvement of accuracy of $G_{\bar{D}}$ estimates by using refinement on PCE: a case with three variables involved (ΔA_{\max} , $\Delta \omega$, and V) and $m = 3$	44
3.1	A sample realization of a 30-minute time series of surge motion for the selected moored floating structure for a sea state represented by $H_s = 3.07$ m and $T_p = 13.79$ s	63
3.2	Comparison of probability of exceedance (G_Z) estimates: MCS (solid) versus PCE (dashed) with $p = 3$ and $N_E = 100$: comparisons are based on 10 sets of MCS and PCE computations	65
3.3	Estimation of G_Z at three levels, 10^{-3} , 10^{-4} , and 10^{-5} , using 10 sets of PCE with different N_E values; comparison is made with 10 sets of MCS	67
3.4	Comparison of probability of exceedance (G_Z) estimates: MCS (solid) versus PCE (dashed) with $p = 4$ and $N_E = 150$: comparisons are based on 10 sets of MCS and PCE computations	68
3.5	Comparison of probability of exceedance (G_Z) estimates: MCS (solid) versus PCE (dashed) with $p = 6$ and $N_E = 280$: comparisons are based on 10 sets of MCS and PCE computations	69
3.6	A subset of 100,000 sampled H_s and T_p values used in MCS	70
3.7	A subset of 1,000 sampled H_s and T_p values used to construct PCE surrogate models (10 sets \times 100 samples for each PCE model)	70
3.8	Selection of importance sampling density function for MCS: (top left) marginal distributions of $f_{H_s}(h)$ and $f_{H_s}^*(h)$, (top right) weight ratio, (bottom left) contours of $f_{H_s, T_p}(h, t)$, (bottom right) contours of $f_{H_s, T_p}^*(h, t)$	74
3.9	Comparison of probability of exceedance (G_Z) estimates by conventional MCS and importance sampling-based MCS: $N_T = 10,000$ for both methods	75
3.10	Comparison of probability of exceedance (G_Z) estimates by conventional MCS and importance sampling-based MCS: $N_T = 100,000$ for MCS and $N_T = 10,000$ for MCS-IS	75

3.11	Comparison of probability of exceedance (G_Z) estimates by conventional MCS and importance sampling-based MCS: $N_T = 100,000$ for both methods	76
3.12	Selection of importance sampling density function for the PCE surrogate: (top left) marginal distributions of $f_{Q_1}(q_1)$ and $f_{Q_1}^*(q_1)$, (top right) weight ratio, (bottom left) contours of $f_{Q_1,Q_2}(q_1, q_2)$, (bottom right) contours of $f_{Q_1,Q_2}^*(q_1, q_2)$	77
3.13	Comparison of probability of exceedance (G_Z) estimates based on conventional MCS, PCE, and importance sampling-based PCE (PCE-IS); $N_T = 100,000$ for all the methods and $p = 3$ and $N_E = 100$ for the PCE surrogate	78
4.1	Comparison of P_f estimates for different b values from 10 MCS, APCE, and HPCE sets for Example 3.	100
4.2	Comparison of P_f estimates for different b values from 10 MCS, APCE, and JPCE sets for Example 4.	102
4.3	Comparison of P_f estimates for different b values from 10 MCS, APCE, and HPCE sets for Example 5.	104
4.4	Flowchart for long-term extreme estimation in probabilistic offshore structure design for Example 6.	106
4.5	Comparison of exceedance probabilities of Z_T for different z values from 10 MCS, APCE, and HPCE sets for Example 6. .	107
5.1	Estimation of pdfs (left column) and exceedance probabilities (right column) of the simple quadratic model by 10 sets of MCS and AS-PCE models for Cases 1 (top), 2 (middle), and 3 (bottom)	132
5.2	Exceedance probability estimation of the quadratic model with a non-polynomial term by 10 sets of MCS and AS-PCE models for Cases 1 (top), 2 (middle), and 3 (bottom)	135
5.3	Probabilities of exceedance of G by 10 sets of MCS and AS-PCE models when $d = 20$ (top), 50 (middle), and 100 (bottom) . .	137
5.4	Probabilities of exceedance of G by 10 sets of MCS and AS-PCE models when $d = 100$ (top), 150 (middle), and 200 (bottom) .	139
5.5	Frequencies ($N_\omega = 51$) selected by model order reduction for prediction of the maximum wave elevation in the North Sea .	141
5.6	Exceedance probabilities (top), mean exceedance probabilities (middle), confidence intervals of low occurrence probability responses (bottom) by 10 sets of full and reduced wave elevation models in the North Sea	142

5.7	Errors in the mean quantile values (z) satisfying $10^{-5} < P[Z > z] < 10^{-1}$ based on 10 sets of full and reduced wave elevation models in the North Sea	143
5.8	Exceedance probabilities of the extreme wave elevation in the North Sea by 10 sets of full (top), reduced, (middle), and PCE surrogate models (bottom)	144
5.9	Exceedance probabilities of the extreme wave elevation in the National Data Buoy Center Station 46022 by 10 sets of full (top), reduced, (middle), and PCE surrogate models (bottom)	146
5.10	Exceedance probabilities of the extreme wave elevation in the Barent Sea by 10 sets of full (top), reduced, (middle), and PCE surrogate models (bottom)	148
5.11	Exceedance probabilities (top), mean exceedance probabilities (middle), confidence intervals of low occurrence probability responses (bottom) by 10 sets of full and reduced response models (Type I) in the North Sea	150
5.12	Error in the mean quantile values (z) satisfying $10^{-5} < P[Z > z] < 10^{-1}$ based on 10 sets of full and reduced response models (Type I) in the North Sea	151
5.13	Exceedance probabilities of the extreme structural response (Type I) in the North Sea by 10 sets of full (top), reduced, (middle), and PCE surrogate models (bottom)	152
5.14	Exceedance probabilities of the extreme structural response (Type II) in the North Sea by 10 sets of full (top), reduced, (middle), and PCE surrogate models (bottom)	154

Chapter 1

Introduction

1.1 Dissertation Structure

This dissertation represents a collection of four papers. It is structured as follows: Chapter 1 provides an overview and introduces the basic concepts addressed in this dissertation. Chapters 2-5 make up four papers describing work carried out in this dissertation.

1.2 Background and Motivation

In reliability-based design, uncertainties in generalized “demand” and “capacity” parameters must be considered and quantified. Monte Carlo Simulation (MCS) is not feasible for high-dimensional problems when assessing any “Quantity of Interest” (QoI) associated with low probability. Other issues such as complex probability distributions and/or dependence structures in the underlying stochastic variables, processes, and fields can complicate the uncertainty quantification. For offshore systems, one must consider background or “long-term” uncertainty, resulting from the environment and associated metocean (meteorological and oceanographic) conditions, as well as “short-term” response/performance uncertainty. For example, different (short-term)

response characteristics of floating platforms, risers, wind turbines, wave energy devices, etc. operate in an uncertain environment defined by (long-term or background) waves, wind, currents, etc. Generally, expensive “short-term” simulations are needed to assess performance against ultimate and fatigue limit states in design; these simulations can involve the use of Computational Fluid Dynamics (CFD), Fluid-Structure Interaction (FSI), Finite Element Analysis (FEA), etc. An alternative to the use of MCS to treat all the long- and short-term uncertainties involves the development and use of “surrogate models” that can manage these uncertainties more efficiently.

1.3 Objectives and Scope

The primary objective of this dissertation is the development of accurate and efficient Uncertainty Quantification (UQ) methods for response prediction of offshore structural systems subject to uncertain ocean environmental conditions, particularly with a view toward design. The objectives and scope of this study are summarized as follows:

- to develop surrogate models for offshore dynamics and design problems using a spectral method, namely Polynomial Chaos Expansion (PCE)
- to introduce a refined non-parametric extension to PCE (namely, arbitrary PCE or aPCE) with special focus on the following cases:
 - generalized input variable definitions/distributions,
 - complex dependence structure,
 - insufficient or imperfect information of input variables;

- to propose a 2-step gradient-based dimension reduction surrogate model development procedure for high-dimensional multivariate functions that involves:
 - (1) model-order reduction in the frequency domain,
 - (2) gradient-based stochastic dimension reduction;
- to validate proposed methods in various offshore structural dynamics/vibration problems for efficient and accurate Uncertainty Quantification (UQ).

1.4 Preliminary Knowledge

1.4.1 Need for Quantifying Uncertainty

Complex engineering systems must deal with uncertainty of two types—aleatory and epistemic. Generally, one need to run numerous costly computer simulations to assess uncertainty in any QoI. Computer simulations are performed to inform some decision (e.g., in design, operation or control) and one might employ low-, medium- or high-fidelity models with different degrees of imperfection. Thus, we need validation of computational models for accurate QoI prediction.

1.4.2 Sources of Uncertainty

Aleatory uncertainty deals with inherent or irreducible randomness, e.g., in ocean waves, wind, and turbulence. Natural geologic/atmospheric hazards (events) can all be included under this type, e.g., earthquakes, floods, and hurricanes. Epistemic uncertainty (reducible) results due to insufficient data, simplifying assumptions, imperfect models, etc.

1.4.3 Computational Model

Complex physical systems are generally assessed using computational models. Because computational models are only implementations that are mathematical approximations of the underlying scientific theory, their validity varies with the nature of the QoIs involved and the desired accuracy in evaluation of those QoIs. Typically, validation refers to systematic comparison of model outputs to reality, truth or measurements—for instance, we can confirm whether a model predicts output or response that is “close” to observations. Such comparisons are necessary but not sufficient for systematic validation. We need to quantify confidence in any prediction or extrapolation based on the model. Validation requires that UQ must handle uncertainty in the data, models and model parameters, as shown in Fig. 1.1.

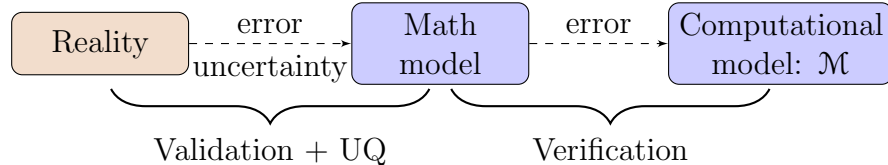


Figure 1.1: Two considerations in computational modeling: (1) mathematical idealization of the physical phenomenon; and (2) computational implementation of numerical solution of the math model.

1.4.4 Uncertainty Quantification (UQ)

Assume that all the uncertainties in the stochastic “input” parameters/variables are described by probability density functions (PDFs), as follows (even though

this may not be the only manner in which uncertainties are described in general):

$$\mathbf{X} \sim f_{\mathbf{X}}. \quad (1.1)$$

A computation model relates inputs to the “response” of interest:

$$\mathcal{M} : Y \equiv \mathcal{M}(\mathbf{X}). \quad (1.2)$$

Uncertainty Quantification (UQ) seeks information on or statistics of Y (e.g., mean and variance, higher moments, PDF, etc.).

1.4.5 UQ Methods

Uncertainty quantification can be carried out using a variety of methods. Some of these are listed below:

- Simulation-based methods
 - Monte Carlo Simulation (MCS)
 - Variance reduction in MCS:
Latin Hypercube, Importance Sampling, Subset Simulation
- Geometric approximations
 - FORM and SORM: First- and Second-Order Reliability Methods
(in analysis)
 - Environmental Contour Method, Inverse FORM (in design)
- Using surrogate models
 - Machine learning, AI, neural nets (training, testing)
 - Kriging (Gaussian processes)
 - Polynomial Chaos Expansion (PCE)

- Post-processing, using limited output or response, Y :
 - Kernel density estimation
 - Maximum entropy distribution
 - Method of moments; maximum likelihood; L-moments

1.4.6 Surrogate Model Development

A surrogate model, $\hat{\mathcal{M}}$, can serve as an approximation of the computational model, \mathcal{M} , and may be constructed using a controllably small number of computation model runs (“truth”) and assumed characteristics of the surrogate (e.g., polynomial form). Developing a reliable surrogate requires rigorous validation (against the “truth”). One can benefit from the use of “surrogate” models that serve as approximations for the “truth” models, as illustrated in Fig. 1.2.

$$\begin{array}{ccc} \mathcal{M}(\mathbf{x}) & \approx & \hat{\mathcal{M}}(\mathbf{x}) \\ \text{Truth} & & \text{Surrogate} \end{array} \quad \begin{array}{c} \text{minutes or hours per run} \\ \text{vs.} \\ \text{seconds per } 10^6 \text{ runs} \end{array}$$

Figure 1.2: The use of “surrogate” models that serve as approximations for the “truth” models

1.5 List of Papers Based on this Study

The following papers are included in the dissertation (as Chapters 2-5):

I **HyeongUk Lim**, Lance Manuel, Ying Min Low and Narakorn Srinil,

Efficient Surrogate Model Development for Riser Fatigue Damage Estimation

II **HyeongUk Lim**, Lance Manuel and Ying Min Low, On Efficient Surrogate Model Development for Prediction of the Long-Term Extreme Response of a Moored Floating Structure

III **HyeongUk Lim** and Lance Manuel, Distribution-Free Polynomial Chaos Expansion Surrogate Models for Efficient Structural Reliability Analysis

IV **HyeongUk Lim** and Lance Manuel, Dimension Reduction in Extreme Response Prediction for Offshore Structures

1.6 Summary of Papers

Paper I:

Prediction of fatigue damage in marine risers undergoing vortex-induced vibration (VIV) remains a challenging problem because great uncertainty is associated with it. In Paper I, an Uncertainty Quantification (UQ) framework is presented—using up to 3 random variables—to assess fatigue damage uncertainty. A distributed wake oscillator model serves as the truth model and Polynomial Chaos Expansion (PCE) is employed for surrogate modeling. Case studies with different PCE surrogate models are compared against Monte Carlo Simulation (MCS) in the truth model, while addressing efficiency and accuracy.

Paper II:

In Paper II, we focus on developing an UQ framework to study the long-term extreme surge motion of a moored floating structure. Uncertainty in such response extremes arises from: (1) variability in sea state conditions (H_s and T_p); and (2) variability in simulated wave trains (time series, given H_s and T_p) arising from random frequency-dependent random amplitudes and phases. A UQ framework is developed that can treat these two sources of uncertainty in different ways. The primary source of uncertainty (due to H_s and T_p) is directly accounted for using PCE, while the secondary source (due to the frequency-dependent random amplitude and phase vector, Θ) is accounted for by the use of multiple PCE models. Validation studies include PCE versus MCS long-term response comparisons for the simple moored floating structure.

Paper III:

Even though PCE can be used to build surrogate models for offshore design as is shown in Papers I and II, incomplete information on the input variables can limit their use because PCE relies on parametric distributions for all the variables and associated basis functions for the polynomial. Also, the dependency structure among the variables can make probabilistic mapping to independent variables needed for PCE cumbersome. In Paper III, a distribution-free PCE approach is proposed to address these challenges. Gram-Schmidt orthogonalization exploits the use of sequences of computed joint raw moments of the variables in developing surrogate models. Using a few examples, we

demonstrate the proposed approach as a surrogate model-building alternative to traditional PCE.

Paper IV:

Response prediction for offshore structures typically involves wave process simulations, which in turn require a very large number of stochastic inputs. As the dimension increases, the associated sample space of inputs increases exponentially; for statistically meaningful results, a large number of input and response samples is needed for high-dimensional problems. Appropriate dimension reduction, when justified, can make building a surrogate model efficient. In Paper IV, a two-step dimension-reduction approach is proposed. The first step involves model order reduction in the frequency domain, while stochastic dimension reduction is subsequently carried out next by making use of response gradients relative to the inputs. The proposed active-subspace approach for dimension reduction is demonstrated for various offshore structural systems subject to different environmental conditions.

1.7 Summary

This dissertation has contributed to the development of accurate and efficient UQ methods that may be used in design and in the response prediction of offshore structural systems subject to uncertain ocean environmental conditions. The four papers included provide examples that demonstrate how surrogate models can help to efficiently deal with uncertainties in such problems.

Paper I:

Chapter 2

Efficient Surrogate Model Development for Riser Fatigue Damage Estimation[†]

Abstract

This study explores the application of polynomial chaos expansion (PCE) to quantify the uncertainty in accumulated fatigue damage in a top-tensioned riser (TTR) due to vortex-induced vibration (VIV) under uniform currents. Time-domain simulations of the response of the selected riser are carried out using a distributed wake oscillator model and fatigue damage is computed using rainflow cycle-counting. Three model parameters—the cylinder maximum amplitude, the ratio of the vortex-shedding frequency to the natural frequency, and the current velocity—are selected as uncertain input variables in the wake oscillator model and the propagation of uncertainty from the wake oscillator model inputs to fatigue damage is studied using PCE. Numerical investigations with regard to location—i.e., where fatigue damage is evaluated on the riser—and material properties affecting fatigue damage predictions are

[†]Some portion of this chapter has been published in: HyeongUk Lim, Lance Manuel, Ying Min Low, and Narakorn Srinil, “Uncertainty Quantification of Riser Fatigue Damage due to VIV Using a Distributed Wake Oscillator Model,” *ASME. International Conference on Ocean, Offshore and Arctic Engineering*, 2017. The dissertation author wrote first drafts of the manuscript, analyzed all the results, and developed the surrogate modeling framework.

also conducted. The efficiency and accuracy resulting from the use of PCE is demonstrated by comparison against Monte Carlo simulation (MCS). The results demonstrate the versatility of a PCE-based approach in fatigue damage prediction for risers undergoing VIV.

2.1 Introduction

Engineering models for any quantity of interest (QoI) and its variability must be generally derived with consideration of various input parameters, some of which may be stochastic. These input parameters have to be selected and specified in an appropriate manner so as to produce desired model outputs, for instance to aid in design. Because engineering models are often imperfect, identifying the behavior of the QoI as a function of the input parameters is a challenging problem. Also, a large number of input parameters and computationally expensive simulations of complex physical phenomena present additional challenges. In such cases, one may investigate a QoI’s sensitivity with respect to the input parameters so as to identify a subset of these parameters whose variation influences the QoI most significantly. In such studies, “surrogate” models are sometimes constructed based on the identified subset of important input parameters and used in lieu of “truth” models when computational resources are limited. Of course, such surrogate models are considered valid only if rigorous validation tests have been coonducted. Even though such validation tests can depend strongly on characteristics of the QoI and on the engineering model, some general guidelines can be found in the

literature [4, 26].

In the field of computational fluid dynamics (CFD), there has been a growing interest in the subject of uncertainty quantification (UQ). There, polynomial chaos expansion (PCE) [2, 21] is commonly employed because of its efficiency and versatility in representing uncertainty in complex high-dimensional problems. Najm [12] has reviewed various applications in CFD that use PCE for UQ. A feature of the PCE approach is that the QoI can be expanded using orthogonal polynomials expressed in terms of the input (random) variables. One may intuitively consider the QoI described by the orthogonal polynomial expansion as a mathematically optimal representation of model outputs associated with the input variables [27]. Also, because of the orthogonality of the selected polynomials, one may conveniently perform variance-based sensitivity analysis without additional runs of the truth model. While PCE may be employed to describe the uncertainty in the QoI, the “curse of dimensionality” when dealing with multiple random variables encountered in estimating PCE coefficients can make it difficult to apply PCE in practice [3]. Also, because the required polynomial order for accuracy is generally not known in advance, application of the PCE approach requires some effort and care.

In CFD applications, characterizing flow unsteadiness and interaction with structures is known to be quite complex due to strong nonlinearities and uncertainties involving system or model parameters in the fluid-structure interaction [24]. The prediction of fatigue life of operating marine risers, for instance, is an important topic today that involves consideration of many

sources of uncertainty [10], especially in a deepwater operating environment where vortex-induced vibration (VIV) is of special concern. There have been also several field measurement studies that have sought to address the uncertainty in fatigue damage in risers resulting from VIV [18, 19, 17]. To accurately predict the response of marine risers undergoing VIV, a distributed wake oscillator model has been proposed and its effectiveness has been demonstrated for different flow conditions and riser configurations [22]; additionally, using this model, uncertainties in fatigue damage resulted from variability in model parameters were studied using PCE [6].

In the present study, procedures for the estimation of fatigue damage in a riser under uniform currents using rainflow cycle-counting are briefly summarized. Next, a PCE-based approach that allows for direct quantification of the uncertainty in riser fatigue damage is outlined and an efficient refinement to the PCE approach presented by Lim et al. [6] is proposed. Polynomial coefficients are estimated using spectral projection. To achieve both efficiency and accuracy when compared with MCS, the appropriate polynomial order and required number of simulation runs at multi-dimensional quadrature points are established for different numerical studies. Also, different locations of interest along the riser's length when considering fatigue damage are investigated by PCE; results from comparison with PCE support claims of the versatility and validation of the PCE-based approach.

2.2 Fluid-Structure Interaction Model for Riser VIV

A schematic diagram of the top-tensioned riser (TTR) selected for this study is presented in Fig. 2.1. The riser with outer diameter, D_{ex} , is subjected to cross-flow VIV due to a uniform current velocity, V ; this TTR has a fully-submerged length L with pinned-pinned supports as depicted. Due to the riser's flexibility resulting from its high aspect ratio, L/D_{ex} , it is treated structurally as a cylinder that exhibits both string-like and beam-like behavior [9].

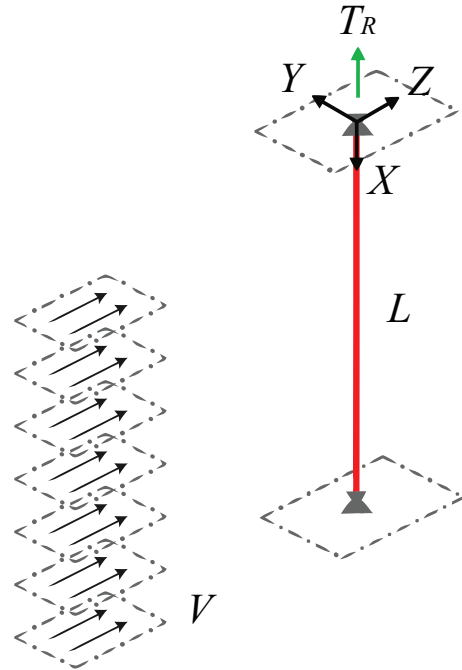


Figure 2.1: Schematic diagram of the selected top-tensioned riser in uniform current flow

The structural and hydrodynamic models that describe the cross-flow motion of the prismatic riser undergoing VIV in a uniform current are de-

scribed in terms of governing partial differential equations. By normalizing all the displacement-related variables with respect to the external diameter, D_{ex} , the equation for cross-flow motion, $v(x, t)$, in the transverse direction, Y , as a function of the spatial coordinate, x , and time, t , may be derived as follows [23]:

$$\frac{d^2v}{dt^2} + \frac{C_d}{M + M_a} \frac{dv}{dt} + \delta \frac{d^4v}{dx^4} - \alpha \frac{d}{dx} \left(T_r(x) \frac{dv}{dx} \right) = \frac{H_y(x, t)}{(M + M_a)D_{\text{ex}}}, \quad (2.1)$$

where C_d is the viscous damping coefficient; M is the mass (per unit length) of the riser; $M_a (= C_A \rho A_f)$ is the added mass of the fluid; C_A is the cross-sectional area associated with the displaced volume, A_f ; ρ is the fluid density; δ is equal to $EI / ((M + M_a) D_{\text{ex}}^4)$ where EI is the bending stiffness; α is equal to $T_R / ((M + M_a) D_{\text{ex}}^2)$ where $T_r(x) = 1 - x D_{\text{ex}} W_e / T_R$; W_e is the riser submerged weight; and T_R is the top tension.

The hydrodynamic lift force, $H_y(x, t)$, in Eq. 2.1 is given as follows:

$$H_y(x, t) = \frac{1}{2} \rho D_{\text{ex}} V^2 C_L(x, t), \quad (2.2)$$

where $C_L(x, t)$ is the associated lift coefficient given as $Q_y(x, t) - 2\gamma \frac{dv}{dt} \frac{1}{\omega_s}$ [20]; γ is the fluid-added damping coefficient; and ω_s is the vortex-shedding frequency (in rad/s) equal to $2\pi StV/D_{\text{ex}}$, where St is the Strouhal number. The variable, Q_y , is described by means of a distributed wake oscillator model [20]:

$$\frac{d^2Q_y}{dt^2} - \omega_s C_{e2} C_{L0}^2 \frac{dQ_y}{dt} + 4\omega_s C_{e2} Q_y^2 \frac{dQ_y}{dt} + \omega_s^2 Q_y = \omega_s C_{e1} \frac{dv}{dt}, \quad (2.3)$$

where C_{L0} is the lift coefficient of the stationary circular cylinder; C_{e1} and C_{e2} are empirical wake coefficients associated with system parameters, which

are functionally related to the cylinder maximum amplitude A_{\max} (normalized with respect to the cylinder diameter) and the frequency ratio, $\omega_{s,A}/\omega_n$, where $\omega_{s,A}$ is the vortex-shedding frequency at A_{\max} and ω_n is the natural frequency in still water.

According to Skop and Balasubramanian [20], the empirical coefficients, C_{e1} and C_{e2} , may be related to system parameters as follows:

$$C_{e1} = \frac{\hat{\mu}(S_G + \gamma)^2}{2}(\Delta^2 + 4)(\Gamma - \Delta), \quad (2.4)$$

$$C_{e2} = \frac{C_{e1}}{2C_{L0}^2(S_G + \gamma)} \frac{3\Delta^2 - 4}{\Delta(\Delta^2 + 4)}, \quad (2.5)$$

$$\Delta = -\left\{ \frac{-(8\Omega - 1) + \sqrt{(8\Omega - 1)^2 + 48\Omega(4\Omega - 1)}}{6\Omega} \right\}^{1/2}, \quad (2.6)$$

$$\Omega = \left\{ \frac{(S_G + \gamma)A_{\max}}{C_{L0}} \right\}^2, \quad \Gamma = \frac{2}{\hat{\mu}(S_G + \gamma)}[\omega_{s,A}/\omega_n - 1], \quad (2.7)$$

$$S_G = \frac{\zeta_n}{\hat{\mu}}, \quad \hat{\mu} = \frac{\rho D_{\text{ex}}^2}{8\pi^2 St^2(M + M_a)}, \quad (2.8)$$

where S_G is the Skop-Griffin parameter and ζ_n is the damping ratio relative to critical.

Combining the structural model (Eq. 2.1) and the hydrodynamic model (Eq. 2.3) with the lift force model (Eq. 2.2), a modal analysis on the cylinder and wake variables can be performed to investigate the multi-mode response of straight cylindrical structures undergoing VIV. For computational convenience, a low-order model is considered in the modal analysis of the riser. Also, lock-in conditions ($\omega_n \approx \omega_s$) are assumed. Rewriting Eqs. 2.1 and 2.3 in their

first-order form, the cylinder and wake variables can be expressed in terms of basis eigenfunctions as follows:

$$\begin{aligned}\frac{dv}{dt} = A \rightarrow v(x, t) &= \sum_{n=1}^{\infty} \varphi_n(x) f_n(t), \\ A(x, t) &= \sum_{n=1}^{\infty} \varphi_n(x) p_n(t),\end{aligned}\tag{2.9}$$

$$\begin{aligned}\frac{dQ_y}{dt} = B \rightarrow Q_y(x, t) &= \sum_{n=1}^{\infty} \varphi_n(x) b_n(t), \\ B(x, t) &= \sum_{n=1}^{\infty} \varphi_n(x) e_n(t),\end{aligned}\tag{2.10}$$

where $\varphi_n(x)$ represents the n th transverse mode shape functions the structure. To obtain accurate information on $\varphi_n(x)$ and ω_n in the case of variable tension and pinned-pinned supports, a semi-analytical numerical approach using a Fourier sine series is employed [25]. Also, $f_n(t)$ and $p_n(t)$ in Eq. 2.9 represent the generalized time-varying displacement and velocity, respectively, of the riser, while $b_n(t)$ and $e_n(t)$ in Eq. 2.10 describe the generalized displacement and velocity, respectively, of the wake. Upon substituting Eqs. 2.9 and 2.10 into Eqs. 2.1, 2.2, and 2.3, a standard Galerkin approach may be used to obtain a reduced-order multi-mode interaction of a coupled riser-wake system in VIV. Pinned-pinned boundary conditions at the ends of the structure are applied and an ortho-normalization of modes is introduced. The reduced multi-mode interaction is then expressed as follows [25]:

$$\frac{df_n}{dt} = p_n, \quad \frac{dp_n}{dt} = -2\xi_n \omega_n p_n - \omega_n^2 f_n + \frac{\xi_n}{S_G} \omega_n^2 (b_n - 2\gamma p_n / \omega_s),\tag{2.11}$$

$$\begin{aligned} \frac{db_n}{dt} &= e_n, \quad \frac{de_n}{dt} = \omega_s C_{e2} C_{L0}^2 e_n - \omega_s^2 b_n + \omega_s C_{e1} p_n \\ &- 4\omega_s C_{e2} \sum_{I=1}^{\infty} \sum_{J=1}^{\infty} \sum_{K=1}^{\infty} \left\{ \int_0^{L/D_{\text{ex}}} \varphi_n \varphi_I \varphi_J \varphi_K dx \right\} b_I b_J e_K. \end{aligned} \quad (2.12)$$

The dynamic stress, $\sigma_y(x, t)$, on the riser due to VIV can be expressed in relation to the dynamic strain as $\sigma_y(x, t) = E\epsilon_y(x, t)$, where E is the elastic modulus of the material of the selected riser. The dynamic strain, $\epsilon_y(x, t)$, at the outer surface of the riser can then be expressed as $\epsilon_y(x, t) = \frac{D_{\text{ex}}}{2} \kappa(x, t)$ where $\kappa(x, t)$ represents the axis curvature.

2.3 Fatigue Damage Estimation

2.3.1 Rainflow Cycle-Counting and MCS

Selection of the uncertain or random variables associated with the selected riser is the first step in the fatigue damage uncertainty assessment. These include (1) a model parameter related to the cylinder maximum amplitude normalized by the diameter, ΔA_{\max} , (2) a model parameter related to the ratio of the vortex-shedding frequency at A_{\max} to the natural frequency, $\Delta\omega$, and (3) the current velocity, V . Thus, the random variable vector is $\mathbf{X} = [\Delta A_{\max}, \Delta\omega, V]^T$.

Note that ΔA_{\max} and $\Delta\omega$ are given as follows:

$$\Delta A_{\max} = A_{\max} - A_{\max}^*, \quad (2.13)$$

$$\Delta\omega = \frac{\omega_{s,A}}{\omega_n} - \left(\frac{\omega_{s,A}}{\omega_n} \right)^*, \quad (2.14)$$

where the two empirical parameters, A_{\max} and $\omega_{s,A}/\omega_n$ are, collected by Skop [20] from several references, in which the 43 sets of $[A_{\max}, \omega_{s,A}/\omega_n]$ pairs are avail-

able for Eqs. 2.13 and 2.14. To fit $[A_{\max}, \omega_{s,A}/\omega_n]$ pairs with S_G , the two regression curves denoted by an asterisk(*) are defined as follows [20]:

$$A_{\max}^* = \frac{0.385}{\sqrt{0.12 + S_G^2}}, \quad (2.15)$$

$$\left(\frac{\omega_{s,A}}{\omega_n}\right)^* = 1.216 + \frac{0.084}{1 + 2.66S_G^2}. \quad (2.16)$$

Fig. 2.2 shows the scattered datasets of A_{\max} and $\omega_{s,A}/\omega_n$ according to different S_G values and the solid lines in the figure represent the fitted curves (i.e., Eqs. 2.15 and 2.16) in a regression manner.

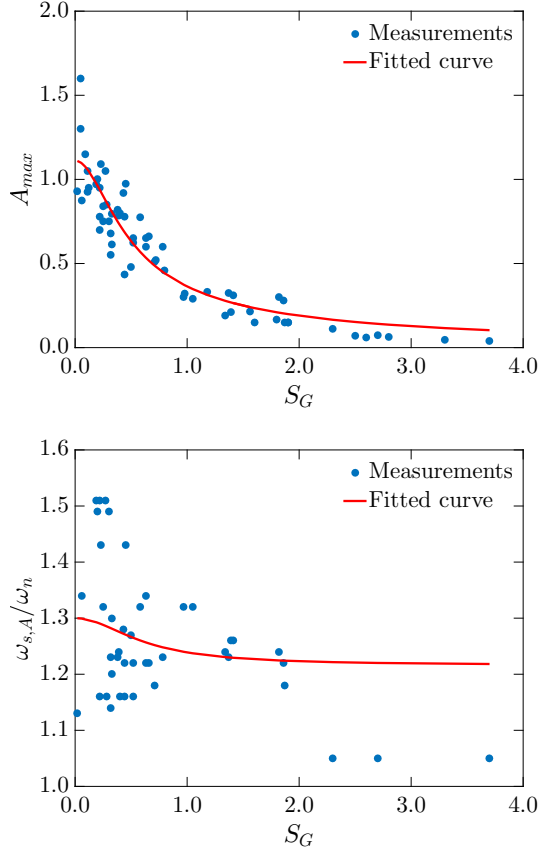


Figure 2.2: Measurement data and the empirical curves (Eqs. 2.15 and 2.16) against S_G : A_{\max} (top) and $\omega_{s,A}/\omega_n$ (bottom)

The model parameters, \mathbf{X} , are treated as random variables whose distributions must be available (one may also use a data-driven approach without the assumptions of distribution types [15]). In this study, the Shifted Generalized Lognormal Distribution (SGLD)[8] defined by the first four central moments of input variables is adopted to fit ΔA_{\max} and $\Delta \omega$. Fig. 2.3 shows the histograms and the SGLD fits of ΔA_{\max} and $\Delta \omega$. The other variable, V (current velocity), is also an important one that is associated with the lock-in

condition during vortex shedding and with the vortex shedding frequency; it is assumed to follow a lognormal distribution whose median value is 0.4 m/s and coefficient of variation is 0.08.

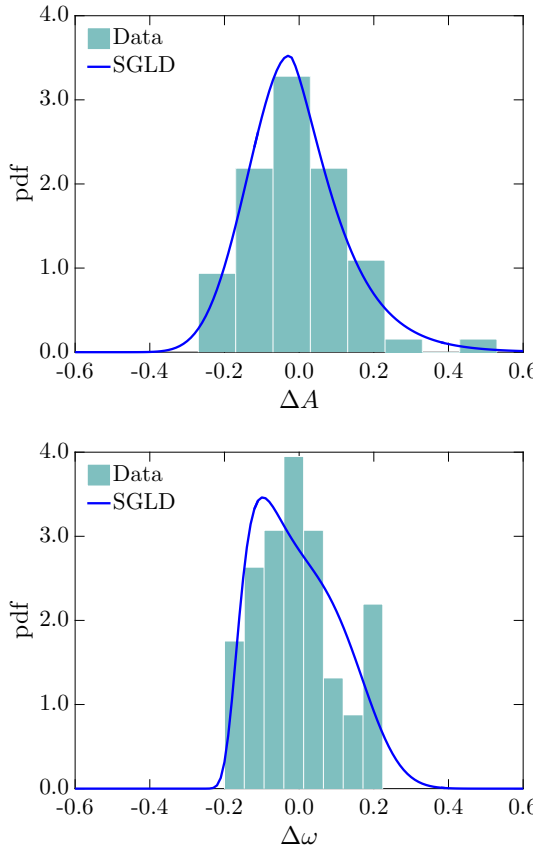


Figure 2.3: Fitted distributions of the residuals (Eqs. 2.13 and 2.14) of the measurement data by SGLD: ΔA_{\max} (top) and $\Delta \omega$ (bottom)

After choosing the model parameters, a transformation, ξ , maps these multiple model parameters in physical space, \mathbf{X} , onto a multi-dimensional independent standard normal variable space, \mathbf{U} . This can generally be achieved using a Rosenblatt transformation [16], although alternative dependence rep-

resentations among the variables in \mathbf{X} may also be employed [13]. After this mapping is preformed, MCS may be conducted; then stress ranges with associated parameters for a k th MCS run (with a k th input parameter sample vector: $\mathbf{X}^{(k)}$) may be counted using rainflow-cycle counting, \mathfrak{R} , as follows:

$$(\mathbf{S}^{(k)}, \mathbf{n}^{(k)}) = \mathfrak{R}\left(\sigma_y^{(k)}(x, t)\right), \quad (2.17)$$

where $\mathbf{S}^{(k)} = [S_1^{(k)}, S_2^{(k)}, \dots, S_{N_T}^{(k)}]^T$ is the vector of constant-amplitude stress ranges, $\mathbf{n}^{(k)} = [n_1^{(k)}, n_2^{(k)}, \dots, n_{N_T}^{(k)}]^T$ is the vector of numbers of cycles accumulated at $\mathbf{S}^{(k)}$, and N_T is the total number of stress range cycles (note that N_T can be varied at each k th MCS run due to uncertainty in $\mathbf{X}^{(k)}$). And, the simulation time, t_{\max} , is to be selected to assure the steady state response. Then fatigue damage is computed using the Miner-Palmgren rule [11], according to which the accumulated fatigue damage in a k th MCS run, $D^{(k)}$, is given as follows:

$$D^{(k)} = \sum_{l=1}^{N_T} \frac{n_l^{(k)}}{N(S_l^{(k)})}, \quad (2.18)$$

where $N(S)$ is the number of cycles to failure associated with stress range, S . Typically, $N(S)$ are described as follows:

$$N(S) = a(S)^{-m}, \quad (2.19)$$

where a and m are material constants determined from laboratory tests. For steel, m values ranging from 3 to 5 are usually considered. Two m values, 3 and 5, are selected for the numerical studies in this paper. Substituting

Eq. 2.19 into Eq. 2.18, $D^{(k)}$ can be represented as follows:

$$D^{(k)} = \frac{1}{a} \sum_{l=1}^{N_T} \left(S_l^{(k)} \right)^m n_l^{(k)}. \quad (2.20)$$

Recall that $D^{(k)}$ in k th MCS run involves the two steps: (1) calculation of the stress time series $\sigma_y^{(k)}(x, t)$, and (2) the rainflow-cycle counting, \mathfrak{R} , and the Miner-Palmgren rule.

It is convenient to express $D^{(k)}$ as a function of the model parameters, i.e., $D^{(k)} \equiv D^{(k)}(\mathbf{X}^{(k)})$. Also, the normalized fatigue damage, $\bar{D}^{(k)}$, will be used, which is defined as follows:

$$\bar{D}^{(k)}(\mathbf{X}^{(k)}) = \frac{D^{(k)}(\mathbf{X}^{(k)})}{D(\mathbf{X}_0)}, \quad (2.21)$$

where \mathbf{X}_0 corresponds to a physical case where $X_1 = X_2 = 0$ and $X_3 = 0.4$ (the median value of V). In the present study, ΔA_{\max} is taken to be X_1 , $\Delta\omega$ is taken to be X_2 , and X_3 is taken to be V . This is merely done for ease of notation and to establish an order or sequence in the definition of the random variables used with PCE.

For notational convenience, let us define the complementary cumulative distribution function (or probability of exceedance) as follows:

$$P(\bar{D} > d) \equiv G_{\bar{D}}(d). \quad (2.22)$$

Now, $G_{\bar{D}}(d)$ must be estimated using MCS because the analytic formulation of \bar{D} as well as the joint probability distribution function (jpdf) of \mathbf{X} are unknown. The MCS estimate is obtained as follows:

$$G_{\bar{D}}^{\text{MC}}(d) = \frac{1}{N_{\text{MC}}} \sum_{k=1}^{N_{\text{MC}}} I(\bar{D}^{(k)}(\mathbf{X}^{(k)}) > d), \quad (2.23)$$

where N_{MC} is the number of MCS samples drawn from the distribution of \mathbf{X} , $I(\mathcal{F})$ is the indicator function which is either 1 or 0 depending on whether \mathcal{F} is true or not, and $\mathbf{X}^{(k)}$ represents a drawn sample set in the k th MCS run. N_{MC} is set to 20,000 in the study.

2.3.2 PCE-based Fatigue Analysis

For PCE, a first step is to represent the selected model parameters, \mathbf{X} , as a summation or expansion of orthogonal polynomials following the Askey scheme [1]. Orthogonal polynomials are selected according to the random model parameters' mapped probability distributions. In Refs. [26, 3], various distributions and associated polynomial families that make up the Askey scheme are summarized. Hermit polynomials are adopted in this study; thus, \mathbf{X} is mapped to a standard normal random variable vector, \mathbf{U} . Recall that this mapping can be done by Rosenblatt or Nataf transformation [16, 13]. In present study, the Nataf transformation is employed; see [7] for detail. Several iterations are conducted to obtain the correlation coefficient between X_1 and X_2 in \mathbf{Y} space (correlated standard normal variable space), satisfying the following:

$$\rho_{Y_1 Y_2} = \int_{-\infty}^{\infty} \int_{-\infty}^{\infty} \left(\frac{x_1 - \mu_{X_1}}{\sigma_{X_1}} \right) \left(\frac{x_2 - \mu_{X_2}}{\sigma_{X_2}} \right) \phi(y_1, y_2, \rho_{Y_1 Y_2}) dy_1 dy_2, \quad (2.24)$$

where μ_{X_r} and σ_{X_r} are a mean and a standard deviation of a random variable, $X_r, r = 1, 2$, ϕ is the bi-variate standard normal probability distribution function (pdf) with a correlation coefficient $\rho_{Y_1 Y_2}$; $\rho_{Y_1 Y_2} = 0.3692$ is found to yield

the equality. The correlation in the physical space is $\rho_{X_1 X_2} = 0.3607$.

After establishing the polynomial basis functions, assuming that all the variables have finite variance, \bar{D} can be expanded as a series involving the polynomial basis functions as follows:

$$\bar{D}(\mathbf{X}) = \sum_{i=0}^{\infty} c_i H_i(\mathbf{U}) = \sum_{i=0}^{\infty} c_i H_i(\xi(\mathbf{X})), \quad (2.25)$$

where $\xi(\cdot)$ are probabilistically mapped functions of the input random variables, \mathbf{X} , c_i are coefficients to be estimated, and $H_i(\cdot)$ represents the i th multivariate orthogonal Hermite polynomial function of the associated input variables, \mathbf{U} .

The i th multivariate orthogonal Hermite polynomial function can be constructed using product of associated univariate Hermite polynomials as follows:

$$H_i(\mathbf{U}) = \prod_{r=1}^{N_X} \bar{H}_{\alpha_i}(U_r), \quad (2.26)$$

where $\bar{H}_{\alpha_i}(U_r)$ is the univariate Hermite polynomial of U_r , $\alpha_i = (\alpha_{i,1}, \dots, \alpha_{i,N_X})$ is the appropriate order sequence of the univariate polynomials for the i th multivariate polynomial function, and N_X is the number of random physical variables ($N_X = 3$ in this study). The total degree (or order), p , is defined as follows:

$$p = \max \left(\sum_{r=1}^{N_X} \alpha_{i,r} \right), \text{ for all } i.$$

For illustration, α_i for $N_X = 3$ and the total degree, $p = 2$, is tabulated in Table. 2.1. The orthogonality of the basis functions implies that:

Table 2.1: Tabulated multi-index for $N_X = 3$ and $p = 2$

$\boldsymbol{\alpha}_i$	$\alpha_{i,1}$	$\alpha_{i,2}$	$\alpha_{i,3}$	$H_i(\mathbf{U})$	$\mathbb{E}[(H_i(\mathbf{U}))^2]$
$\boldsymbol{\alpha}_0$	0	0	0	$\bar{H}_0(U_1)\bar{H}_0(U_2)\bar{H}_0(U_3) = 1$	1
$\boldsymbol{\alpha}_1$	1	0	0	$\bar{H}_1(U_1)\bar{H}_0(U_2)\bar{H}_0(U_3) = U_1$	1
$\boldsymbol{\alpha}_2$	0	1	0	$\bar{H}_0(U_1)\bar{H}_1(U_2)\bar{H}_0(U_3) = U_2$	1
$\boldsymbol{\alpha}_3$	0	0	1	$\bar{H}_0(U_1)\bar{H}_0(U_2)\bar{H}_1(U_3) = U_3$	1
$\boldsymbol{\alpha}_4$	2	0	0	$\bar{H}_2(U_1)\bar{H}_0(U_2)\bar{H}_0(U_3) = U_1^2 - 1$	2
$\boldsymbol{\alpha}_5$	1	1	0	$\bar{H}_1(U_1)\bar{H}_1(U_2)\bar{H}_0(U_3) = U_1U_2$	1
$\boldsymbol{\alpha}_6$	1	0	1	$\bar{H}_1(U_1)\bar{H}_0(U_2)\bar{H}_1(U_3) = U_1U_3$	1
$\boldsymbol{\alpha}_7$	0	2	0	$\bar{H}_0(U_1)\bar{H}_2(U_2)\bar{H}_0(U_3) = U_2^2 - 1$	2
$\boldsymbol{\alpha}_8$	0	1	1	$\bar{H}_0(U_1)\bar{H}_1(U_2)\bar{H}_1(U_3) = U_2U_3$	1
$\boldsymbol{\alpha}_9$	0	0	2	$\bar{H}_0(U_1)\bar{H}_0(U_2)\bar{H}_2(U_3) = U_3^2 - 1$	2

$$E[H_i H_j] = \delta_{ij} E[H_i^2], \quad E[H_i^2] = i! \quad (2.27)$$

where δ_{ij} is the Kronecker delta, equal to 1 if $i = j$ and 0 otherwise, and $E[\cdot]$ is the expectation operator.

A truncated PCE for \bar{D} that involves polynomials only up to order p can be represented as:

$$\bar{D}(\mathbf{X}) \approx \bar{D}^{\text{PCE}}(\mathbf{X}) = \sum_{i=0}^{N_p-1} c_i H_i(\xi(\mathbf{X})), \quad (2.28)$$

where N_p denotes the number of unknown PCE coefficients in polynomials of order not exceeding p , and it can be computed as follows:

$$N_p = \binom{N_X + p}{N_X}. \quad (2.29)$$

The next step in PCE is to estimate the coefficients, c_i . Several methods for estimating these coefficients have been developed. They include spectral projection, stochastic collocation, and linear regression, and have been applied to

offshore structural problems [6, 14, 5]. In the present study, spectral projection (involving quadrature-based integration) is used to compute the coefficients as follows:

$$c_i = \frac{E[\bar{D}(\mathbf{X})H_i(\xi(\mathbf{X}))]}{E[H_i^2(\xi(\mathbf{X}))]}. \quad (2.30)$$

For $N_X = 3$, the numerator in Eq. 2.30 is given as follows:

$$\begin{aligned} E[\bar{D}(\mathbf{X})H_i(\xi(\mathbf{X}))] &= \\ \int \int \int \bar{D}(\mathbf{X})H_i(\xi(\mathbf{X}))f_{\mathbf{X}}(\mathbf{x})dx_1dx_2dx_3, \end{aligned} \quad (2.31)$$

where $f_{\mathbf{X}}(\mathbf{x})$ is a joint pdf of \mathbf{X} . The numerator may require a multi-dimensional integration by using a quadrature rule. Note that integration in standard normal space, \mathbf{U} , than physical space, \mathbf{X} , is convenient. Using the Gauss-Hermite quadrature rule with N_q quadrature points, the numerator can be approximated as follows:

$$\begin{aligned} E[\bar{D}(\mathbf{X})H_i(\xi(\mathbf{X}))] &= E[\bar{D}(\xi^{-1}(\mathbf{U}))H_i(\mathbf{U})] \approx \\ \sum_{u_{1q}=1}^{N_q} \sum_{u_{2q}=1}^{N_q} \sum_{u_{3q}=1}^{N_q} \bar{D}\left(\xi^{-1}(u_{1q}, u_{2q}, u_{3q})\right) H_i(u_{1q}, u_{2q}, u_{3q}) \\ w_{1q}w_{2q}w_{3q}, \end{aligned} \quad (2.32)$$

where w_{rq} for $r = 1, 2, 3$ are weights corresponding to Gauss-Hermite quadrature points, u_{rq} . The denominator is given in a closed form as follows:

$$E(H_i^2(\xi(\mathbf{X}))) = E(H_i^2(\mathbf{U})) = \prod_{r=1}^3 \alpha_{i,r}!. \quad (2.33)$$

One may construct an orthonormal polynomial functions by $\Psi_i(\mathbf{U}) = H_i(\mathbf{U})/\sqrt{E(H_i^2(\mathbf{U}))}$ which satisfies a condition, $E[\Psi_i\Psi_j] = \delta_{ij}$.

The PCE estimate for Eq. 2.22 is given as follows:

$$G_{\bar{D}}^{\text{PCE}}(d) = \frac{1}{N_{\text{PCE}}} \sum_{k=1}^{N_{\text{PCE}}} I(\bar{D}^{\text{PCE}}(\xi(\mathbf{X}^{(k)})) > d), \quad (2.34)$$

where N_{PCE} is the number of computations involving use of a PCE surrogate model. It is noted that $G_{\bar{D}}^{\text{PCE}}$ is also calculated by MCS but using the PCE surrogate model, \bar{D}^{PCE} , not the truth model \bar{D} . Because \bar{D}^{PCE} is given as a closed form, N_{PCE} can chosen much greater than N_{MCS} .

2.4 Numerical Studies

We now discuss fatigue damage estimation in the selected top-tensioned riser due to VIV. Recall that an uniform current velocity of $V = 0.4$ m/s is considered and a corresponding Reynolds number is around 1×10^5 . Important properties of the model are presented in Table 2.2. The simulations are run until the response reaches a steady state (until around 40 s) after the initial transients (that last around 20 s) have passed. It is at the middle of the riser where the sum of the axial and bending stresses are computed for fatigue damage estimation.

2.4.1 Example with 3 Variables

Fatigue damage estimation using PCE and with the three variables as random (ΔA_{\max} , $\Delta \omega$, and V) is considered. For illustration purposes, 1,000 different sets of the 3 variables are randomly generated. It is noted that these realizations are done using the truth model to see the overall perspective before

Table 2.2: Properties of the selected TTR

Property	Value
Young's modulus (E)	2.05×10^{11} N/m ²
Outer diameter (D_{ex})	0.268 m
Wall thickness (t_w)	14 mm
Length of the riser (L)	500 m
Water density (ρ)	1025 kg/m ³
Top tension/submerged weight	8.3
Mass ratio ($M/(\rho\pi D_{\text{ex}}^2/4)$)	1.52
Aspect ratio (L/D_{ex})	1866

proceeding with PCE. Fig. 2.4 shows these MCS samples in a manner that reveals combinations of two random variables at a time (ΔA_{\max} and $\Delta\omega$, ΔA_{\max} and V , or $\Delta\omega$ and V). Note that, in each row, the uncorrelated samples (top) and the correlated samples (between ΔA_{\max} and $\Delta\omega$ —bottom) are plotted. The color of each sample goes from blue to red as \bar{D} increases. Greater fatigue damage results from higher ΔA_{\max} and V values and from lower $\Delta\omega$ values. It can be seen that, due to the positive correlation between ΔA_{\max} and $\Delta\omega$ — $\rho_{\Delta A_{\max}, \Delta\omega} = \rho_{X_1 X_2} = 0.3607$, \bar{D} for the correlated case exhibit lower values than the uncorrelated case, because, as stated earlier, \bar{D} increases with ΔA_{\max} while decreases with $\Delta\omega$.

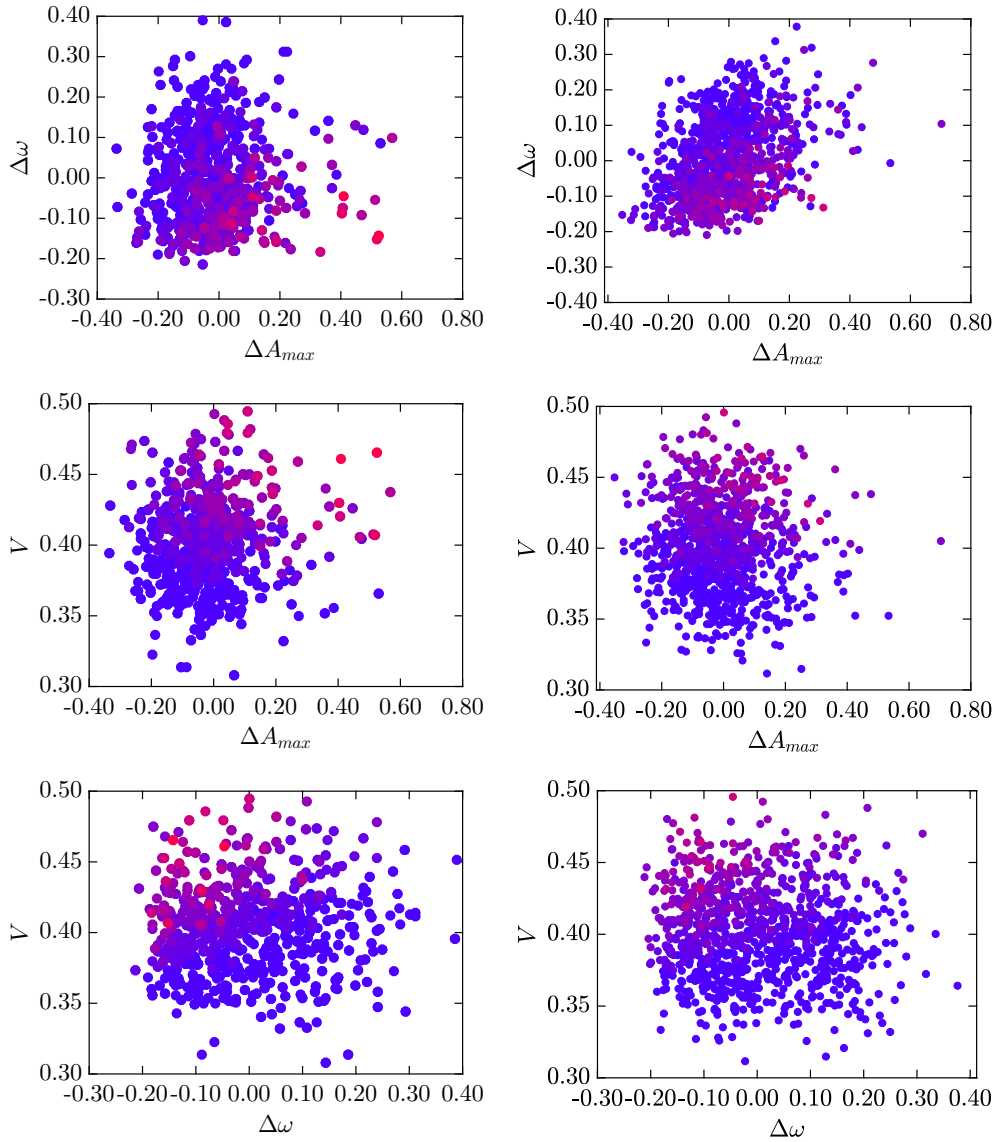


Figure 2.4: Scatter plots of the relationships between three variables (ΔA_{max} , $\Delta \omega$, and V): uncorrelated (left column) and correlated (right column), using 1000 MCS in the truth model— $\rho_{\Delta A_{max}, \Delta \omega} = \rho_{X_1 X_2} = 0.3607$

In Fig. 2.5, 10 sets of pdfs, Q-Q plots, and exceedance probability plots

for \bar{D} using a PCE scheme with a polynomial order, $p = 5$, are shown; comparisons are made versus MCS in the truth model. Note that these comparisons are made between MCS in the “surrogate model” and MCS in the “truth model”. For simplicity, these comparisons will be represented by “MCS” versus “PCE” from now on. The number of quadrature points for Eq. 2.32 is set to $N_q = 5^{N_x} = 5^3$ in this example. We see that the pdfs by the 5-order PCE scheme match well with the MCS-based pdfs for \bar{D} . In the Q-Q plots, the PCE models with a polynomial order 5 appear to indicate again very good agreement with MCS over all damage ranges, and perhaps is acceptable for a surrogate model for \bar{D} . The exceedance probability plots also show that the PCE models estimate G_D quite well; over the range, $0 < d < 10$, the 5-order PCE schemes predict exceedance probabilities that lie within the MCS 99% confidence interval, which is computed by bootstrapping by 1000 replications.

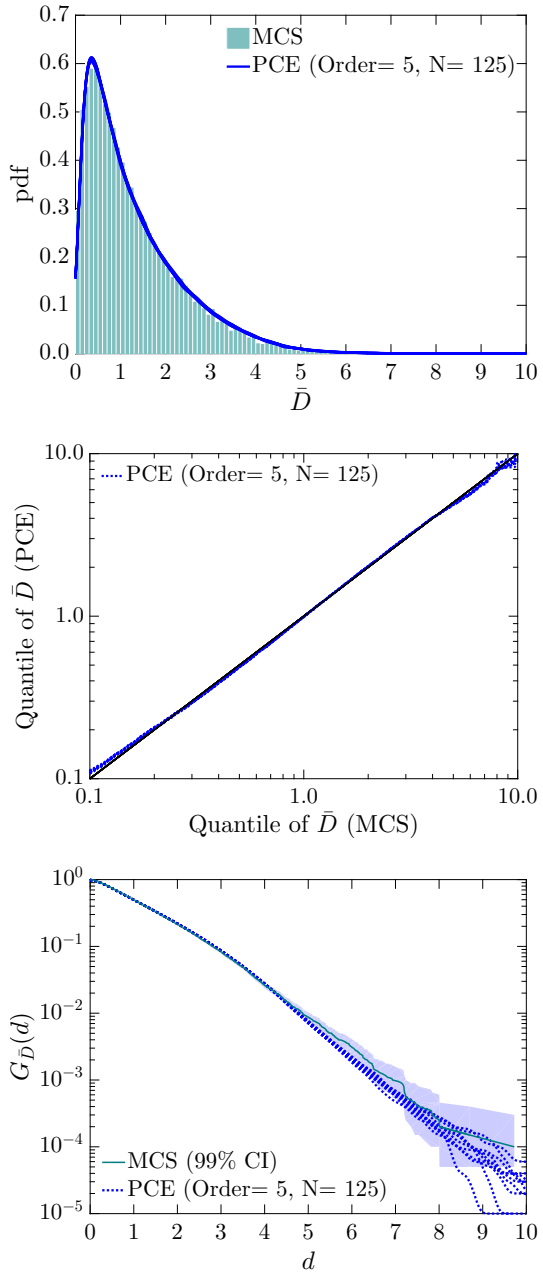


Figure 2.5: Comparisons of pdf's (top), Q-Q plots (middle), and exceedance probability (bottom) plots for a polynomial order-5 PCE model—10 sets with three uncertain variables

2.4.2 Uncertainties of PCE Surrogate Models for Various Choices of Input Parameters

In the authors' previous study [6], we have seen that variability in normalized fatigue damage, \bar{D} , arises from different choice and/or combinations of uncertain input parameters such as ΔA_{\max} , $\Delta \omega$, and V that are involving with system parameters of a structure and a flow. Also, the results show that an order-5 PCE model with 5^{N_x} quadrature integration scheme is fairly accurate in estimation of \bar{D} when compared against MCS. These results may suggest a guideline for choosing appropriate parameters associated with PCE—a PCE polynomial order, p , and a required number of simulations, $N_q^{N_x}$, at multi-dimensional quadrature points.

To compare influence of different choices of the uncertain input parameters on \bar{D} , Fig. 2.6 presents PCE-based mean exceedance probability curves for various choices/combinations of model parameters and comparisons against MCS. Here, MCS is performed using 3 random variables (ΔA_{\max} , $\Delta \omega$, and V with the correlation— $\rho_{\Delta A_{\max}, \Delta \omega} = \rho_{X_1, X_2} = 0.3607$) and all PCE models adopt an order-5 and use 5^{N_x} quadrature schemes (e.g., 5 for one, 5^2 for two, and 5^3 for three variables). The different PCE-based exceedance probability curves suggest contrasting levels of influence of the input variables. In other words, if we disregard the variability of one variable or more in fatigue damage prediction, large errors would have been introduced; the PCE models with two variables (dash-dot curves) exhibit large errors when compared against the MCS curve, and accuracy of the PCE model with one variable (solid or

dashed curves) is worse than the PCE with the two variables.

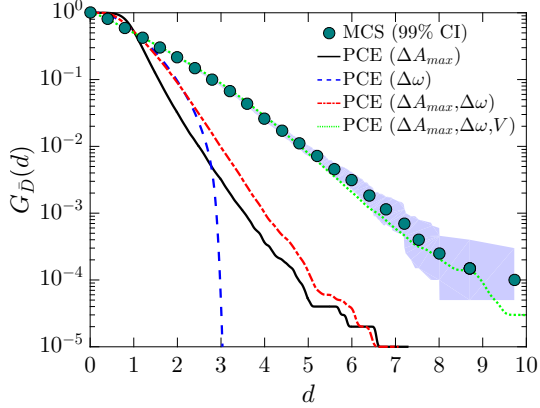


Figure 2.6: Comparisons of the mean exceedance probabilities for each PCE model of various model input selections: one variable (ΔA_{\max} or $\Delta \omega$), two variable (ΔA_{\max} and $\Delta \omega$), and three variables (ΔA_{\max} , $\Delta \omega$, and V)

2.4.3 Different Locations of Interest Along the Riser

We investigate next variability in estimation of \bar{D} at different locations of interest along the riser's length. The procedures and results are presented in the same manner as with the previous numerical studies, however, the focus is now on differences in the variability of \bar{D} at three locations ($x = L/4$, $L/2$, and $3L/4$ —from the top). For illustration, Fig. 2.7 shows stress range histograms obtained using rainflow cycle-counting for the three different locations; at each location, ΔA_{\max} , $\Delta \omega$, and V are set to $\mathbf{X}_0 = [0, 0, 0.4]^T$, and the fatigue damage, $D(\mathbf{X}_0)$, are normalized with respect to $D_0(\mathbf{X}_0)$, which is defined as the fatigue damage at the middle of the riser. The abscissa and ordinate in the plots in Fig. 2.7 represent the stress ranges and numbers of cycles, respectively, for the three locations. Note that D/D_0 values at each location

are: $D_{x=L/4}/D_0 = 0.478$, $D_{x=L/2}/D_0 = 1$, and $D_{x=3L/4}/D_0 = 0.437$.

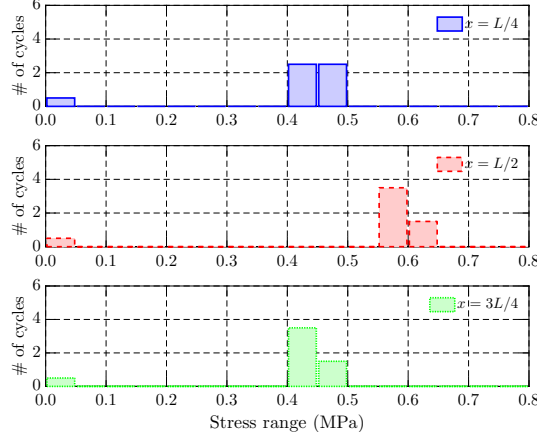


Figure 2.7: Stress range histograms obtained by rainflow cycle-counting at three different locations along the riser ($x = L/4$, $L/2$, and $3L/4$ —from the top) under $V = 0.4$ m/s

Although phases and amplitudes of the response process, $v(x, t)/D_{ex}$, at $x = L/4$ and $x = 3L/4$, do not differ very noticeably as shown in Fig. 2.8, the D/D_0 estimates at the two locations— $D_{x=L/4}/D_0 = 0.478$ and $D_{x=3L/4}/D_0 = 0.437$ —show non-negligible differences that result from differences in the cycle counts seen in the stress range histograms for $x = L/4$ and $3L/4$ in Fig. 2.7. We note again that the initial transients (from 0 to around 20 s) are not considered in the rainflow cycle-counting, as is indicated by the dashed vertical line in Fig. 2.8. It is clearly seen that the fatigue damage at the middle of the riser—i.e., $D/D_0 = 1$ at $x = L/2$ —is significantly greater than the normalized values of 0.478 and 0.437 at $x = L/4$ and $x = 3L/4$, respectively. This is likely due to excitation of the third mode of vibration of this riser that results with the selected uniform current velocity profile. Note that in other modes

of vibration, it may well be the case that other locations than the middle of the riser may experience greater fatigue damage and is even possible that the middle of the riser is an anti-node. In this study, our focus is on developing a PCE-based fatigue damage surrogate model that will work at any location along the riser.

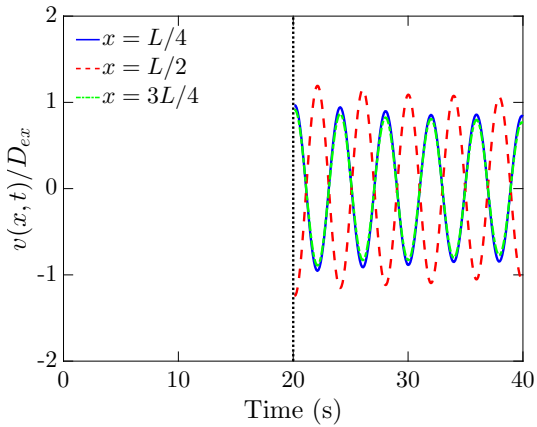


Figure 2.8: Cross flow motion time history $v(x, t)$ at different locations ($x = L/4, L/2, 3L/4$ —from the top in the riser) under $V = 0.4$

From preceding discussions, it is expected that exceedance probabilities of \bar{D} at different locations of interest could exhibit some degree of variability; $G_{\bar{D}}$ estimate at the three selected locations are investigated next. A comparison between MCS and PCE is not done for this study that is focused on location of fatigue damage. Our justification is that we wish to focus primarily on variability in \bar{D} at the three locations as established by PCE surrogate models for \bar{D} . As such, Fig. 2.9 shows order-5 PCE-based fatigue damage exceedance probability curves at the three locations— $x = L/4, L/2$, and $3L/4$ —along the

riser. These curves confirm the contrasting degrees of influence of input variable variability on fatigue damage at each selected location, it is noted that in the case considered, the middle of the riser experiences both the largest fatigue damage in general as well as the greatest variability. Of the other two locations, fatigue damage estimates at $x = L/4$ are seen to systematically greater than those at $x = 3L/4$; some differences are to be expected in a top-tensioned riser.

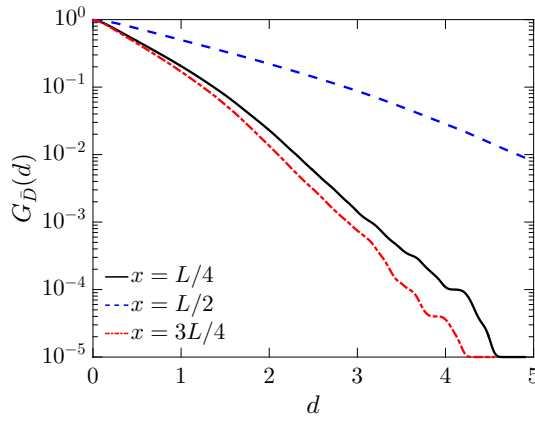


Figure 2.9: Order-5 PCE-based fatigue damage exceedance probability curves at three locations along the riser ($x = L/4$, $L/2$, and $3L/4$ —from the top) arising from consideration of three uncertain variables (ΔA_{\max} , $\Delta \omega$, and V).

2.4.4 Influence of S-N Parameters: $m = 5$

One of the material constants related to calculations of \bar{D} (namely, S-N parameters), m , which governs non-linearity between stress and fatigue damage as formulated in Eq. 2.20, can greatly influence on the estimation of \bar{D} . Hence, it is worthwhile to investigate and check accuracy of the PCE scheme for

$m = 5$ —a 5-order PCE with an integration scheme that involves $N = 5^3$ quadrature points. However, it is expected that such a PCE scheme will not be sufficient to provide accuracy when compared against MCS. The reason is that high non-linearity arising from the change of a m value to 5 from 3 may require a sophisticated model to have accuracy: a higher polynomial order than $p = 5$. Also, one should be cautious to avoid overfitting during the construction of PCE surrogate models by spectral projection, that can worsen the estimation. As such, a order-7 PCE scheme while keeping $N = 5^3$ is selected for the prediction. Fig. 2.10 shows that such a PCE scheme performs well; it can be seen that the 10 PCE-based exceedance probability curves exhibit lower variability than predictions from the 10 MCS sets with bootstrapping (1,000 replications). Also, note that the prediction at the lower probability levels is improved when compared to the lower-order PCE polynomial choice ($p = 5$).

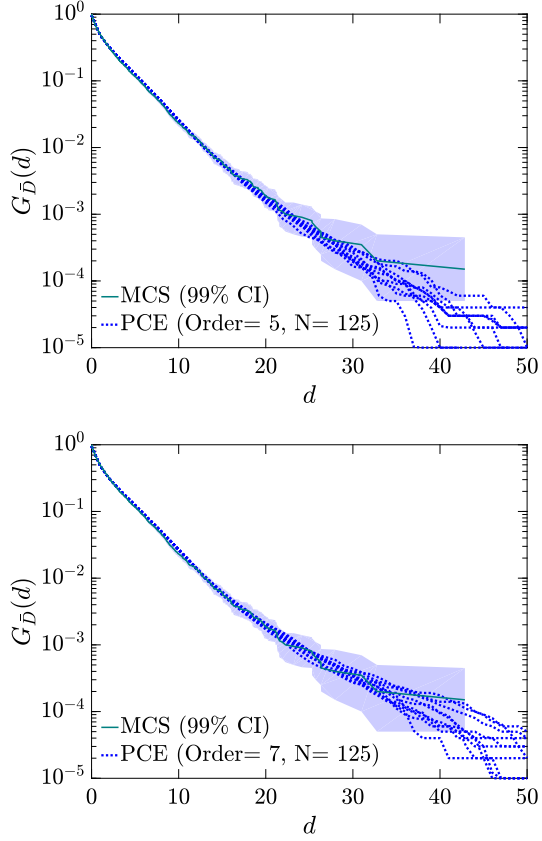


Figure 2.10: Comparisons of 10 sets of order-5 (top) and order-7 (bottom) PCE-based exceedance probability curves for $m = 5$ against the MCS-based curve with 99% confidence intervals

2.5 Refined PCE Analysis

To improve PCE accuracy, rather than increasing PCE polynomial order p (or number of quadrature points, N_q), we now turn to a simple but effective refinement on PCE. We take the logarithm of the positive-valued QoI in the refined PCE (rPCE), motivated by work done with the refined point estimate method (rPEM) based on the point estimate method (PEM) [10]. For the sake

of brevity, the detailed steps of PEM and rPEM are not presented here but, for comparisons, the exceedance probability curves by PEM and rPEM are presented in Fig. 2.11. From the figure, it is clear that PEM and rPEM do not estimate well $G_{\bar{D}}$ for the case where three variables are involved— ΔA_{\max} , $\Delta \omega$, and V —although the estimations for the case two variables involved— ΔA_{\max} and $\Delta \omega$ —are quite accurate for $0 < d < 4$ when compared against the MCS-based exceedance probability curve. One possible reason might be that PEM and rPEM are not suitable to capture the complicated interaction involving V in a wake oscillator model; it should be noted that, in PEM or rPEM, $G_{\bar{D}}$ are calculated by (1) estimations of the first four moments of each single-variable function associated with each input random variable, (2) estimations of \bar{D} 's first four moments by using the results of (1), and (3) fitting of \bar{D} by a parametric distribution such as a SGLD fit [8].

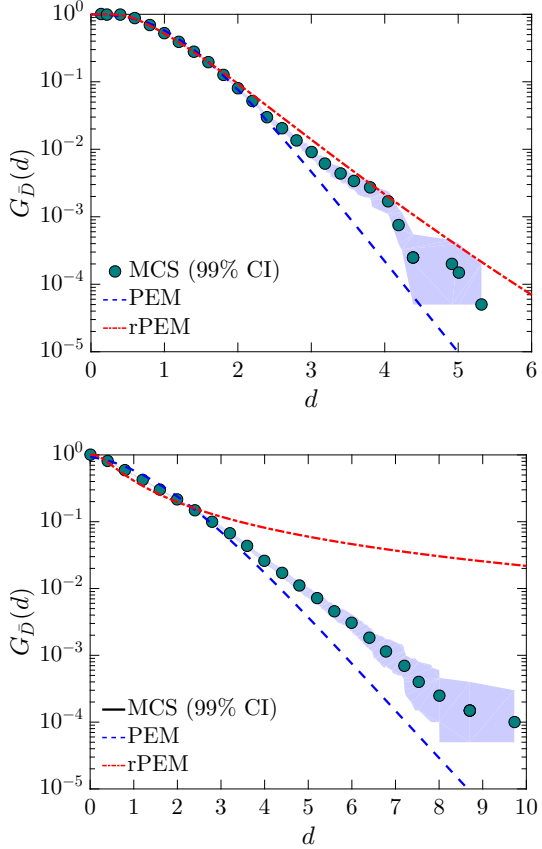


Figure 2.11: Estimations of exceedance probabilities for the cases two (top) and three (bottom) variables involved, by PEM and rPEM; comparisons are made against MCS of 99% confidence intervals

The fatigue damage, D , is guaranteed to be non-negative because the stress ranges, S_l , calculated by the rainflow cycle-counting in Eq. 2.20, are non-negative and, in the same sense, a , m , and n_l are non-negative. Hence, for the refinement, it may be acceptable to construct a PCE surrogate model by taking the logarithm, i.e., $\ln \bar{D}^{\text{PCE}}$; effectively, this amounts to using a new

QoI, which is the logarithm of the QoI used before. Thus, we have:

$$\ln(\bar{D}^{\text{PCE}}(\mathbf{X})) = \sum_{i=0}^{N_p-1} \hat{c}_i H_i(\xi(\mathbf{X})), \quad (2.35)$$

where \hat{c} are coefficients to be estimated, which are given as:

$$\hat{c}_i = \frac{E[\ln(\bar{D}(\mathbf{X})) H_i(\xi(\mathbf{X}))]}{E(H_i^2(\xi(\mathbf{X})))}. \quad (2.36)$$

Now, using the fact that $P(\bar{D} > d) = P(\ln \bar{D} > \ln d)$, $G_{\bar{D}}$ for the rPCE is given as follows:

$$G_{\bar{D}}^{\text{rPCE}}(d) = \frac{1}{N_{\text{PCE}}} \sum_{k=1}^{N_{\text{PCE}}} I(\ln(\bar{D}^{\text{PCE}}(\mathbf{X}^{(k)})) > \ln(d)). \quad (2.37)$$

In Fig. 2.12, it is seen that rPCE works well for the case of three variables involved when $m = 3$; the ten rPCE-based exceedance probability curves exhibit smaller variability than the ten PCE sets. Also bias is reduced for rPCE compared to the PCE model.

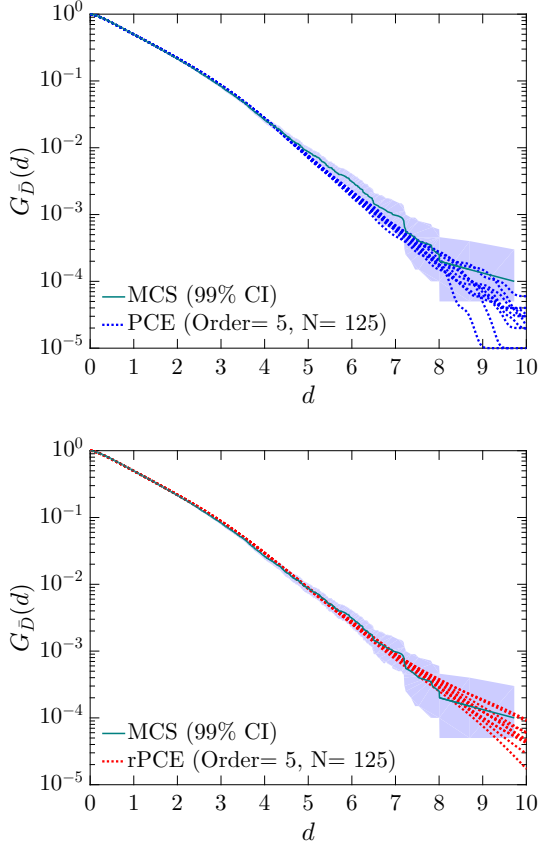


Figure 2.12: Improvement of accuracy of $G_{\bar{D}}$ estimates by using refinement on PCE: a case with three variables involved (ΔA_{\max} , $\Delta \omega$, and V) and $m = 3$

2.6 Conclusions

In this study, the fatigue damage estimation due to VIV in a marine riser is carried out by employing PCE with a choice of model parameters that are considered uncertain— ΔA_{\max} , $\Delta \omega$, and V . A distributed wake oscillator model is used to perform numerical studies with the selected uncertain parameters. A PCE order-5 scheme is found to be quite accurate with an integration scheme

that involves 5^3 quadrature points when compared against MCS predictions.

In a separate but related study, the variability of fatigue damage at different measurement locations— $x = L/4, L/2, 3L/4$ from the top—on the riser is investigated. Again, the PCE order-5 scheme with 5^3 quadrature points is used in order to estimate exceedance probability curves at the locations and the results also confirm the versatility of the PCE-based approach.

The efficiency and accuracy of the PCE-based approach in fatigue damage estimation is also demonstrated by investigating the impact of a change of m on the fatigue damage—to 5 from 3. The results show that the fatigue damage estimation for $m = 5$ is reasonably accurate when a PCE order-7 scheme with 5^3 quadrature points is used, when comparison is made against MCS predictions.

To improve the accuracy of the PCE surrogate, a simple but effective refinement is proposed, which only involves taking the logarithm of \bar{D} . This changes the quantity of interest in the polynomial chaos expansion; results with $\ln \bar{D}$ confirm the improved accuracy.

Bibliography

- [1] George E Andrews and Richard Askey. Classical orthogonal polynomials. In *Polynômes orthogonaux et applications*, pages 36–62. Springer, 1985.
- [2] Roger G Ghanem and Pol D Spanos. *Stochastic finite elements: a spectral approach*. Courier Corporation, 2003.
- [3] Chao Hu and Byeng D Youn. Adaptive-sparse polynomial chaos expansion for reliability analysis and design of complex engineering systems. *Structural and Multidisciplinary Optimization*, 43(3):419–442, 2011.
- [4] Bin Liang and Sankaran Mahadevan. Error and uncertainty quantification and sensitivity analysis in mechanics computational models. *International Journal for Uncertainty Quantification*, 1(2), 2011.
- [5] HyeongUk Lim, Lance Manuel, and Ying Min Low. On efficient long-term extreme response estimation for a moored floating structure. *ASME. International Conference on Offshore Mechanics and Arctic Engineering*, 2018.
- [6] HyeongUk Lim, Lance Manuel, Ying Min Low, and Narakorn Srinil. Uncertainty quantification of riser fatigue damage due to VIV using a distributed wake oscillator model. *ASME. International Conference on Ocean, Offshore and Arctic Engineering*, 2017.

- [7] Pei-Ling Liu and Armen Der Kiureghian. Multivariate distribution models with prescribed marginals and covariances. *Probabilistic Engineering Mechanics*, 1(2):105–112, 1986.
- [8] Ying Min Low. A new distribution for fitting four moments and its applications to reliability analysis. *Structural Safety*, 42:12–25, 2013.
- [9] Ying Min Low and Narakorn Srinil. Sensitivity study of wake oscillator parameters influencing the fatigue damage of a riser undergoing VIV. *ASME. International Conference on Ocean, Offshore and Arctic Engineering*, 2015.
- [10] Ying Min Low and Narakorn Srinil. VIV fatigue reliability analysis of marine risers with uncertainties in the wake oscillator model. *Engineering Structures*, 106:96–108, 2016.
- [11] Milton A Miner. Cumulative damage in fatigue. *Journal of Applied Mechanics*, 12(3):159–164, 1945.
- [12] Habib N Najm. Uncertainty quantification and polynomial chaos techniques in computational fluid dynamics. *Annual Review of Fluid Mechanics*, 41:35–52, 2009.
- [13] Andre Nataf. Determination des distribution don t les marges sont donnees. *Comptes Rendus de l Academie des Sciences*, 225:42–43, 1962.
- [14] Phong TT Nguyen, Lance Manuel, and Ryan G Coe. On the development of an efficient surrogate model for predicting long-term extreme loads on

a wave energy converter. *ASME. International Conference on Offshore Mechanics and Arctic Engineering*, 2018.

- [15] Sergey Oladyshkin and Wolfgang Nowak. Data-driven uncertainty quantification using the arbitrary polynomial chaos expansion. *Reliability Engineering & System Safety*, 106:179–190, 2012.
- [16] Murray Rosenblatt. Remarks on a multivariate transformation. *The Annals of Mathematical Statistics*, 23(3):470–472, 1952.
- [17] Chen Shi and Lance Manuel. Non-parametric prediction of the long-term fatigue damage for an instrumented top-tensioned riser. *Applied Ocean Research*, 82:245 – 258, 2019.
- [18] Chen Shi, Lance Manuel, and Michael A Tognarelli. Empirical procedures for long-term prediction of fatigue damage for an instrumented marine riser. *Journal of Offshore Mechanics and Arctic Engineering*, 136(3):031402, 2014.
- [19] Chen Shi, Lance Manuel, and Michael A Tognarelli. A comparison of empirical procedures for fatigue damage prediction in instrumented risers undergoing vortex-induced vibration. *Applied Sciences*, 8(11), 2018.
- [20] Richard A Skop and Sathish Balasubramanian. A new twist on an old model for vortex-excited vibrations. *Journal of Fluids and Structures*, 11(4):395–412, 1997.

- [21] Christian Soize and Roger Ghanem. Physical systems with random uncertainties: chaos representations with arbitrary probability measure. *SIAM Journal on Scientific Computing*, 26(2):395–410, 2004.
- [22] Narakorn Srinil. Multi-mode interactions in vortex-induced vibrations of flexible curved/straight structures with geometric nonlinearities. *Journal of Fluids and Structures*, 26(7):1098–1122, 2010.
- [23] Narakorn Srinil. Analysis and prediction of vortex-induced vibrations of variable-tension vertical risers in linearly sheared currents. *Applied Ocean Research*, 33(1):41–53, 2011.
- [24] Narakorn Srinil, Pierre-Adrien Opinel, and Francesca Tagliaferri. Empirical sensitivity of two-dimensional nonlinear wake–cylinder oscillators in cross-flow/in-line vortex-induced vibrations. *Journal of Fluids and Structures*, 83:310–338, 2018.
- [25] Narakorn Srinil, Marian Wiercigroch, and Patrick O’Brien. Reduced-order modelling of vortex-induced vibration of catenary riser. *Ocean Engineering*, 36(17):1404–1414, 2009.
- [26] Bruno Sudret. Meta-models for structural reliability and uncertainty quantification. *arXiv preprint arXiv:1203.2062*, 2012.
- [27] Dongbin Xiu and George Em Karniadakis. The Wiener–Askey polynomial chaos for stochastic differential equations. *SIAM Journal on Scientific Computing*, 24(2):619–644, 2002.

Paper II:

Chapter 3

On Efficient Surrogate Model Development for Prediction of the Long-Term Extreme Response of a Moored Floating Structure[†]

Abstract

This study focuses on the development of efficient surrogate models by polynomial chaos expansion (PCE) for prediction of the long-term extreme surge motion of a moored floating offshore structure. The structure is subjected to first-order and second-order (difference-frequency) wave loading. Uncertainty in the long-term response arises from the contrasting sea state conditions, characterized by the significant wave height, H_s , and the spectral peak period, T_p , and their relative likelihood of occurrence; these two variables are explicitly included in the PCE-based uncertainty quantification (UQ). In a given sea state, however, response simulations must be run for the associated H_s and T_p ; in such simulations, typically, a set of random amplitudes and phases define an irregular wave train consistent with that sea state. These

[†]Some portion of this chapter has been published in: HyeongUk Lim, Lance Manuel, and Ying Min Low, “On Efficient Long-Term Extreme Response Estimation for a Moored Floating Structure,” *ASME. International Conference on Ocean, Offshore and Arctic Engineering*, 2018. The dissertation author wrote first drafts of the manuscript, analyzed all the results, and developed the surrogate modeling framework.

random amplitudes and phases for all the frequency components in the wave train introduce additional uncertainty in the simulated waves and in the response. The UQ framework treats these two sources of uncertainty—from H_s and T_p on the one hand, and the amplitude and phase vectors on the other—in a nested manner that is shown to efficiently yield long-term surge motion extreme predictions consistent with more expensive Monte Carlo simulations (MCS) that serve as the “truth” system for this exercise. To reduce uncertainty in response extremes that result from sea states with a low likelihood of occurrence, importance sampling is employed with both MCS- and PCE-based extreme response predictions. Satisfactory performance with the proposed UQ approach suggests that such inexpensive surrogate models can be useful in assessing the long-term response of various offshore structures.

3.1 Introduction

Quantities of Interest (QoIs) such as the extreme response of a structure in a design process, that often need to be evaluated, generally involve the use of models that in turn employ stochastic input parameters. Any such QoI and its associated uncertainty must be estimated using repetitive computations involving a large number of sampled model parameters; simulations for each parameter set can be computationally expensive. Then, one might consider the use of “surrogate” models that serve as approximations of the “truth” system. Of course, the development of such surrogates is validated only if the QoI and its associated uncertainty are shown to be reasonably similar to those

obtained when the truth system is employed.

Polynomial chaos expansion (PCE) [5, 18] offers a robust framework for the development of surrogate models due to its efficiency and versatility in accounting for uncertainties in complex high-dimensional problems. A desirable feature of PCE-based surrogate models for engineering applications is that the QoI is expanded using orthogonal basis functions (polynomials) defined in terms of random variables, suitably mapped to generalized uncertain physical parameters. A QoI surrogate defined using PCE can be thought of as a mathematically optimal representation of model output(s) associated with uncertain input variables or parameters [15].

The long-term surge motion extremes of a moored floating structure are of interest in this study. Suppose the T -year surge displacement ($T > 1$) is of interest; for design $T = 50$ or 100 is common. If the surge motion in a sea state of a short duration, say 30 minutes, is assumed stationary, then for such a sea state defined by parameters (such as H_s and T_p), one can carry out response simulations for irregular/stochastic wave loading consistent with those parameters. By sweeping over different H_s and T_p values, while accounting for their relative likelihoods of occurrence, and generating suites of irregular wave trains each time, one can establish fully the uncertainty in, say, the 30-minute surge extreme. If this is done for a very large number of sampled sea states, “long-term” extreme response values for very low probability of exceedance levels can be estimated, although this procedure can be expensive. The estimation of a QoI defined as the T -year return period surge motion of

a floating structure is the objective of this study; it is equivalent to assessing as QoI, that surge motion level which is exceeded with probability $1/(T \times 365.25 \times 24 \times 2)$ in 30 minutes. It is this quantity and its uncertainty that we are interested in.

While PCE may be employed for problems dealing with prediction of the long-term extreme response for offshore structures, the “curse of dimensionality” when dealing with all the random variables involved (in describing the sea state parameters as well as in the short-term response process) makes it a challenge to apply in practice [9]. In addition, the appropriate order of the selected polynomial basis functions for the most efficient and accurate surrogate is not known in advance; a portion of this work seeks to investigate the influence of the selected parameters, the polynomial order, and the number of evaluations of the truth system that are needed in developing a PCE surrogate model for studies such as this one.

A discussion of the response for the selected moored floating offshore structure is first presented; next, the PCE-based analysis is outlined and the pertinent QoI for long-term surge motion is defined. The truth system that entails use of Monte Carlo simulation (MCS) is discussed; a comparison of PCE and MCS estimates of the QoI and associated uncertainty is the focus of this work. Consistent with well-established variance-reduction practices employed in practice, to reduce sampling variability in response extreme prediction, biased samples around regions with high H_s values are employed in importance sampling considered with the PCE-based surrogate models (with appropriate

adjustments for bias resulting from the use of the importance sampling distributions). Results confirm the versatility of the PCE-based approach to predict long-term surge motions for the selected moored floating structure subjected to first-order and second-order wave loads.

3.2 Problem Formulation

A single-degree-of-freedom system is employed to describe the surge motion of the selected moored floating structure subjected to first- and second-order wave loads. The governing equation of motion is as follows:

$$M\ddot{u}(t) + 2\zeta\sqrt{KM}\dot{u}(t) + Ku(t) = F_{WF}(t) + F_{LF}(t), \quad (3.1)$$

where $M = 1 \times 10^8$ kg, $\zeta = 0.1$, and $K = 2.8 \times 10^5$ N/m are the mass, damping ratio, and stiffness, respectively [11]. Also, $u(t)$ represents the surge motion at time, t , while $F_{WF}(t)$ represents the first-order wave-frequency forces and $F_{LF}(t)$, the second-order (difference-frequency) forces. These two wave-related force components are defined in the frequency domain (ω) as follows [3]:

$$F^{(1)}(\omega_r) = T^{(1)}(\omega_r)\eta(\omega_r), \quad (3.2)$$

$$F^{(2)}(\omega_r, \omega_s) = T^{(2)}(\omega_r, \omega_s)\eta(\omega_r)\eta(\omega_s), \quad (3.3)$$

where $T^{(1)}$ and $T^{(2)}$ represent the linear transfer function and the quadratic transfer function (QTF), respectively. Note that the QTF is defined here using Newman's approximation [13], where non-diagonal terms of the QTF are approximated by the arithmetic mean of the associated diagonal terms—i.e., $T^{(2)}(\omega_r, \omega_s) = 0.5[T^{(2)}(\omega_r, \omega_r) + T^{(2)}(\omega_s, \omega_s)]$. The surge motion $u(t)$ can

be computed as follows:

$$u(t) = \sum_{r=1}^R H(\omega_r) T^{(1)}(\omega_r) A_r \exp(i\omega_r t) + \sum_{r=1}^R \sum_{\substack{s=1 \\ r \neq s}}^R H(\omega_r - \omega_s) T^{(2)}(\omega_r, \omega_s) A_r A_s^* \exp[i(\omega_r - \omega_s)t], \quad (3.4)$$

where $H(\omega) = (-\omega^2 M + i\omega C + K)^{-1}$ is the frequency response function, and $C = 2\zeta\sqrt{KM}$. Also, $A_r = a_r \exp(i\phi_r)$ is the complex Fourier amplitude for the r th harmonic component (in each simulation, a_r represents a sampled Rayleigh-distributed random amplitude that is defined in terms of the sea state parameters, H_s and T_p , while ϕ_r represent a randomly sampled phase); the asterisk in Eq. 3.4 refers to the complex conjugate. It should be noted that the surge motion of the selected structure is non-Gaussian due to the second-order difference-frequency contribution to this motion; extremes of non-Gaussian processes can be difficult to predict in general. The present study considers non-Gaussian extremes and, as such, offers a relatively tractable but challenging problem to assess the PCE surrogate model development for response extreme prediction.

3.3 Environmental Conditions

Metocean statistical parameters that describe the wave climate are the significant wave height, H_s , and spectral peak period, T_p . In a short-term response simulation, given H_s and T_p , a target power spectral density function, $S_\eta(\omega)$ (where $\eta(t)$ is the sea surface elevation) must be defined; the JONSWAP spec-

trum is selected for $S_\eta(\omega)$ in this study [6].

3.4 Short-Term Extreme Response and QoI

In the short-term simulations of 30-minute duration, the sea surface elevation and response processes are assumed to be stationary for the given H_s and T_p associated with the sea state. The selected wave spectrum, $S_\eta(\omega)$, is discretized into R components of equal frequency interval $\Delta\omega$. A simulated time series for $\eta(t)$ may be generated as:

$$\eta(t) = \sum_{r=1}^R a_r \cos(\omega_r t + \phi_r), \quad (3.5)$$

where a_r are independent random wave amplitudes (Rayleigh distributed with mean-square value equal to $2S_\eta(\omega_r)\Delta\omega$) [22] while ϕ_r are independent random phase angles (uniformly distributed between 0 and 2π). (Note that sometimes a_r is taken deterministically as equal to $\sqrt{2S_\eta(\omega_r)\Delta\omega}$, relying on a valid assumption that $\eta(t)$ will be asymptotically Gaussian for large R .) It is convenient to define a $2R$ -dimensional vector, $\Theta = [a_1 \ a_2 \ \dots \ a_R \ \phi_1 \ \phi_2 \ \dots \ \phi_R]^T$ comprised of the R independent random amplitudes and phase angles that introduce short-term uncertainty in the response, given H_s and T_p . The present study recognizes that long-term uncertainty in the 30-minute extreme of $u(t)$ results both from uncertainty in H_s and T_p as well as from the short-term uncertainty in Θ .

Given the simulated response process defined over duration, T , for a given pair of H_s and T_p values and the simulated stochastic process, $u(t)$, the

extreme response, Z , is defined as follows [11]:

$$Z = \max\{u(t); 0 \leq t \leq T\}. \quad (3.6)$$

Note that Z depends on H_s , T_p , and Θ —i.e., $Z \equiv Z(H_s, T_p, \Theta)$. For notational convenience, let us define the complementary cumulative distribution function (or probability of exceedance) as

$$P(Z > z) = G_Z(z). \quad (3.7)$$

Thus, for a selected sea state and associated H_s and T_p values, $G_{Z|H_s, T_p}(z)$ denotes the conditional probability of exceedance of level z by the short-term extreme value of $u(t)$ in duration, T . We shall see that it is $G_Z(z)$, which describes the unconditional probability of exceedance of level z , obtained by considering all H_s and T_p values that we must establish to fully define our QoI.

3.5 Long-Term Extreme Response

Long-term statistics of H_s and T_p are described by the joint probability density function (jpdf), namely $f_{H_s, T_p}(h, t)$; this jpdf is available for the site of interest in the North Sea [8, 7]. It is given as follows:

$$f_{H_s, T_p}(h, t) = f_{H_s}(h)f_{T_p|H_s}(t|h), \quad (3.8)$$

$$f_{H_s}(h) = \frac{1}{\sqrt{2\pi}\zeta_{H_s}h} \exp\left[-\frac{(\ln h - \lambda_{H_s})^2}{2\zeta_{H_s}^2}\right], \quad \text{if } h \leq \hat{\eta}, \quad (3.9)$$

$$= \frac{\gamma}{\rho} \left(\frac{h}{\rho}\right)^{\gamma-1} \exp\left[-\left(\frac{h}{\rho}\right)^\gamma\right], \quad \text{if } h > \hat{\eta}, \quad (3.10)$$

$$f_{T_p|H_s}(t|h) = \frac{1}{\sqrt{2\pi}\zeta_{T_p|H_s}(h)t} \exp\left[-\frac{(\ln t - \lambda_{T_p|H_s}(h))^2}{2\{\zeta_{T_p|H_s}(h)\}^2}\right], \quad (3.11)$$

where $\zeta_{H_s} = 0.6565$, $\lambda_{H_s} = 0.77$, $\gamma = 1.503$, $\rho = 2.691\text{m}$, $\hat{\eta} = 2.90 \text{ m}$, $\zeta_{T_p|H_s}(h) = (0.005 + 0.120 \exp(-0.455h))^{1/2}$, $\lambda_{T_p|H_s}(h) = 1.134 + 0.892h^{0.225}$. Considering all sea states, the unconditional probability of exceedance $G_Z(z)$ is given as follows:

$$G_Z(z) = \iint G_{Z|H_s, T_p}(z) f_{H_s, T_p}(h, t) dh dt. \quad (3.12)$$

Note that $G_Z(z)$ in Eq. 3.12 may be evaluated for any z if Monte Carlo simulation is applied in the “forward” way. Efficient alternatives to Monte Carlo simulation exist; one such uses “inverse” reliability approaches [16, 17, 1, 12] that focus on the metocean random variables alone or optionally account for response variability. However, in those approaches, only z values that ensure a target value of $G_Z(z)$ are derived; moreover, these methods are approximate. In the present study, an alternative approach is proposed that makes use of polynomial chaos expansion to derive a surrogate model for $G_Z(z)$.

3.6 Polynomial Chaos Expansion

A first step in PCE is to express the QoI as a summation or expansion of orthogonal polynomials involving all of the selected uncertain model parameters, \mathbf{X} , following an Askey scheme [2]. In the present study, these model parameters include H_s and T_p —thus, $\mathbf{X} = [H_s, T_p]^T$. Appropriate orthogonal polynomials are selected for the expansion according to the probability distributions of auxiliary random variables to which \mathbf{X} must be mapped [20, 9]. Because the appropriate order is not known in advance for engineering applications in general, a convergence study is necessary. Hermite polynomials, $H_i(\cdot)$

are adopted in the present study; thus, \mathbf{X} is mapped to a standard normal random variable vector, \mathbf{Q} . After establishing the polynomial basis functions and assuming that all the physical variables in \mathbf{X} have finite variance, our QoI, Z , may be expressed as a series involving these basis functions as:

$$Z(\mathbf{X}) = \sum_{i=0}^{\infty} c_i H_i(\mathbf{Q}) = \sum_{i=0}^{\infty} c_i H_i(\xi(\mathbf{X})), \quad (3.13)$$

where $\xi(\cdot)$ are probabilistically mapped functions of the input random variables (\mathbf{X}), c_i are coefficients to be estimated, $H_i(\cdot)$ represents the i th multivariate orthogonal Hermite polynomial function expressed in terms of the input variables, and $Z(\mathbf{X})$ represents the QoI. Again, $\xi(\cdot)$ describes the mapping from the physical variable space, \mathbf{X} , of the model parameters to the independent standard normal space, \mathbf{Q} (mappings using, for example, Nataf, Rosenblatt, or copula transformation models that describe the dependence structure among variables in different ways may be employed—see, for example, Manuel et al [12]). In the present study, given the jpdf for H_s and T_p , the mapping that describes ξ : $\mathbf{Q} \leftrightarrow \mathbf{X}$ is defined using the Rosenblatt transformation as follows:

$$\Phi(q_1) = F_{H_s}(h), \quad (3.14)$$

$$\Phi(q_2) = F_{T_p|H_s}(t|h), \quad (3.15)$$

where $\Phi(\cdot)$ represent the univariate cumulative distribution function of a standard normal variable, while $F_{H_s}(\cdot)$ and $F_{T_p|H_s}(\cdot)$ represent, respectively, the cumulative distribution functions of the input variables while q_1 and q_2 represent standard normal variables corresponding to H_s and T_p .

The i th multivariate orthogonal Hermite polynomial function in Eq. 3.13 is constructed using the product of associated univariate Hermite polynomials as follows:

$$H_i(\mathbf{Q}) = \prod_{l=1}^{N_X} \bar{H}_{\alpha_l}(Q_l), \quad (3.16)$$

where $\bar{H}_{\alpha_l}(Q_l)$ is the l th univariate Hermite polynomial, α_l is the appropriate index of the univariate polynomial order for the i th multivariate polynomial function [21], and N_X is the number of random physical variables ($N_X = 2$ in this study).

Orthogonality of the selected basis functions implies that:

$$\mathbb{E}[H_i H_j] = \delta_{ij} \mathbb{E}[H_i^2], \quad (3.17)$$

where δ_{ij} is the Kronecker delta, equal to unity when $i = j$ and zero otherwise, and $\mathbb{E}[\cdot]$ is the expectation operator. Also, $\mathbb{E}[H_i^2]$ is available in closed form for all i .

A truncated PCE for Z that involves polynomials up to order p can be represented as:

$$Z(\mathbf{X}) \approx Z^{\text{PCE}}(\mathbf{X}) = \sum_{i=0}^{N-1} c_i H_i(\xi(\mathbf{X})), \quad (3.18)$$

where N denotes the number of unknown PCE coefficients in polynomials of order not exceeding p . This number, N , is computed using combinatorics as follows:

$$N = \binom{N_X + p}{N_X}. \quad (3.19)$$

The next step in PCE is to estimate the coefficients of the orthogonal polynomials. Several methods for doing so have been suggested; they include spectral projection, stochastic collocation, and linear regression. Spectral projection has been employed on a very similar problem to that addressed in the present study; it has been applied to predict the long-term response of a point absorber wave energy converter [14]. Spectral projection has also been employed in developing a PCE surrogate for assessing the fatigue damage resulting from vortex-induced vibration of a riser using a distributed wake oscillator model [10]. In the present study, linear regression is employed; accordingly, the PCE coefficients are computed by minimizing the sum of the squared residuals between the truncated PCE and the truth system, $Z(\mathbf{X})$. The coefficients can be then be obtained as follows:

$$\mathbf{c} = \arg \min_{c_i} \sum_{m=1}^{N_E} \left[Z(\mathbf{X}^{(m)}) - \sum_{i=0}^{N-1} c_i H_i(\xi(\mathbf{X}^{(m)})) \right]^2, \quad (3.20)$$

where N_E is the number of simulations performed with the truth system as part of the linear regression.

Note that a procedure for constructing a surrogate model for Z using PCE is outlined above but it does not explicitly include nor account for the influence of short-term uncertainty arising from Θ . We recognize this limitation of our PCE-based QoI and denote it as $Z^{\text{PCE}}(\mathbf{X}) \equiv \hat{Z}$, recalling that, as defined, \mathbf{X} does not contain Θ , i.e., $\mathbf{X} = [H_s, T_p]^T$. The introduction of short-term uncertainty in the simulated response process, $u(t)$ (and its extreme value in time, T), arising from Θ , must be addressed in careful estimation of \mathbf{c} in

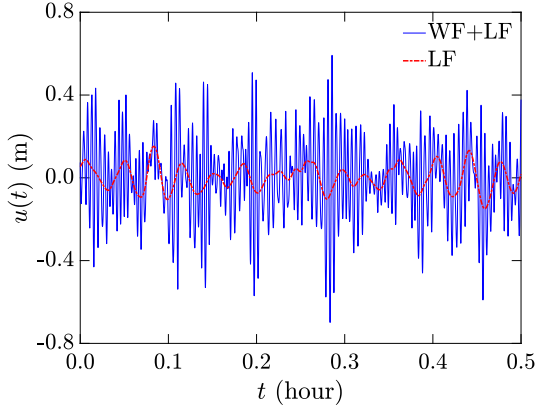


Figure 3.1: A sample realization of a 30-minute time series of surge motion for the selected moored floating structure for a sea state represented by $H_s = 3.07$ m and $T_p = 13.79$ s

Eq. 3.20 that needs to thus include different realizations of Θ for each \mathbf{X} . This is explained next.

3.7 Monte Carlo Simulations and PCE-based Surrogate Models

Now, $G_Z(z)$ must be estimated using Monte Carlo Simulation (MCS) as well as PCE. The MCS estimate is obtained as follows:

$$G_Z^{\text{MC}}(z) = \frac{1}{N_T} \sum_{k=1}^{N_T} I(Z > z | H_s^{(k)}, T_p^{(k)}, \Theta^{(k)}), \quad (3.21)$$

where N_T represents the number of MCS samples drawn for (H_s, T_p, Θ) , $I(\mathcal{F})$ is the indicator function which is equal to either 1 or 0 depending on whether \mathcal{F} is true or not and $H_s^{(k)}$, $T_p^{(k)}$, $\Theta^{(k)}$ represents drawn samples of all random variables in the k th trial. Note that T is set to 30 min (in Eq. 3.6) and N_T is set to 100,000 in the MCS computations. An illustrative realization of a

30-minute time series of the surge motion, $u(t)$, is presented in Fig. 3.1. Also, the corresponding PCE estimate is given as follows:

$$G_{\hat{Z}}^{\text{PCE}}(z) = \frac{1}{N_T} \sum_{k=1}^{N_T} I(\hat{Z} > z | H_s^{(k)}, T_p^{(k)}), \quad (3.22)$$

where $H_s^{(k)}$ and $T_p^{(k)}$ are fed into the surrogate \bar{Z} in the associated \mathbf{Q} space; thus, the mapping (Eqs. 3.14 and 3.15) must be performed. Note that, for PCE, a choice for the polynomial order (p) and for the number of the simulations (N_E) of the truth system is needed. Sudret [19] has suggested that, in general, p must be at least 3 in order to achieve satisfactory accuracy for events associated with probabilities on the order of 10^{-4} . Also, according to Blatman [4], we must have $N_E \leq 3N$ where N represents the number of PCE coefficients to be estimated. To start, one may investigate $p = 3$ and select N_E equal to $3N$ (i.e., $N_E = 30$) to attempt to accurately approximate $G_Z(z)$ at probability levels around 10^{-4} . However, when compared to MCS, it is expected that such a PCE scheme will likely not work. The reason is that, while the PCE approach accounts for uncertainty introduced via \mathbf{X} , the short-term response uncertainty (in Θ) is not considered; as a result, $Z^{\text{PCE}}(\mathbf{X})$ or \hat{Z} derived using a PCE surrogate will be highly variable depending on the actual samples of Θ . Thus, it would not be adequate to use $p = 3$ and $N_E = 3N = 30$ in order to have reasonable accuracy.

From preceding discussions, it is expected that short-term uncertainties due to the irregular wave train (resulting from random amplitudes and phases for each wave frequency component) need to be accounted for in the

PCE models so as to accurately predict the long-term extreme response of the moored structure. Thus, a sample for regression in Eq. 3.20 of size greater than $N_E = 3N = 30$ is needed. Accordingly, we investigate next whether $N_E = 10N = 100$ will work for $p = 3$. Figure 3.2 shows that such a PCE scheme performs well; it can be seen that the 10 MCS-based exceedance probability curves exhibit slightly lower variability than predictions from 10 PCE sets but there is no bias in the PCE predictions. It is important to point out that these curves required 10^6 simulations (10×10^5) for MCS but only 10^3 simulations (10×100) for PCE; this represents a factor of 1,000 advantage of PCE over MCS.

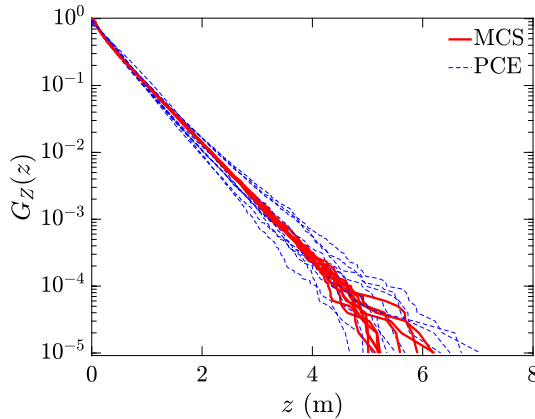


Figure 3.2: Comparison of probability of exceedance (G_Z) estimates: MCS (solid) versus PCE (dashed) with $p = 3$ and $N_E = 100$: comparisons are based on 10 sets of MCS and PCE computations

To investigate the PCE models with different N_E selections, $G_{\hat{Z}}^{\text{PCE}}(z)$, i.e., with $N_E = 30, 70, 90, 100$ are computed; probability levels, $G_Z = 10^{-3}$, 10^{-4} , 10^{-5} , are selected for comparison. In Fig. 3.3, 10 sets of MCS and PCE

estimates of G_Z at the three different probability levels are shown. It is seen that the G_Z estimates PCE with $N_E = 10N = 100$ perform better than the others at all three probability levels; with that choice, the range in values of z at each G_Z level are smallest.

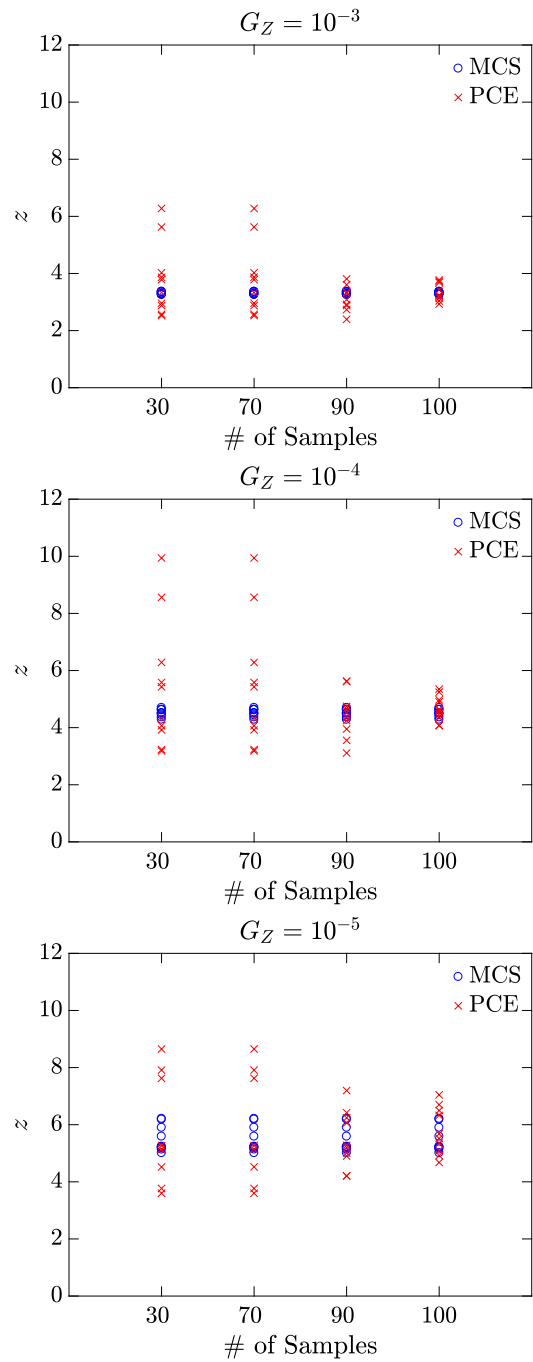


Figure 3.3: Estimation of G_Z at three levels, 10^{-3} , 10^{-4} , and 10^{-5} , using 10 sets of PCE with different N_E values; comparison is made with 10 sets of MCS

To increase PCE accuracy, the choice of $p = 4$ (higher polynomial order) is investigated while still keeping $N_E = 10N$. Since N depends on p (Eq. 3.19), the value of N_E for $p = 4$ increases from 100 to 150. Figure 3.4 shows that the increase in PCE polynomial order from 3 to 4 leads to very large variability in predicted extremes compared to MCS. Note that a few PCE-based curves indicate great discrepancy from the MCS estimates. These results suggests that an increase in polynomial order, p , does not guarantee improved accuracy in PCE-based prediction. Overfitting to the sampled data through regression during construction of the PCE model can lead to problems in extreme response prediction. To highlight such overfitting in predictions, Fig. 3.5 shows how an increase in polynomial order, p , to 6 (which requires estimation of 28 PCE coefficients) leads to significant discrepancies relative to MCS predictions, especially at lower exceedance probability levels, compared to the lower-order PCE polynomial choice seen in Fig. 3.2.

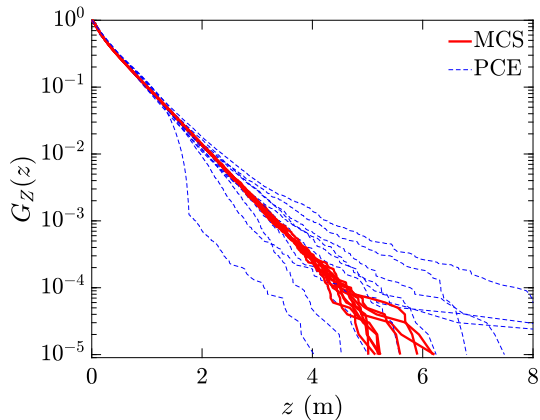


Figure 3.4: Comparison of probability of exceedance (G_Z) estimates: MCS (solid) versus PCE (dashed) with $p = 4$ and $N_E = 150$: comparisons are based on 10 sets of MCS and PCE computations

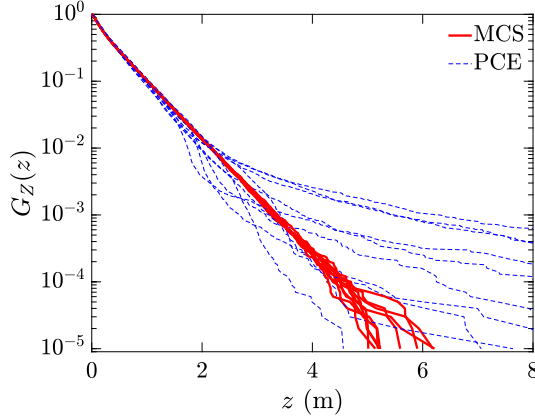


Figure 3.5: Comparison of probability of exceedance (G_Z) estimates: MCS (solid) versus PCE (dashed) with $p = 6$ and $N_E = 280$: comparisons are based on 10 sets of MCS and PCE computations

We investigate next the accuracy in PCE prediction of the short-term extreme response due to irregular waves for selected sea states (i.e., H_s , T_p pairs). Recall that the long-term extreme response probability of exceedance (G_Z in Eq. 3.12) results theoretically from integration of the short-term probability distribution $G_{Z|H_s, T_p}$ over all sea states. Hence, it is not unreasonable that inaccuracy in G_Z prediction based on the PCE model may result from deficient approximation of the short-term extreme response, Z , at some (H_s , T_p) values. For illustration purposes, the selected samples of H_s - T_p pairs for MCS (Eq. 3.21) and PCE (Eq. 3.22) are presented in Figs. 3.6 and 3.7, respectively. In these figures, each dot represents a drawn sample of H_s and T_p ; the colors of these dots go from blue to red as Z increases. While the number of drawn samples is a hundred fold larger for MCS versus PCE, differences in the relative density of drawn samples, particularly in high H_s and high T_p

regions, leading to fewer data from these regions used in the PCE regression may explain the variability in the PCE extreme response predictions as well as in deviations relative to MCS.

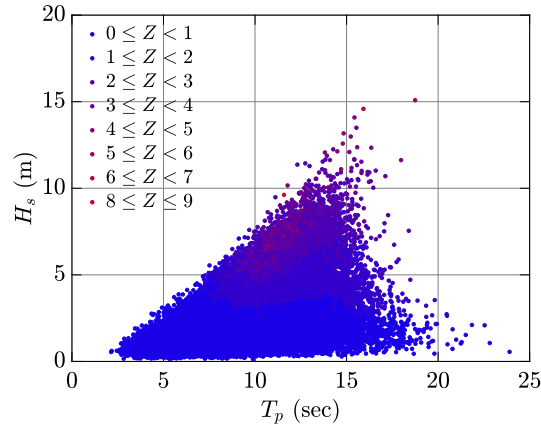


Figure 3.6: A subset of 100,000 sampled H_s and T_p values used in MCS

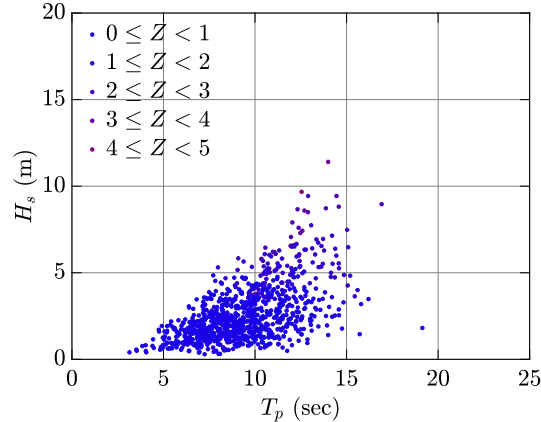


Figure 3.7: A subset of 1,000 sampled H_s and T_p values used to construct PCE surrogate models (10 sets \times 100 samples for each PCE model)

To further investigate the variability in short-term extreme response prediction for specific sea states, Table 3.1 shows comparisons of Z estimates

Table 3.1: Comparisons of short-term Z values in meters, predicted by the truth system (MCS) and by using 10 PCE surrogate models ($p = 3, N_E = 100$) for selected H_s - T_p pairs

H_s (m)	T_p (s)	Truth System
0.73	7.14	0.034
2.16	8.98	0.250
5.58	11.56	1.340

PCE1	PCE2	PCE3	PCE4	PCE5
0.041	0.036	0.011	-0.012	0.076
0.232	0.266	0.285	0.271	0.238
1.220	1.216	1.317	1.419	1.215

PCE6	PCE7	PCE8	PCE9	PCE10	Mean
0.079	0.047	-0.072	0.026	0.025	0.026
0.234	0.244	0.294	0.282	0.262	0.261
1.246	1.347	1.495	1.264	1.374	1.311

(i.e., the 30-minute surge motion extreme) resulting from ten PCE models evaluated for three H_s - T_p pairs. The H_s values selected correspond to 0.1, 0.5, and 0.9 non-exceedance marginal quantiles of H_s ; associated T_p values are selected as conditional median values for these three H_s values. For the truth system, the short-term extreme, Z , for each H_s - T_p pair is computed using Eq. 3.6. Note that Z for the truth system for each of the three pairs is averaged from 100 different realizations of random amplitudes and phases. It is seen from the table that, for the three selected pairs (sea states), the 10 PCE models exhibit some degree of variability while their mean values are fairly close to the truth system (MCS) estimates.

3.8 MCS and PCE with Important Sampling

For variance reduction, importance sampling, if employed, can make use of biased samples to estimate G_Z for desired target probability levels of interest (e.g., $G_Z = 10^{-4}$ or 10^{-5}), while keeping the eventual estimation unbiased by using weights to compensate for the biased samples (the weights are proportional to the ratio of the true jpdf to the “importance sampling” biased jpdf). It should be noted that the biased samples need to be chosen appropriately; otherwise estimation can be worsened. The estimator of G_Z by MCS with importance sampling can be given as follows:

$$G_Z^{\text{MCS-IS}}(z) = \frac{1}{N_T} \sum_{k=1}^{N_T} I(Z > z | H_s^{(k)}, T_p^{(k)}, \Theta^{(k)}) \frac{f_{H_s, T_p, \Theta}(H_s^{(k)}, T_p^{(k)}, a_1^{(k)}, \dots, a_R^{(k)}, \theta_1^{(k)}, \dots, \theta_R^{(k)})}{f_{H_s, T_p, \Theta}^*(H_s^{(k)}, T_p^{(k)}, a_1^{(k)}, \dots, a_R^{(k)}, \theta_1^{(k)}, \dots, \theta_R^{(k)})}, \quad (3.23)$$

where $f_{H_s, T_p, \Theta}$ and $f_{H_s, T_p, \Theta}^*$ are the original jpdf and the importance sampling jpdf of H_s, T_p, Θ , respectively. The importance sampling jpdf $f_{H_s, T_p, \Theta}^*$ is to be selected; however, $f_{H_s, T_p, \Theta}^*$ involves $2R + 2$ random variables, which are not easy to manipulate when R is large. Here, we limit the importance sampling to only two variables, H_s and T_p , to reduce the sampling variability resulted from long-term uncertainty. As a consequence, Eq. 3.23 can be simplified as follows:

$$G_Z^{\text{MCS-IS}}(z) = \frac{1}{N_T} \sum_{k=1}^{N_T} I(Z > z | H_s^{(k)}, T_p^{(k)}, \Theta^{(k)}) \frac{f_{H_s, T_p}(H_s^{(k)}, T_p^{(k)})}{f_{H_s, T_p}^*(H_s^{(k)}, T_p^{(k)})}, \quad (3.24)$$

where f_{H_s, T_p}^* is the importance sampling jpdf of H_s and T_p .

Furthermore, by changing only the marginal distribution of H_s in f_{H_s, T_p}^* , i.e., by setting $f_{H_s, T_p}^* = f_{H_s}^* f_{T_p|H_s}$ (while ensuring that the volume integral of f_{H_s, T_p}^* over H_s and T_p equals unity), Eq. 3.24 can be reduced to the following:

$$G_Z^{\text{MCS-IS}}(z) = \frac{1}{N_T} \sum_{k=1}^{N_T} I(Z > z | H_s^{(k)}, T_p^{(k)}, \Theta^{(k)}) \frac{f_{H_s}(H_s^{(k)})}{f_{H_s}^*(H_s^{(k)})}, \quad (3.25)$$

where $f_{H_s}^*$ is the marginal importance sampling density for H_s . A lognormal marginal probability density function (pdf) is selected as follows:

$$f_{H_s}^*(h) = \frac{1}{\sqrt{2\pi}\zeta_{H_s} h} \exp \left[-\frac{(\ln h - \lambda'_{H_s})^2}{2\zeta_{H_s}^2} \right], \quad \text{for } h > 0, \quad (3.26)$$

where λ'_{H_s} is set to 1.0482 (note that $\lambda_{H_s} = 0.77$). The value of λ'_{H_s} is chosen so that the mean value of H_s based on $f_{H_s}^*$ is equal to the mean value based on f_{H_s} plus 1 meter; that is:

$$\int h f_{H_s}(h) dh + 1 = \int h f_{H_s}^*(h) dh. \quad (3.27)$$

Note that the left-hand side of Eq. 3.27 is evaluated numerically (and is equal to 3.54 m) while the right-hand side is given in closed form, i.e., it is equal to $\exp \left(\lambda'_{H_s} + \frac{\zeta_{H_s}^2}{2} \right)$.

Summary plots (marginal distributions, weight ratio, contours of f_{H_s, T_p} and f_{H_s, T_p}^*) for the importance sampling density selection are presented in Fig. 3.8. As intended, $f_{H_s}^*$ has shifted probability mass to right so as to have a higher mean value; this is also evident in the difference in the two jpdf contours for H_s and T_p . The weight ratio (adjustment for bias in the importance sampling) get lower as higher h values are sampled; weights below unity enable

us to estimate G_Z values below $1/N_T$ (while MCS estimates G_Z only go down to $1/N_T$).

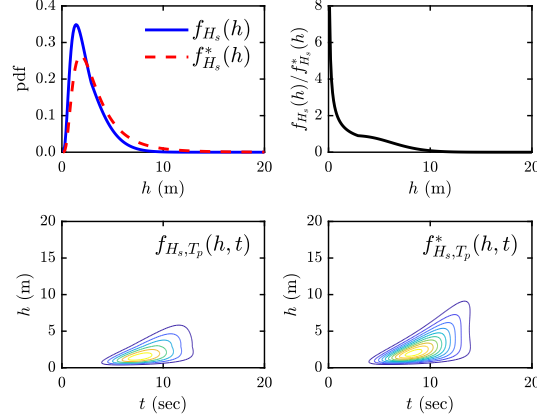


Figure 3.8: Selection of importance sampling density function for MCS: (top left) marginal distributions of $f_{H_s}(h)$ and $f_{H_s}^*(h)$, (top right) weight ratio, (bottom left) contours of $f_{H_s,T_p}(h,t)$, (bottom right) contours of $f_{H_s,T_p}^*(h,t)$

A comparison of 10 sets of G_Z^{MCS} and $G_Z^{\text{MCS-IS}}$ is presented in Fig. 3.9; N_T is set to 10,000 for each set of conventional MCS and importance sampling-based MCS. It is seen that MCS-IS can lead to unbiased estimates of G_Z and also have reduced variance, when compared against conventional MCS. Due to the weights that are applied, $G_Z^{\text{MCS-IS}}$ estimates below a 10^{-4} probability level can also be obtained. To assess the accuracy of MCS-IS at $G_Z(z) = 10^{-4}$ levels and lower, MCS for $N_T = 100,000$ is additionally performed. Figure 3.10 shows that MCS-IS estimates for $10^{-5} < G_Z(z) < 10^{-4}$ compare well against MCS. Note that different N_T values are used for MCS and MCS-IS in Fig. 3.10. MCS-IS with $N_T = 100,000$ shows lower variance than MCS with the same N_T , as shown in Fig. 3.11.

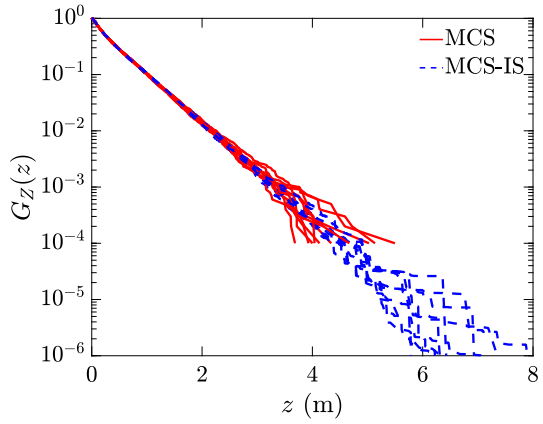


Figure 3.9: Comparison of probability of exceedance (G_Z) estimates by conventional MCS and importance sampling-based MCS: $N_T = 10,000$ for both methods

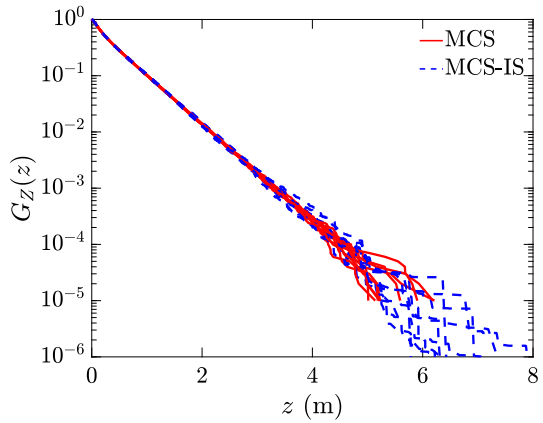


Figure 3.10: Comparison of probability of exceedance (G_Z) estimates by conventional MCS and importance sampling-based MCS: $N_T = 100,000$ for MCS and $N_T = 10,000$ for MCS-IS

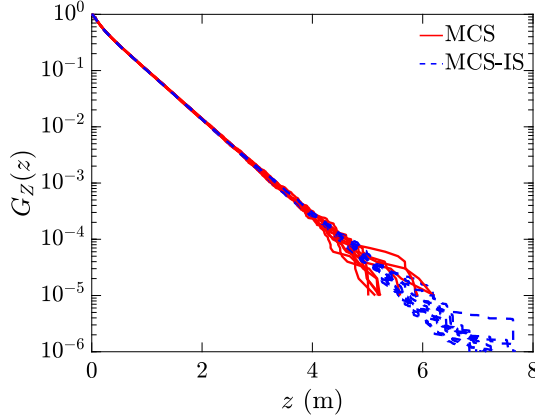


Figure 3.11: Comparison of probability of exceedance (G_Z) estimates by conventional MCS and importance sampling-based MCS: $N_T = 100,000$ for both methods

Finally, we consider importance sampling but now with the PCE surrogate models. The importance sampling can be applied to MCS based on the PCE surrogate models, not the truth system. Because the PCE surrogates are constructed in an independent standard normal variable space (\mathbf{Q}), selection of an importance sampling density function is to be considered with the standard normal random variables. In the same manner as with the choice of a importance sampling density function for MCS-IS, the marginal distribution for Q_1 , corresponding to H_s , is the target to change for importance sampling. The importance sampling-based PCE estimate for G_Z is given as follows:

$$G_{\hat{Z}}^{\text{PCE-IS}}(z) = \frac{1}{N_T} \sum_{k=1}^{N_T} I(\hat{Z} > z | H_s^{(k)}, T_p^{(k)}) \frac{\varphi(Q_1^{(k)})}{\varphi^*(Q_1^{(k)})}, \quad (3.28)$$

where $\varphi(\cdot)$ is the univariate standard normal pdf, $Q_1^{(k)}$ is the k th drawn sample from φ^* , the importance sampling density function of Q_1 . Note that the map-

pling represented by Eq. 3.14 between Q_1 and H_s is needed in the estimation.

The selected importance sampling density function is a normal pdf with variance $\sigma_{Q_1}^2 = 1$ but with mean value, μ_{Q_1} , set to 0.77 which is equivalent to the importance sampling-based mean value, $H_s = 3.54$ m as was considered before, i.e., $F_{H_s}^{-1}(\Phi(0.77)) = 3.54$ m.

Summary plots of the importance sampling density function for PCE are presented in Fig. 3.12. In the same fashion as for Fig. 3.8, it is seen that $f_{Q_1}^*$ is selected to have a higher mean value than that of f_{Q_1} . Also, note that, because the PCE sampling is carried out in \mathbf{Q} space, the marginal distribution, $f_{Q_1}^*$, has the classical shape of an univariate normal distribution with a positive shift in the Q_1 direction.

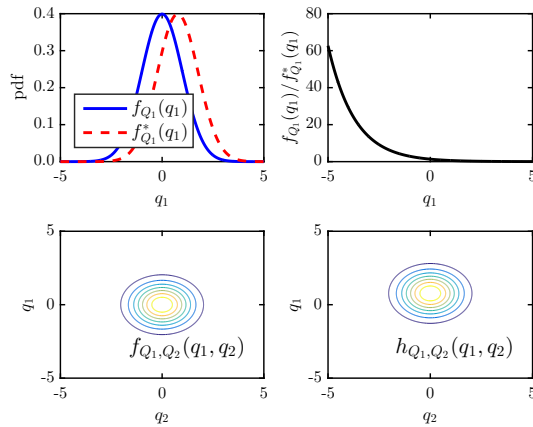


Figure 3.12: Selection of importance sampling density function for the PCE surrogate: (top left) marginal distributions of $f_{Q_1}(q_1)$ and $f_{Q_1}^*(q_1)$, (top right) weight ratio, (bottom left) contours of $f_{Q_1,Q_2}(q_1, q_2)$, (bottom right) contours of $f_{Q_1,Q_2}^*(q_1, q_2)$

A comparison of estimations based on MCS, PCE, and PCE with im-

portance sampling is presented in Fig. 3.13; N_T is set to 100,000 and, $p = 3$ and $N_E = 100$ are used for the PCE surrogate. It is seen that PCE-IS estimates of G_Z have no bias relative to MCS and have very low small sampling variability at the lowest probability levels.

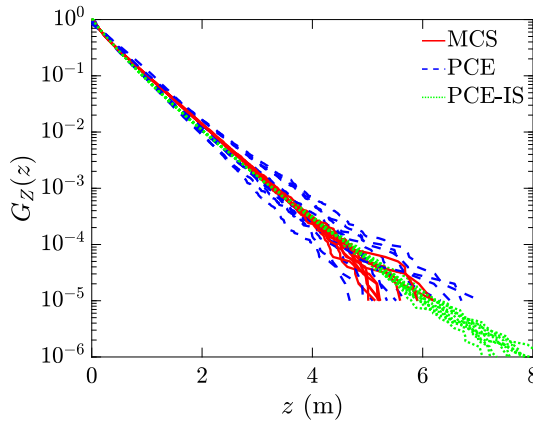


Figure 3.13: Comparison of probability of exceedance (G_Z) estimates based on conventional MCS, PCE, and importance sampling-based PCE (PCE-IS); $N_T = 100,000$ for all the methods and $p = 3$ and $N_E = 100$ for the PCE surrogate

3.9 Conclusions

In this study, prediction of the long-term extreme response (surge motion) of a simple moored floating offshore structure is carried out using polynomial chaos expansion (PCE) with model parameters, H_s and T_p , considered as uncertain. This offshore structure, subjected to first-order and second-order wave loads, is considered in numerical studies with explicit treatment of these two uncertain parameters. Variability in the short-term response resulting from random amplitudes and phases in wave harmonic components is accounted for by con-

sidering multiple suites of data in linear regression, which is used to estimate PCE coefficients. Different orders of polynomials (p) in the PCE scheme are considered; caveats regarding overfitting in estimation of the short-term response are discussed. Both short- and long-term response extreme prediction are reasonably accurate when a PCE model with $p = 3$ and $N_E = 10N$ is used and comparison is made against MCS predictions. To reduce sampling variability resulting from H_s and T_p , an importance sampling enhancement is applied to the PCE scheme. It is expected that the demonstrated efficiency and accuracy of the PCE-based long-term extreme response prediction for this simple moored offshore floating structure can be extended to other structures; the benefit resulting from significantly less computation is obvious. Optimal PCE schemes with increased accuracy are also being explored, building from lessons learned in this pilot study.

Bibliography

- [1] Puneet Agarwal and Lance Manuel. On the modeling of nonlinear waves for prediction of long-term offshore wind turbine loads. *Journal of Offshore Mechanics and Arctic Engineering*, 131(4), 2009.
- [2] George E Andrews and Richard Askey. Classical orthogonal polynomials. In *Polynômes orthogonaux et applications*, pages 36–62. Springer, 1985.
- [3] Nigel DP Barltrop. *Floating structures: a guide for design and analysis*, volume 1. Oilfield Publications Incorporated, 1998.
- [4] Géraud Blatman and Bruno Sudret. An adaptive algorithm to build up sparse polynomial chaos expansions for stochastic finite element analysis. *Probabilistic Engineering Mechanics*, 25(2):183–197, 2010.
- [5] Roger G Ghanem and Pol D Spanos. *Stochastic finite elements: a spectral approach*. Courier Corporation, 2003.
- [6] Klaus Hasselmann. Measurements of wind wave growth and swell decay during the joint north sea wave project (JONSWAP). *Deutches Hydrographisches Institut*, 8:95, 1973.
- [7] Sverre Haver. On the prediction of extreme wave crest heights. *International Workshop on Wave Hindcasting and Forecasting*, 2002.

- [8] Sverre Haver and Kjell A Nyhus. A wave climate description for long term response calculations. *OMAE. International Symposium*, 4:27–34, 1986.
- [9] Chao Hu and Byeng D Youn. Adaptive-sparse polynomial chaos expansion for reliability analysis and design of complex engineering systems. *Structural and Multidisciplinary Optimization*, 43(3):419–442, 2011.
- [10] HyeongUk Lim, Lance Manuel, Ying Min Low, and Narakorn Srinil. Uncertainty quantification of riser fatigue damage due to VIV using a distributed wake oscillator model. *ASME. International Conference on Ocean, Offshore and Arctic Engineering*, 2017.
- [11] Ying Min Low and Xiaoxu Huang. Long-term extreme response analysis of offshore structures by combining importance sampling with subset simulation. *Structural Safety*, 69:79–95, 2017.
- [12] Lance Manuel, Phong TT Nguyen, Jarred Canning, Ryan G Coe, Aubrey C Eckert-Gallup, and Nevin Martin. Alternative approaches to develop environmental contours from metocean data. *Journal of Ocean Engineering and Marine Energy*, 4(4):293–310, Nov 2018.
- [13] John N Newman. Second-order, slowly-varying forces on vessels in irregular waves. *Marine Vehicles*, pages 182–186, 1974.
- [14] Phong TT Nguyen, Lance Manuel, and Ryan G Coe. On the development of an efficient surrogate model for predicting long-term extreme loads

- on a wave energy converter. *Journal of Offshore Mechanics and Arctic Engineering*, 141(6):061103, 2019.
- [15] Sergey Oladyshkin and Wolfgang Nowak. Data-driven uncertainty quantification using the arbitrary polynomial chaos expansion. *Reliability Engineering & System Safety*, 106:179–190, 2012.
- [16] Korn Saranyasoontorn and Lance Manuel. A comparison of wind turbine design loads in different environments using inverse reliability techniques. *Journal of Solar Energy Engineering*, 126(4):1060–1068, 2004.
- [17] Korn Saranyasoontorn and Lance Manuel. On assessing the accuracy of offshore wind turbine reliability-based design loads from the environmental contour method. *International Journal of Offshore and Polar Engineering*, 15(2):132–140, 2005.
- [18] Christian Soize and Roger Ghanem. Physical systems with random uncertainties: chaos representations with arbitrary probability measure. *SIAM Journal on Scientific Computing*, 26(2):395–410, 2004.
- [19] Bruno Sudret. Uncertainty propagation and sensitivity analysis in mechanical models—contributions to structural reliability and stochastic spectral methods. *Habilitationa diriger des recherches, Université Blaise Pascal, Clermont-Ferrand, France*, 2007.
- [20] Bruno Sudret. Meta-models for structural reliability and uncertainty quantification. *arXiv preprint arXiv:1203.2062*, 2012.

- [21] Bruno Sudret, Marc Berveiller, and Maurice Lemaire. A stochastic finite element procedure for moment and reliability analysis. *European Journal of Computational Mechanics/Revue Européenne de Mécanique Numérique*, 15(7-8):825–866, 2006.
- [22] Det Norske Veritas. *Environmental conditions and environmental loads*. Recommended Practice, DNV-RP-C205, Norway, 2010.

Paper III:

Chapter 4

Distribution-Free Polynomial Chaos Expansion Surrogate Models for Efficient Structural Reliability Analysis

Abstract

In complex stochastic high-dimensional reliability studies, polynomial chaos expansion (PCE) has been widely used to build surrogate models in lieu of prohibitively expensive Monte Carlo simulation (MCS). PCE relies on parametric distributions for associated variables and appropriate basis functions. However, incomplete or imperfect information on the stochastic variables can limit its use; accepted parametric forms for variable distributions, for instance, may not be justified when variables display multimodal character or mixed discrete-continuous support. Also, the dependency structure among the random variables may be complex, which can make probabilistic mapping or transformation to independent variables needed for PCE cumbersome. Non-linearities in such transformations can affect the accuracy of PCE surrogate models and lead to slower convergence relative to “truth” system computations of desired QoIs (quantities of interest). To address these challenges, a distribution-free PCE approach is proposed. We compute joint raw moments of underlying random input variables for Gram-Schmidt orthogonalization in

developing surrogate models. Using illustrative examples, we demonstrate the proposed approach as an efficient and accurate surrogate model-building alternative to traditional PCE.

4.1 Introduction

Evaluation of the reliability and safety of structural systems typically involves computation that must provide accurate prediction of the probability of failure or of some undesired load/demand level. A variety of methods for assessing structural reliability have been developed [18] and can be categorized as geometrical approximations [23, 11], efficient sampling methods [2, 4, 20], moment methods [31, 30], and surrogate modeling methods [24, 5].

Surrogate modeling has gained interest recently due to its efficiency and accuracy in response prediction at low probability levels. Surrogate modeling aims to obtain an appropriate analytical function that can be used instead of the truth model.

It is often the case that performance or limit state functions may be expressed only in implicit manner and can involve the use of computationally expensive simulation models (e.g., finite element analysis or computational fluid dynamics) that, in turn, employ uncertain input parameters. Then, one can benefit from the use of “surrogate” functions (models) that serve as approximations for the “truth” performance or limit state functions. Of course, these surrogate limit state functions are validated only if the evaluations of the developed surrogate limit state functions and associated uncertainty are

reasonably similar to those of the truth limit state function.

Polynomial chaos expansion (PCE) offers a robust framework for the development of surrogate models [10]. A feature of PCE-based surrogates is that the QoIs are expressed as a series of orthogonal polynomial basis functions defined in terms of the input random variables. It has been suggested that the QoIs defined using PCE can be thought of as mathematically optimal representations of model outputs associated with uncertain input variables or parameters [29, 6]. PCE has been widely used in structural reliability [7] and several variants of it have been developed [3, 19].

However, incomplete or imperfect information on the underlying stochastic variables can limit the use of PCE. Also, traditional PCE cannot efficiently deal with variables that display multimodal character or mixed discrete-continuous support. Worse, a complex dependency structure among the random variables can make probabilistic transformation to independent variables needed for traditional PCE cumbersome.

Accordingly, a distribution-free PCE approach is proposed for surrogate model development for use in reliability studies. Traditional PCE is briefly summarized first; then, the distribution-free framework that exploits sequences of joint raw moments of underlying random variables is presented. Benchmark problems including one example regarding a floating ocean structure in an uncertain environment and undergoing complex vibrational response are presented.

4.2 Polynomial Chaos Expansion

4.2.1 Underlying Assumptions

Consider a structural system with a limit state function, $g_{\mathbf{X}}(\mathbf{x})$, where $\mathbf{X} = [X_1, \dots, X_d]^T \in \mathbb{R}^d$ are d -dimensional dependent uncertain input variables. Since non-normal correlated random variables can be transformed into independent standard normal variables (e.g., by Nataf or Rosenblatt transformations [21, 15, 25]), $g_{\mathbf{X}}(\mathbf{x})$ can be rewritten as $g_{\mathbf{Q}}(\mathbf{q})$ where $\mathbf{Q} = [Q_1, \dots, Q_d]^T \in \mathbb{R}^d$ are independent standard normal variables.

It should be noted that the Nataf transformation works with equivalent Gaussian correlated random variables from the original non-Gaussian variables; inaccuracies may result when more general non-Gaussian dependency must be considered and Nataf transformation is used. Also, it is not always an easy task to identify or define a dependence hierarchy and structure between all the random variables for use of the Rosenblatt transformation.

Introduced first by Wiener [27], the original PCE as defined for independent Gaussian random variables, can be generalized for independent non-Gaussian variables [29]. This generalization is known as the so-called Askey scheme [1], and is referred as traditional PCE in our paper. Traditional PCE, which is inherently tied to the selected associated random variable space, relies on an independence assumption among the random variables; for multi-dimensional problems, it uses tensor-product polynomial basis functions.

4.2.2 Traditional PCE Formulation

In PCE, a performance function, $g(\mathbf{X})$, can be thought of as a QoI that is expanded using orthogonal polynomials given in terms of all the selected uncertain model parameters in a d -dimensional vector, $\mathbf{X} = [X_1, \dots, X_d]^T$. The orthogonal polynomial basis functions depend on the probability distributions of the auxiliary (independent) random variables to which \mathbf{X} must be mapped [26].

Assuming all the physical variables in \mathbf{X} have finite variance, the expansion for $g(\mathbf{X})$ involves multi-indicial coefficients, $\boldsymbol{\alpha} = [\alpha_1, \dots, \alpha_d]^T \in \mathbb{N}^d$:

$$g(\mathbf{X}) = \sum_{\boldsymbol{\alpha} \in \mathbb{N}^d} c_{\boldsymbol{\alpha}} \Psi_{\boldsymbol{\alpha}}(T(\mathbf{X})), \quad (4.1)$$

where $T(\cdot)$ represents a probabilistic mapping from a dependent input random variable vector to the associated independent random variable vector, $c_{\boldsymbol{\alpha}}$ are coefficients to be estimated, and $\Psi_{\boldsymbol{\alpha}}(\cdot)$ describe the multivariate orthogonal polynomial functions.

A PCE model for $g(\mathbf{X})$ truncated at polynomial order p can be represented as:

$$g(\mathbf{X}) \approx \hat{g}_{\text{PCE}}(\mathbf{X}) = \sum_{|\boldsymbol{\alpha}| \leq p} c_{\boldsymbol{\alpha}} \Psi_{\boldsymbol{\alpha}}(T(\mathbf{X})), \quad (4.2)$$

where the total order is defined as $|\boldsymbol{\alpha}| = \sum_{n=1}^d \alpha_n$. A multi-index vector of the set \mathcal{A} can be defined as:

$$\mathcal{A} = \{\boldsymbol{\alpha} \in \mathbb{N}^d : |\boldsymbol{\alpha}| = \sum_{n=1}^d \alpha_n \leq p\}. \quad (4.3)$$

The number of elements in the set \mathcal{A} is defined as follows:

$$\text{card}(\mathcal{A}) = N_p = \binom{d+p}{d}. \quad (4.4)$$

Orthogonality of the selected basis functions implies that:

$$E[\Psi_\alpha \Psi_\beta] = \delta_{\alpha\beta} E[\Psi_\alpha^2], \quad (4.5)$$

where $\delta_{\alpha\beta}$ is the Kronecker delta, equal to unity when α and β are identical and zero otherwise, and $E[\cdot]$ is the expectation operator. Note that $E[\Psi_\alpha^2]$ is available in a closed form for the input variable types within the Askey scheme.

There are at least two limitations to the use of traditional PCE in some cases: (1) incomplete or imperfect information on the stochastic variables, and (2) ambiguous and/or complex dependency structure among the variables.

4.2.3 PCE Coefficient Estimation

The PCE coefficients, $\mathbf{c} = [c_1, \dots, c_{N_p}]^\top$, can be estimated by spectral projection, stochastic collocation, or linear regression. This study uses linear regression, which allows coefficients to be estimated by minimizing the sum of the squared residuals between the truncated PCE and the truth system as follows:

$$\mathbf{c} = \arg \min_{\mathbf{c} \in \mathbb{R}^{N_p}} \sum_{k=1}^{N_s} \left[g(\mathbf{x}^{(k)}) - \sum_{\alpha \in \mathcal{A}} c_\alpha \Psi_\alpha(T(\mathbf{x}^{(k)})) \right]^2, \quad (4.6)$$

where N_s is the number of simulations performed with the truth system as part of the linear regression. For a review of procedures for estimation of c_α and selection of the basis functions in PCE, see [26].

4.3 Distribution-Free Polynomial Chaos Expansion

4.3.1 Univariate Basis Polynomial Functions Using Gram-Schmidt Orthogonalization

A univariate polynomial basis function of order p , generated by Gram-Schmidt orthogonalization [28, 22], can be written as follows:

$$P_X^{(p)}(x) = \sum_{j=0}^p c_{j,(p)} x^j, \quad (4.7)$$

where the coefficients $c_{j,(p)}$ are computed by solving the linear matrix equation [22]:

$$\begin{bmatrix} m_0 & m_1 & \dots & m_p \\ m_1 & m_2 & \dots & m_{p+1} \\ \vdots & \vdots & \vdots & \vdots \\ m_{p-1} & m_p & \dots & m_{2p-1} \\ 0 & 0 & \dots & 1 \end{bmatrix} \begin{bmatrix} c_{0,(p)} \\ c_{1,(p)} \\ \vdots \\ c_{p-1,(p)} \\ c_{p,(p)} \end{bmatrix} = \begin{bmatrix} 0 \\ 0 \\ \vdots \\ 0 \\ 1 \end{bmatrix}, \quad (4.8)$$

where m_k is the k th raw moment of the random variable, X , and the leading coefficient $c_{p,(p)}$ is assumed to be unity (i.e., a monic polynomial).

Note that $P_X^{(p)}(x)$ can be reformulated as follows [13]:

$$P_X^{(p)}(x) = \det \begin{bmatrix} m_0 & m_1 & \dots & m_p \\ m_1 & m_2 & \dots & m_{p+1} \\ \vdots & \vdots & \vdots & \vdots \\ m_{p-1} & m_p & \dots & m_{2p-1} \\ 1 & x & \dots & x^p \end{bmatrix}. \quad (4.9)$$

The computed orthogonal polynomial functions by Eq. 4.9 can be tensorized to define a multivariate orthogonal polynomial function. But non-product type probability measures in the dependent variables cannot be accounted for by tensorization.

4.3.2 Distribution-Free Multivariate Basis Polynomial Functions

Consider now a distribution-free PCE framework. We define a monomial, x^α , as follows:

$$x^\alpha = x_1^{\alpha_1} \cdots x_d^{\alpha_d}, \quad (4.10)$$

and define, as well, the space of homogeneous polynomials of degree n as follows:

$$\mathcal{P}_n^d \equiv \text{span}\{x^\alpha : |\alpha| = \sum_{n=1}^d \alpha_n = n\}. \quad (4.11)$$

Then, homogeneous polynomials of degree at most n are defined as follows:

$$\Pi_n^d \equiv \text{span}\{x^\alpha : |\alpha| \leq n\}. \quad (4.12)$$

Consider next all inner products defined in terms of polynomials of the d variables as follows:

$$\langle P, Q \rangle = \int_{\mathbb{R}^d} P(\mathbf{x})Q(\mathbf{x})f(\mathbf{x})d\mathbf{x}, \quad (4.13)$$

where $f(\cdot)$ is the joint probability density function (jpdf) of \mathbf{X} .

A polynomial $P \in \mathcal{P}_n^d$ is an orthogonal polynomial of degree n with respect to Q if

$$\langle P, Q \rangle = 0, \quad \forall Q \in \Pi_n^d \text{ with } \deg(Q) < \deg(P). \quad (4.14)$$

Accordingly, P is orthogonal with respect to all polynomials of lower degree, but it may not be orthogonal to other polynomials of the same degree. For

example, P with $\boldsymbol{\alpha} = [1, 1]^T$ may not be orthogonal with respect to Q with $\boldsymbol{\alpha} = [2, 0]^T$. This is defined as “weak” orthogonality in contrast with “strong” orthogonality which allows tensorized construction of univariate polynomial spaces, as in traditional PCE.

Given an inner product, we can assign to the set $\{x^\alpha\}$ a linear order and apply Gram-Schmidt orthogonalization process to generate a sequence of multivariate orthogonal polynomials. For each n , \mathbf{x}^n denotes a column vector, $\mathbf{x}^n \equiv [\forall x^\alpha]^T$, such that $|\boldsymbol{\alpha}| = n$. For example, \mathbf{x}^2 is defined as $[x_1^2, x_1x_2, x_2^2]^T$ when $d = 2$.

Consider, then, a moment matrix, $\mathbf{m}_{\{i\}+\{j\}}$, and a moment vector, $\mathbf{m}_{\boldsymbol{\alpha},i}$, defined as follows:

$$\mathbf{m}_{\{i\}+\{j\}} \equiv \mathbb{E}[\mathbf{x}^i(\mathbf{x}^j)^T]; \quad \mathbf{m}_{\boldsymbol{\alpha},i} \equiv \mathbb{E}[x^\alpha \mathbf{x}^i]. \quad (4.15)$$

Next, define $P_\alpha(\mathbf{x})$ as follows [9]:

$$P_\alpha(\mathbf{x}) = \frac{1}{\Delta_{n-1,d}} \cdot \det \begin{bmatrix} \mathbf{m}_{\{0\}+\{0\}} & \cdots & \mathbf{m}_{\{0\}+\{n-1\}} & \mathbf{m}_{\boldsymbol{\alpha},0} \\ \vdots & \ddots & \vdots & \vdots \\ \mathbf{m}_{\{n-1\}+\{0\}} & \cdots & \mathbf{m}_{\{n-1\}+\{n-1\}} & \mathbf{m}_{\boldsymbol{\alpha},n-1} \\ (\mathbf{x}^0)^T & \cdots & (\mathbf{x}^{n-1})^T & x^\alpha \end{bmatrix}, \quad (4.16)$$

where

$$\Delta_{n-1,d} = \det \begin{bmatrix} \mathbf{m}_{\{0\}+\{0\}} & \cdots & \mathbf{m}_{\{0\}+\{n-1\}} \\ \vdots & \ddots & \vdots \\ \mathbf{m}_{\{n-1\}+\{0\}} & \cdots & \mathbf{m}_{\{n-1\}+\{n-1\}} \end{bmatrix}. \quad (4.17)$$

Note that $\mathbf{m}_{\{i\}+\{j\}}$ and $\mathbf{m}_{\alpha,i}$ may be estimated using sampled joint raw moments of variables in \mathbf{X} . For example, $P_{\alpha=[1,1]}(\mathbf{x})$ can be defined as follows:

$$P_{\alpha=[1,1]}(\mathbf{x}) = \frac{1}{\Delta_{1,2}} \det \begin{bmatrix} 1 & \mathbb{E}[x_1] & \mathbb{E}[x_2] & \mathbb{E}[x_1x_2] \\ \mathbb{E}[x_1] & \mathbb{E}[x_1^2] & \mathbb{E}[x_1x_2] & \mathbb{E}[x_1^2x_2] \\ \mathbb{E}[x_2] & \mathbb{E}[x_1x_2] & \mathbb{E}[x_2^2] & \mathbb{E}[x_1x_2^2] \\ 1 & x_1 & x_2 & x_1x_2 \end{bmatrix}. \quad (4.18)$$

Analogous to Eq. 4.2 and traditional PCE, a surrogate performance function of order p using P_α , denoted Arbitrary PCE (APCE) hereinafter, is given as follows:

$$g(\mathbf{X}) \approx \hat{g}_{\text{APCE}}(\mathbf{X}) = \sum_{|\alpha| \leq p} c_\alpha P_\alpha(\mathbf{X}). \quad (4.19)$$

4.4 Numerical Examples

Six illustrative examples are selected to assess the proposed APCE framework:

- (1) a noisy limit state function;
- (2) a quadratic limit state function;
- (3) a linear limit state function involving correlated non-normal random variables;
- (4) a highly nonlinear performance function involving multimodal random variables;
- (5) a quadratic limit state function with mixed discrete-continuous support;
- and (6) an implicit performance function relating the long-term extreme response of a floating ocean structure in an uncertain environment.

In the examples, we consider two types of performance functions: (1) strength and (2) serviceability. The strength performance function can be defined as follows:

$$g(\mathbf{X}) = R - S, \quad (4.20)$$

where R and S represent resistance and load variables, respectively, for the system; instability, buckling, and overturning analysis can fall into this type. The serviceability performance function can be defined as follows:

$$g(\mathbf{X}) = b - h(\mathbf{X}), \quad (4.21)$$

where b is a deterministic threshold and $h(\mathbf{X})$ represents demand on the system; this demand might serve as a proxy for deflection, vibration, crack size, etc.

In customary usage, $g(\mathbf{X}) < 0$ often represents an undesired state. In Eq. 4.21, estimating the failure probability, $P_f = P[g(\mathbf{X}) < 0]$, is equivalent to the estimation of $P[h(\mathbf{X}) > b]$; however, changing b allows assessing the performance of different system “capacity” levels.

For the serviceability performance functions, estimated failure probabilities for various threshold (b) values are compared using 10 sets of the “truth” system using MCS versus 10 surrogate model estimates. Note that for estimation of the PCE coefficients (of either kind, traditional or arbitrary), the number of randomly drawn samples of input and output variables is selected as $N_s = 3 \times \binom{d+p}{d}$.

For the strength performance functions, statistics regarding the failure probability are computed using 100 sets of the truth system with MCS as well a 100 surrogate model estimates.

The failure probability can be computed by MCS in a PCE surrogate

model as:

$$P_f \equiv P(g < 0) \approx \frac{1}{N_{\text{MC}}} \sum_{k=1}^{N_{\text{MC}}} I(\hat{g}(\mathbf{x}^{(k)}) < 0), \quad (4.22)$$

where $I(\mathcal{F})$ is the indicator function which is either 1 or 0 depending on whether \mathcal{F} is true or not, and N_{MC} is the number of evaluations.

The root-mean-square error (RMSE) which is used to assess models is defined as follows:

$$\text{RMSE} = \sqrt{\frac{1}{N_T} \sum_{k=1}^{N_T} (g^{(k)}(\mathbf{x}) - \hat{g}^{(k)}(\mathbf{x}))^2}, \quad (4.23)$$

where N_T is the total number of evaluations.

4.4.1 Example 1: Noisy Limit State Function

The first example involves a noisy limit state function which is given as follows [16]:

$$g_{\mathbf{x}}(\mathbf{x}) = x_1 + 2x_2 + 2x_3 + x_4 - 5x_5 - 5x_6 + 0.001 \sum_{i=1}^6 \sin(100x_i), \quad (4.24)$$

where $\mathbf{X} = \{X_1, \dots, X_6\}$ are mutually independent random variables whose distributions are listed in Table 4.1.

Because the linear terms are dominant in the limit state function, the linear APCE models (i.e., $p = 1$) accurately estimate the statistics as is seen in Table 4.2. No large errors are introduced; i.e., small RMSE values are found. On the other hand, the traditional PCE scheme (HPCE denotes traditional PCE using Hermite polynomials) requires polynomials of higher order ($p > 1$) and more training samples to yield the same COV as MCS.

Table 4.1: Random variables in Example 1

Variable	Distribution	Mean	COV
X_1	Lognormal	120	0.10
X_2	Lognormal	120	0.10
X_3	Lognormal	120	0.10
X_4	Lognormal	120	0.10
X_5	Lognormal	50	0.30
X_6	Lognormal	40	0.30

Table 4.2: Comparison of statistics based on APCE and HPCE for Example 1

	MCS	APCE		HPCE
		$p = 1$	$p = 4$	
σ_{P_f}	3.28×10^{-4}	3.28×10^{-4}	3.28×10^{-4}	
μ_{P_f}	1.23×10^{-2}	1.23×10^{-2}	1.23×10^{-2}	
COV	2.68×10^{-2}	2.68×10^{-2}	2.68×10^{-2}	
RMSE		2.10×10^{-3}	1.12×10^{-1}	
N_s		21	630	

4.4.2 Example 2: Quadratic Function

This example considers a quadratic limit state function as follows [16]:

$$\begin{aligned}
g_{\mathbf{x}}(\mathbf{x}) = & 1.1 - 0.00115x_1x_2 + 0.00157x_2^2 + 0.00117x_1^2 \\
& + 0.0135x_2x_3 - 0.0705x_2 - 0.00534x_1 \\
& - 0.0149x_1x_3 - 0.0611x_2x_4 + 0.0717x_1x_4 \\
& - 0.226x_3 + 0.0333x_3^2 - 0.558x_3x_4 \\
& + 0.998x_4 - 1.339x_4^2. \tag{4.25}
\end{aligned}$$

The random variables, $X_{i=1,\dots,4}$, are mutually independent; their distributions are listed in Table. 4.3.

Table 4.3: Random variables in Example 2

Variable	Distribution	Mean	COV
X_1	Type II Extreme	10	0.50
X_2	Normal	25	0.20
X_3	Normal	0.8	0.25
X_4	Lognormal	0.0625	1.00

Computed statistics based on APCE and HPCE are presented in Table 4.4. The APCE models with $p = 2$ are able to accurately estimate the QoI statistics with a relatively small number of samples compared to that with HPCE.

Table 4.4: Comparison of statistics based on APCE and HPCE for Example 2

	Truth	APCE		HPCE
		$p = 2$	$p = 10$	
σ_{P_f}	6.89×10^{-4}	6.89×10^{-4}	6.96×10^{-4}	
μ_{P_f}	5.57×10^{-2}	5.57×10^{-2}	5.57×10^{-2}	
COV	1.24×10^{-2}	1.24×10^{-2}	1.25×10^{-2}	
RMSE		6.90×10^{-16}	1.40×10^{-1}	
N_s		45	3003	

4.4.3 Example 3: Correlated Non-Normal Variables

Consider an extension to the benchmark problem proposed by Liu & Kureghian [8] that describes a linear limit state function involving non-normal

random variables:

$$g_{\mathbf{X}}(\mathbf{x}) = b - (x_1 - x_2), \quad (4.26)$$

where X_1 is a uniformly distributed variable ranging from 0 to 100 while X_2 is unit-mean exponentially distributed variable, as shown in Table 4.5. A correlation coefficient between the two variables, $\rho_{X_1, X_2} = 0.5$, is assumed.

Table 4.5: Random variables in Example 3

Variable	Distribution	Mean	COV
X_1	Uniform	50	0.58
X_2	Exponential	1	1

The order-1 APCE surrogate shows remarkable agreement, when compared with MCS, in estimation of P_f for various b values as shown in Fig. 4.1; note that MCS is based on 1×10^6 truth model evaluations. The proposed APCE approach requires only 9 evaluations of the truth model (i.e., $N_s = 9$), whereas traditional PCE using Hermite polynomials (HPCE) requires 900 evaluations, and is still not satisfactory in the region where $P_f < 10^{-4}$.

Note that we use the Nataf transformation [21] in HPCE because it needs to be built in an independent standard normal variable space; nonlinearity in the transformation makes convergence of the HPCE models to the truth function difficult.

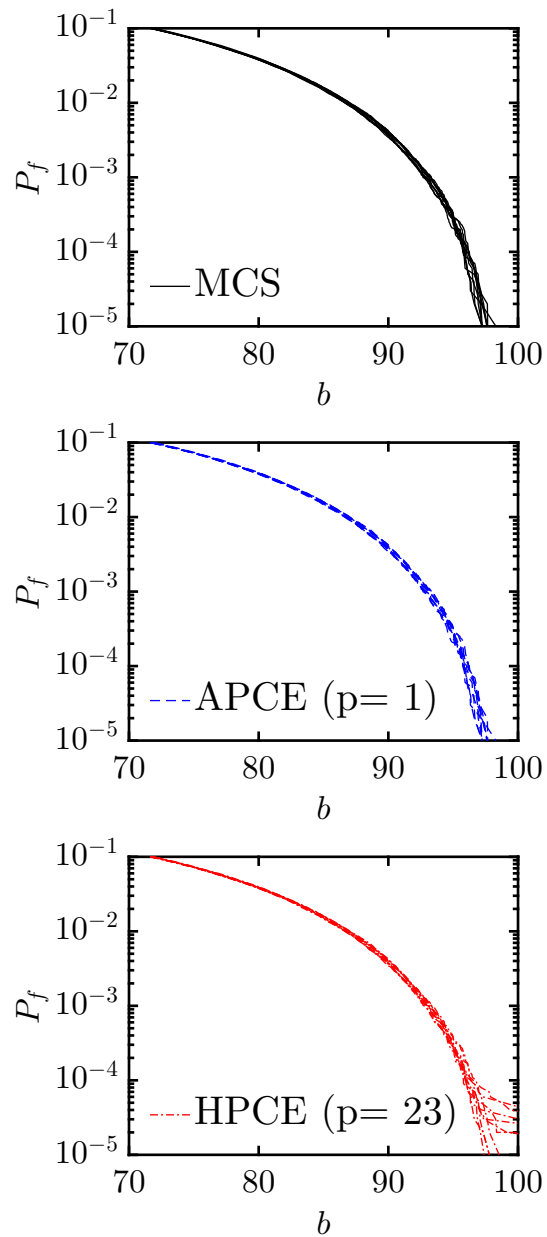


Figure 4.1: Comparison of P_f estimates for different b values from 10 MCS, APCE, and HPCE sets for Example 3.

4.4.4 Example 4: Multimodal Random Variables

This example considers the modified Ishigami function, with modification in the support for the variables, so as to allow for multimodal characteristics (the original Ishigami function involved uniform variables [12]). The function is as follows:

$$g_{\mathbf{x}}(\mathbf{x}) = b - (\sin x_1 + 7 \sin^2 x_2 + 0.1x_3^4 \sin x_1). \quad (4.27)$$

Each of the independent random variables, X_i ($i = 1, 2, 3$), follows a mixture distribution with a pdf:

$$f(x) = \sum_{i=1}^3 w_i \phi_i(x), \quad (4.28)$$

where the weights, w_i , are set to 1/3 and $\phi_i(\cdot)$ are three Gaussian pdfs with means and standard deviations as follows: $(\mu, \sigma) = (2.0, 0.1), (2.5, 0.5), (3.5, 0.2)$. Estimates of P_f for various b values from 10 sets of the truth and surrogate models are presented in Fig. 4.2. The proposed APCE method is found to predict accurate results even in this case with random variables that exhibit multimodal characteristics. With traditional PCE, the multimodal random variables are mapped to shifted beta distributions; accordingly, Jacobi polynomials (denoted by JPCE) serve as orthogonal basis functions but the method clearly fails.

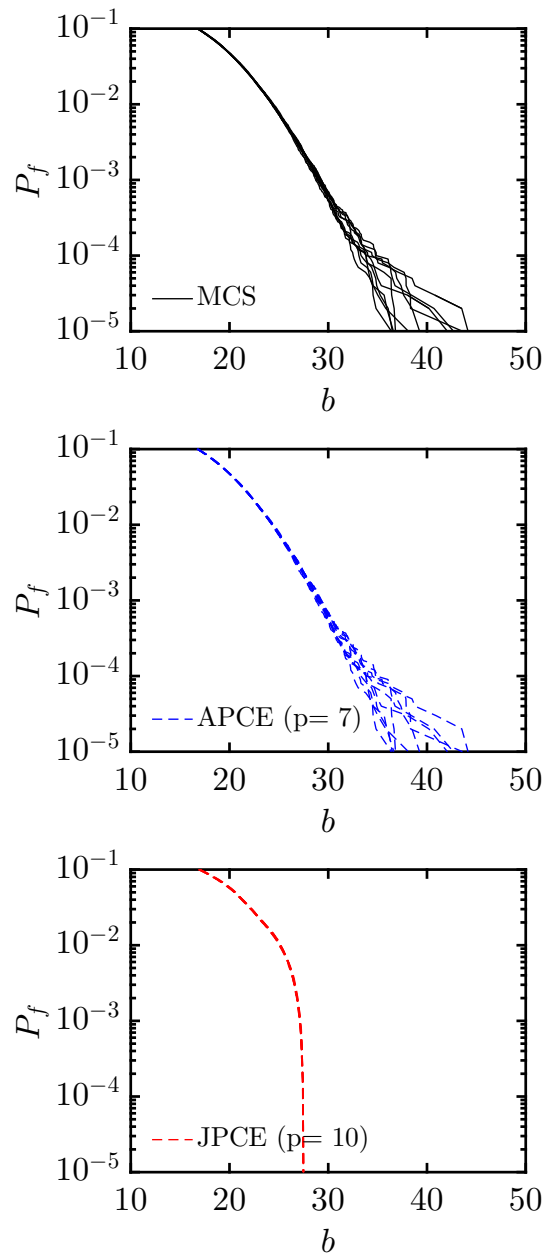


Figure 4.2: Comparison of P_f estimates for different b values from 10 MCS, APCE, and JPCE sets for Example 4.

4.4.5 Example 5: Mixed Discrete-Continuous Support

Consider a quadratic performance function given as:

$$\begin{aligned} g_{\mathbf{x}}(\mathbf{x}) = & b - (15 + 4x_1x_2 + 4x_1x_3 + 4x_2x_3 \\ & + 3x_1 + 3x_2 + 3x_3 - x_1^2 - x_2^2 - x_3^2), \end{aligned} \quad (4.29)$$

where the variables, X_i ($i = 1, 2, 3$), are described by mixed discrete-continuous pdfs as follows:

$$f_X(x) = 0.7 \left(\frac{1}{\sqrt{2\pi}} \exp\left(-\frac{x^2}{2}\right) \right) + 0.3\delta(x - 2.0), \quad (4.30)$$

where $\delta(\cdot)$ is the Dirac delta function. Estimates of P_f for various b values from 10 sets of the truth and surrogate models are presented in Fig. 4.3. The order-2 APCE surrogate is seen to yield accurate results, even with the mixed discrete-continuous support for the random variables, while HPCE again clearly does not.

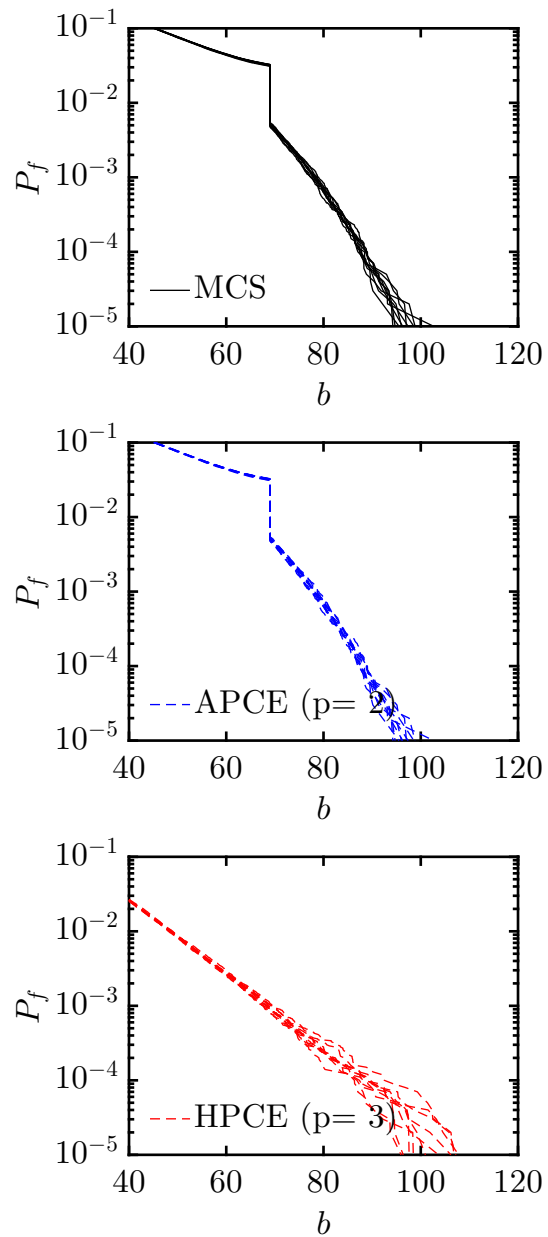


Figure 4.3: Comparison of P_f estimates for different b values from 10 MCS, APCE, and HPCE sets for Example 5.

4.4.6 Example 6: Computational Time-Domain Solver for Performance Function

In this final example, an implicit performance function often considered in the design of offshore structures, with a target reliability, is investigated. The performance function is given as follows:

$$g = z - Z_T(\mathbf{X}), \quad (4.31)$$

where z is a threshold value (similar to b in the previous examples) while Z_T is the T -year long-term extreme response. Note that computation of Z_T and establishing uncertainty in its estimate involves: (1) long-term or background environment/climate uncertainty; and (2) short-term time-domain simulations of a response of interest. This is described schematically in Fig. 4.4. The exceedance probability, P_T , associated with the long-term response, z , is defined as follows:

$$P_T = P[Z_T > z] = \int_{\mathbf{X}} P[Z_T > z | \mathbf{X}] f_{\mathbf{X}}(\mathbf{x}) d\mathbf{x}, \quad (4.32)$$

where $f_{\mathbf{X}}$ is the jpdf of the environmental variables. Note that when 30-minute long time-domain simulations are run for specified realizations of the environmental variables, \mathbf{X} , the “design” process is concerned with estimation of the quantile of Z_T that is associated with a target probability of exceedance. For instance, the T -year response is a QoI that is associated with $P_T = 1/(T \times 365.25 \times 24 \times 2)$. Note that direct integration implied by Eq. 4.32 is computationally demanding and involves MCS for random variables, \mathbf{X} , in

the outer loop and random process simulation in the inner loop with high-dimensional frequency-dependent random phases and amplitudes, Θ , for the waves. Figure 4.5 presents $P[Z_T > z]$ estimates for a floating structure with complex dynamics [14, 17]. The proposed APCE surrogate with polynomial order, 2, is more accurate relative to HPCE, as can be easily verified.

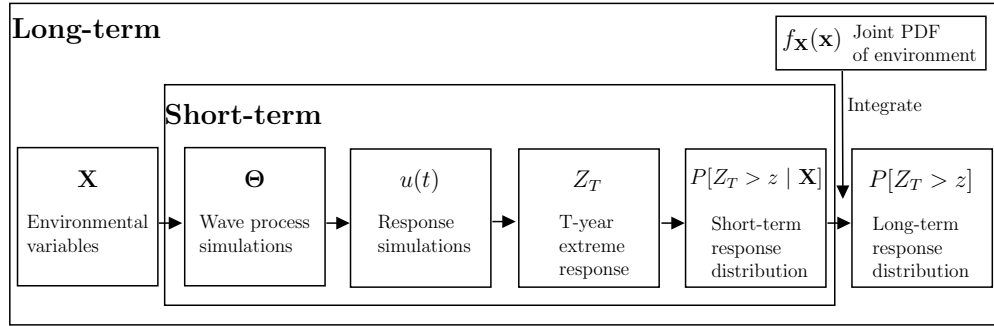


Figure 4.4: Flowchart for long-term extreme estimation in probabilistic offshore structure design for Example 6.

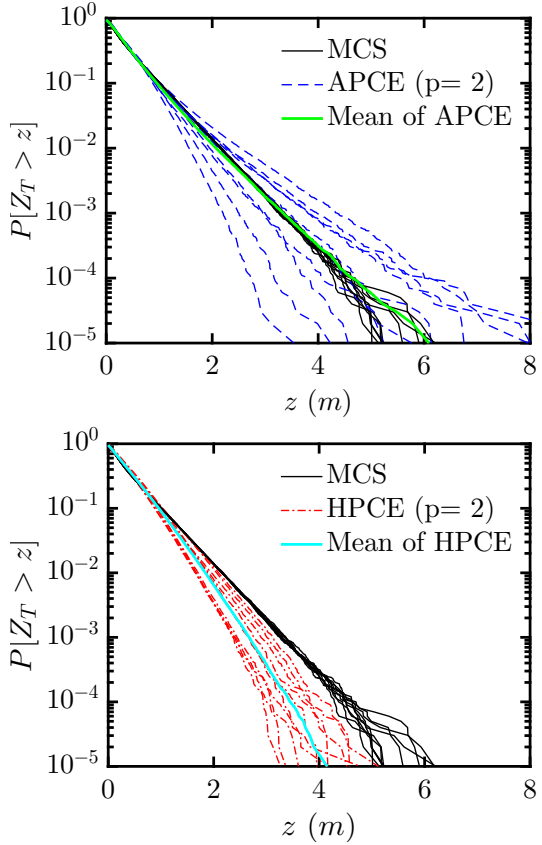


Figure 4.5: Comparison of exceedance probabilities of Z_T for different z values from 10 MCS, APCE, and HPCE sets for Example 6.

4.5 Conclusions

A distribution-free PCE framework for efficient probabilistic analysis of various QoIs is proposed. Gram-Schmidt orthogonalization, involved in the computational framework, employs sequences of computed joint raw moments of underlying random variables to construct multivariate polynomial basis functions for dependent variables generally. The proposed method is validated

using benchmark problems as well as an offshore design problem; results suggest that APCE is more versatile and accurate compared to traditional PCE.

Certain types of limit state functions, such as fractional polynomial functions and highly oscillatory functions and any associated QoIs, may not be predicted well by the proposed APCE method. Further investigations for those types of limit state functions are necessary.

Bibliography

- [1] Richard Askey and James A Wilson. *Some basic hypergeometric orthogonal polynomials that generalize Jacobi polynomials*, volume 319. American Mathematical Society, 1985.
- [2] Siu-Kui Au and James L Beck. Estimation of small failure probabilities in high dimensions by subset simulation. *Probabilistic Engineering Mechanics*, 16(4):263–277, 2001.
- [3] Géraud Blatman and Bruno Sudret. Efficient computation of global sensitivity indices using sparse polynomial chaos expansions. *Reliability Engineering & System Safety*, 95(11):1216–1229, 2010.
- [4] Christian G Bucher. Adaptive sampling – an iterative fast Monte Carlo procedure. *Structural Safety*, 5(2):119–126, 1988.
- [5] Christian G Bucher and Ulrich Bourgund. A fast and efficient response surface approach for structural reliability problems. *Structural Safety*, 7(1):57–66, 1990.
- [6] Robert H Cameron and William T Martin. The orthogonal development of non-linear functionals in series of Fourier-Hermite functionals. *Annals of Mathematics*, pages 385–392, 1947.

- [7] Seung-Kyun Choi, Ramana V Grandhi, and Robert A Canfield. Structural reliability under non-gaussian stochastic behavior. *Computers & Structures*, 82(13-14):1113–1121, 2004.
- [8] Armen Der Kiureghian and Pei-Ling Liu. Structural reliability under incomplete probability information. *Journal of Engineering Mechanics*, 112(1):85–104, 1986.
- [9] Charles F Dunkl and Yuan Xu. *Orthogonal polynomials of several variables*. Number 155. Cambridge University Press, 2014.
- [10] Roger G Ghanem and Pol D Spanos. *Stochastic finite elements: a spectral approach*. Courier Corporation, 2003.
- [11] Abraham M Hasofer and Niels C Lind. Exact and invariant second-moment code format. *Journal of the Engineering Mechanics division*, 100(1):111–121, 1974.
- [12] Tsutomu Ishigami and Toshimitsu Homma. An importance quantification technique in uncertainty analysis for computer models. *International Symposium on Uncertainty Modeling and Analysis*, pages 398–403, 1990.
- [13] Mourad Ismail, JJ Foncannon, and Osmo Pekonen. Classical and quantum orthogonal polynomials in one variable. *The Mathematical Intelligencer*, 30(1):54–60, 2008.
- [14] HyeongUk Lim, Lance Manuel, and Ying Min Low. On efficient long-term extreme response estimation for a moored floating structure. *ASME*.

International Conference on Offshore Mechanics and Arctic Engineering,
2018.

- [15] Pei-Ling Liu and Armen Der Kiureghian. Multivariate distribution models with prescribed marginals and covariances. *Probabilistic Engineering Mechanics*, 1(2):105–112, 1986.
- [16] Pei-Ling Liu and Armen Der Kiureghian. Optimization algorithms for structural reliability. *Structural Safety*, 9(3):161–177, 1991.
- [17] Ying Min Low and Robin S Langley. A comparison of methods for the coupled analysis of floating structures. *ASME. International Conference on Offshore Mechanics and Arctic Engineering*, pages 249–258, 2007.
- [18] Henrik O Madsen, Steen Krenk, and Niels C Lind. *Methods of structural safety*. Courier Corporation, 2006.
- [19] Chu V Mai, Minas D Spiridonakos, Eleni N Chatzi, and Bruno Sudret. Surrogate modeling for stochastic dynamical systems by combining non-linear autoregressive with exogenous input models and polynomial chaos expansions. *International Journal for Uncertainty Quantification*, 6(4), 2016.
- [20] Yasuhiro Mori and Bruce R Ellingwood. Time-dependent system reliability analysis by adaptive importance sampling. *Structural Safety*, 12(1):59–73, 1993.

- [21] Andre Nataf. Determination des distribution don t les marges sont donnees. *Comptes Rendus de l Academie des Sciences*, 225:42–43, 1962.
- [22] Sergey Oladyshkin and Wolfgang Nowak. Data-driven uncertainty quantification using the arbitrary polynomial chaos expansion. *Reliability Engineering & System Safety*, 106:179–190, 2012.
- [23] Rüdiger Rackwitz and Bernd Flessler. Structural reliability under combined random load sequences. *Computers & Structures*, 9(5):489–494, 1978.
- [24] Malur R Rajashekhar and Bruce R Ellingwood. A new look at the response surface approach for reliability analysis. *Structural Safety*, 12(3):205–220, 1993.
- [25] Murray Rosenblatt. Remarks on a multivariate transformation. *The Annals of Mathematical Statistics*, 23(3):470–472, 1952.
- [26] Bruno Sudret. Meta-models for structural reliability and uncertainty quantification. *arXiv preprint arXiv:1203.2062*, 2012.
- [27] Norbert Wiener. The homogeneous chaos. *American Journal of Mathematics*, 60(4):897–936, 1938.
- [28] Jeroen AS Witteveen and Hester Bijl. Modeling arbitrary uncertainties using Gram-Schmidt polynomial chaos. *AIAA. Aerospace Sciences Meeting and Exhibit*, page 896, 2006.

- [29] Dongbin Xiu and George Em Karniadakis. The Wiener–Askey polynomial chaos for stochastic differential equations. *SIAM Journal on Scientific Computing*, 24(2):619–644, 2002.
- [30] Xufang Zhang and Mahesh D Pandey. Structural reliability analysis based on the concepts of entropy, fractional moment and dimensional reduction method. *Structural Safety*, 43:28–40, 2013.
- [31] Yan-Gang Zhao and Tetsuro Ono. Moment methods for structural reliability. *Structural Safety*, 23(1):47–75, 2001.

Paper IV:

Chapter 5

Dimension Reduction in Extreme Response Prediction for Offshore Structures

Abstract

This study proposes a two-step dimension reduction method for long-term extreme response prediction of offshore structures in an uncertain ocean environment. Uncertainty in the response arises from contrasting sea state conditions defined by the significant wave height H_s and the spectral peak period T_p . In a given sea state, short-term response simulations are carried out for sampled pairs of H_s and T_p ; in such simulations, a large number of harmonics, that are comprised of random amplitude and phase vectors $\Theta = [\mathbf{a}, \boldsymbol{\theta}]^T$, are typically required. To address the high dimensionality, the proposed method includes: (1) model order reduction in the frequency domain for the short-term response analysis, and (2) gradient-based stochastic dimension reduction for the long-term extreme response prediction. Surrogate models are then built in terms of the reduced dimension variables that is a transformed set from the original variables, $\mathbf{X} = [H_s, T_p, \Theta]^T$. The reduced-order surrogate models are accurate in long-term extreme response prediction for various offshore structures and consistent with more expensive Monte Carlo simulations.

5.1 Introduction

The evaluation of quantities of interest (QoIs) for various engineering problems involves the use of computational models that employ uncertain input parameters. Each QoI and its associated uncertainty is estimated using repetitive computations. Simulations for each parameter set can be computationally expensive if one uses a high-fidelity model such as a refined finite element model or computational fluid dynamics analysis. Also, one may need a very large number of runs with a computational solver to obtain convergent outputs when the input dimension is high. For such cases, it is beneficial to find a low-dimensional representation of the uncertain input parameters that can explain the QoIs without loss of information. Then, one can construct “surrogate” models in terms of the low-dimension variables that can serve as approximations for the high-dimensional “truth” system.

Polynomial chaos expansion (PCE) [5, 20] offers a robust framework for the development of surrogate models due to its accuracy and efficiency in accounting for uncertainties in complex engineering problems. While PCE may be employed in many applications, the “curse of dimensionality” makes it a challenge to apply in practice [10, 9]. For example, the response simulation for offshore dynamics problems typically requires hundreds or thousands of uncertain input variables, that may not be conducive to the use of PCE. We study efficient surrogate modeling that can account for most of the response’s variability by means of dimension reduction.

The long-term extreme response of an offshore structure is of interest in

this study. Suppose the T -year motion of such a structure is of interest; often, for design $T = 50$ or 100 . If the motion in a sea state of a short duration, say 30 minutes, is considered stationary, it is common practice to define such a sea state by parameters such as H_s and T_p and then carry out response simulations for irregular/stochastic wave loading consistent with those parameters. By sweeping over various H_s and T_p values, while accounting for their relative likelihood of occurrence, and generating suites of irregular wave trains each time, one can establish fully the uncertainty in say, the 30-minute extreme. The establishment of a QoI defined as the T -year return period motion is the objective of this study; it is equivalent to assessing as QoI, the motion level that is exceeded with probability $1/(T \times 365.25 \times 24 \times 2)$ in T -minutes. It is this quantity and its uncertainty that we will assess.

In this study, we will first define the response of interest and its uncertainties due to the ocean environment. We discuss how to conduct model order reduction in the frequency domain to avoid excessive gradient calculations that will later be needed for dimension reduction. We define a covariance matrix of QoI gradients with respect to the inputs, for the reduced model, to identify directions along which the response varies greatly. Then, the gradient vector needed for the covariance matrix is estimated by the elementary effects approach. Eigendecomposition of the covariance matrix helps identify new input coordinates using linear transformation. PCE surrogate models are built in the reduced dimension space. Numerical results serve to assess the proposed approach for long-term response prediction of various offshore structures.

5.2 Problem Formulation

A single-degree-of-freedom (SDOF) system may be employed to describe the motion of an offshore structure undergoing uncertain environmental loading. The governing equation of motion is as follows [11]:

$$M\ddot{u}(t) + 2\zeta\sqrt{KM}\dot{u}(t) + Ku(t) = F(t), \quad (5.1)$$

where M , ζ , and K represent the mass, damping ratio, and stiffness, respectively; the time series of the response (motion), $u(t)$, is evaluated for any excitation, $F(t)$. The motion can be expressed as follows:

$$u(t) = \sum_{r=1}^R H(\omega_r)T(\omega_r)A_r \exp(i\omega_r t) \quad (5.2)$$

where $H(\omega) = (-\omega^2 M + i\omega C + K)^{-1}$ is the frequency response function, $T(\omega)$ is a transfer function (from waves to force), $C = 2\zeta\sqrt{KM}$ is the damping coefficient, and $A_r = a_r \exp(i\phi_r)$ is the complex Fourier amplitude of the r th harmonic component, where a_r is a random amplitude defined in terms of H_s and T_p , and ϕ_r is a random phase angle. In some problems, to account for second-order effects, a quadratic frequency function (QTF) can be employed [3].

5.3 Metocean Conditions

Metocean statistical parameters that describe the wave climate are the significant wave height H_s and spectral peak period T_p . In a short-term response simulation given H_s and T_p , the wave spectrum must be defined; for example,

the JONSWAP (Joint North Sea Wave Project) spectrum can be employed for a site of interest [6].

5.4 Uncertainties in Extreme Response

5.4.1 Short-Term Extreme Response and QoI

In the short-term simulations of T -minute duration, the sea surface elevation and response process are assumed to be stationary for the given H_s and T_p pair. The selected wave spectrum, $S_\eta(\omega)$, can be discretized into R components of equal frequency interval $\Delta\omega$. The simulated time series for $\eta(t)$ may be represented as:

$$\eta(t) = \sum_{r=1}^R a_r \cos(\omega_r t + \phi_r), \quad (5.3)$$

where a_r are independent random wave amplitudes and ϕ_r are independent random phase angles [22]. The amplitudes follow a Rayleigh distributions with mean-squared values equal to $2S_\eta(\omega_r)\Delta\omega$ while the phases follow a uniform distribution between 0 and 2π . It is convenient to define a $2R$ -dimensional vector, $\Theta = [a_1, a_2, \dots, a_R, \phi_1, \phi_2, \dots, \phi_R]^T$ that results in short-term uncertainty in the response. This study recognizes that long-term uncertainty in the T -minute extreme of u results both from uncertainty in H_s and T_p as well as from short-term uncertainty in Θ . Typically, hundreds to thousands of frequency components are required for time series realization given a target wave spectrum; this can make the prediction of the uncertainty in response extremes difficult.

Given the simulated response process, $u(t)$ defined over duration T for

a given pair of H_s and T_p values, the extreme response (QoI) is defined as follows [11]:

$$Z = \max\{u(t); 0 \leq t \leq T\}. \quad (5.4)$$

Note that Z depends on H_s , T_p , and Θ —i.e., $Z \equiv Z(H_s, T_p, \Theta)$. For notational convenience, let us define the complementary cumulative distribution function (or probability of exceedance) as

$$P(Z > z) = G_Z(z). \quad (5.5)$$

Thus, for a selected sea state and associated H_s and T_p values, $G_{Z|H_s,T_p}(z)$ denotes the conditional probability of exceedance of level z by the short-term extreme value of u in duration, T . We shall see that it is $G_Z(z)$ that describes the unconditional probability of exceedance of level z , obtained by considering all H_s and T_p values that we must establish to fully define our QoI and its associated uncertainty.

5.4.2 Long-Term Extreme Response

Long-term statistics of H_s and T_p are described by the joint probability density function (jpdf), namely $f_{H_s, T_p}(h, t)$. Considering all sea states, the unconditional probability of exceedance $G_Z(z)$ is given as follows:

$$G_Z(z) = \iint G_{Z|H_s,T_p}(z) f_{H_s, T_p}(h, t) dh dt. \quad (5.6)$$

Note that $G_Z(z)$ in Eq. 5.6 may be evaluated for any z if Monte Carlo simulation is applied in the “forward” way. Efficient alternatives to Monte Carlo

simulation exist; one such uses “inverse” reliability approaches [18, 19, 1] that focuses on the metocean random variables alone or optionally accounts for response variability. However, in those approaches, only z values that ensure a target value of $G_Z(z)$ are derived; moreover, these methods are approximate. In the present study, an alternative approach is proposed that makes use of PCE to derive a surrogate model for $G_Z(z)$ in reduced dimension.

5.5 Monte Carlo Simulations

The use of Eq. 5.2 allows the simulation of response time series quite efficiently using the Inverse Fast Fourier Transform (IFFT). Then, $G_Z(z)$ can be estimated using MCS; the MCS estimate is obtained as follows:

$$G_Z^{\text{MC}}(z) = \frac{1}{N_T} \sum_{k=1}^{N_T} I(Z > z | H_s^{(k)}, T_p^{(k)}, \Theta^{(k)}), \quad (5.7)$$

where N_T represents the number of MCS samples, $I(\mathcal{F})$ is the indicator function which is either 1 or 0 depending on whether \mathcal{F} is true or not and $H_s^{(k)}$, $T_p^{(k)}$, $\Theta^{(k)}$ represents the drawn samples in the k th trial.

5.6 Dimension Reduction

5.6.1 Model Order Reduction

We often need an excessive computation effort to obtain meaningful statistics when the truth system is given in a high-dimensional input space; we may benefit first from reducing the dimension if we are to require QoI gradients in terms of all the input parameters/variables. For response prediction of offshore

structure, we propose a two-step dimension reduction method: (1) model order reduction in the frequency domain, and (2) gradient-based stochastic dimension reduction.

In design, interest is in the maximum or undesired response in simulated time series comprised of a number of harmonics; depending on the bandwidth of the input wave spectrum, we might expect that this quantity is likely dominated by only some harmonics. For example, wave energy spectra in severe sea states may be dominant contributors to the maximum response at low probabilities of exceedance. In model order reduction, N_ω frequency components are selected while keeping the total wave energy in the “reduced” model the same as that with the “full” model by scaling the wave spectrum ordinates. Accuracy of the reduced model depends on appropriate selection of the frequencies; it needs to consider the short-term influence (that might depend on the structure type) as well as metocean conditions (e.g., different sea states and wave energy spectra).

The simulated time series for $\hat{\eta}(t)$ by model order reduction can be expressed as follows:

$$\hat{\eta}(t) = \sum_{k=1}^{N_\omega} \hat{a}_k \cos(\omega_k t + \phi_k), \quad (5.8)$$

where the index k represents the chosen frequency sequence, \hat{a}_k , which are random amplitudes that follow Rayleigh distributions with mean-squared values of $2\hat{S}_\eta(\omega)\Delta\omega$ and $\hat{S}_\eta(\omega)$ is the scaled wave spectrum to maintain the right variance for the sea state. The wave elevation variance for a sea state given

H_s and T_p is given as follows:

$$\text{Var}[\eta(t)] = \left(\frac{H_s}{4}\right)^2. \quad (5.9)$$

The random amplitudes in the reduced model are then subject to this condition:

$$\text{Var}[\hat{\eta}(t)] = \text{Var}[\eta(t)]. \quad (5.10)$$

By Parseval's theorem, this condition can be written in frequency domain as follows:

$$\sum_{r=1}^R S_\eta(\omega_r) \Delta\omega = \sum_{k=1}^{N_\omega} \hat{S}_\eta(\omega_k) \Delta\omega. \quad (5.11)$$

We use a uniform frequency interval, $\Delta\omega$, for IFFTs with the reduced model, consistent with the full model. Thus, the spectral ordinates of all frequencies not included in the reduced model are all set to zero.

The response $\hat{u}(t)$ by model order reduction, when a linear transfer function is considered, can be expressed as follows:

$$\hat{u}(t) = \sum_{k=1}^{N_\omega} H(\omega_k) T(\omega_k) \hat{A}_k \exp(i\omega_k t), \quad (5.12)$$

where

$$\hat{A}_k = \hat{a}_k \exp(i\phi_k), \quad (5.13)$$

$$\hat{a}_k \sim \text{Rayleigh}\left(\sqrt{\hat{S}_\eta(\omega_k) \Delta\omega}\right). \quad (5.14)$$

The extreme response \hat{Z} is then defined by the reduced model, as follows:

$$\hat{Z} = \max\{\hat{u}(t), 0 \leq t \leq T\}. \quad (5.15)$$

A convergence study is needed to assess whether the reduced-order model accurately estimates the extreme response and converges to same level as the full model as N_ω increases.

5.6.2 Construction of Active Subspace

We use the “active subspace” approach for stochastic dimension reduction [4]. It seeks a subset of the original input space, that can optimally explain the response’s variability.

Consider an extreme response with n independent and identically distributed random variables, \mathbf{Q} , as follows:

$$Z = Z_{\mathbf{Q}}(\mathbf{q}), \quad \mathbf{q} \in \mathbb{R}^n. \quad (5.16)$$

A mapping from \mathbf{X} to \mathbf{Q} can be achieved by an iso-probabilistic transformation such as Nataf or Rosenblatt transformations [13, 17]. A gradient vector can be then defined as follows:

$$\mathbf{G} = \left[\frac{\partial Z}{\partial q_1}, \dots, \frac{\partial Z}{\partial q_n} \right]^T.$$

Now, an uncentered covariance matrix of the gradient vector is defined as:

$$\mathbf{C} = \mathbb{E}[\mathbf{G}\mathbf{G}^T]. \quad (5.17)$$

Note that \mathbf{C} is symmetric and positive semi-definite. By real eigenvalue decomposition, \mathbf{C} can be decomposed as follows:

$$\mathbf{C} = \mathbf{W}\Lambda\mathbf{W}^T, \quad (5.18)$$

$$\Lambda = \text{diag}(\lambda_1, \dots, \lambda_n), \quad \lambda_1 \geq \dots \geq \lambda_n \geq 0. \quad (5.19)$$

The matrices of eigenvalues and eigenvectors can be partitioned as follows:

$$\Lambda = \begin{bmatrix} \Lambda_1 & \\ & \Lambda_2 \end{bmatrix}, \quad (5.20)$$

$$\mathbf{W} = [\mathbf{W}_1 \ \mathbf{W}_2]. \quad (5.21)$$

The rotated coordinates comprised of “active” and “inactive” subspaces are defined as follows:

$$\mathbf{y}_1 = \mathbf{W}_1^T \mathbf{q}, \quad \mathbf{y} \in \mathbb{R}^m, \quad (5.22)$$

$$\mathbf{y}_2 = \mathbf{W}_2^T \mathbf{q}, \quad \mathbf{y} \in \mathbb{R}^{n-m}. \quad (5.23)$$

The eigenvalues represent the mean-squared directional derivatives of Z with respect to the eigenvector as follows:

$$\lambda_i = \int \cdots \int (\mathbf{w}_i^T \mathbf{G})^2 f(\mathbf{q}) d\mathbf{q}, \quad (5.24)$$

where $\mathbf{w}_i^T \mathbf{G}$ is the directional derivative (dot product of the vector and the gradient vector) and $f(\cdot)$ is the jpdf.

The extreme response Z varies more dominantly along \mathbf{y}_1 than \mathbf{y}_2 , if the eigenvalues corresponding to \mathbf{W}_1 are strongly dominant, i.e., $\lambda_1 \geq \cdots \geq \lambda_m \gg \lambda_{m+1} \geq \cdots \geq \lambda_n \geq 0$. For example, a zero eigenvalue, λ_i , indicates that Z is constant in the direction of \mathbf{w}_i . Therefore, most of the variability in Z can be accounted for by considering \mathbf{y}_1 , while ignoring \mathbf{y}_2 .

5.6.3 Gradient Vector and Covariance Matrix Approximation

The QoI gradient vector estimation can be challenging when response computation involves the use of a time-consuming “solver” and/or calculating gradi-

ents directly in the solver is not possible. Then, it is necessary to estimate the gradient vector numerically and build the covariance matrix of the gradients subsequently.

We use the elementary effects approach for gradient vector approximation [12]. It can account for joint effects of input random variables in the gradient computation. A gradient vector by elementary effects can be approximated as follows:

$$\mathbf{G} \approx \hat{\mathbf{G}} = [d_1, \dots, d_n]^T, \quad (5.25)$$

where the elementary effects d_i are defined as follows:

$$d_i = \frac{Z(q_1, \dots, q_{i-1}, q_i + \Delta_i, q_{i+1}, \dots, q_n) - Z(q_1, \dots, q_n)}{\Delta_i}, \quad (5.26)$$

where Δ_i is a step size for the elementary effect; a fixed or random step size can be employed. An uncentered covariance matrix of a gradient vector can be approximated as follows:

$$\mathbf{C} \approx \hat{\mathbf{C}} = \frac{1}{N_G} \sum_{l=1}^{N_G} (\hat{\mathbf{G}}_{(l)} \hat{\mathbf{G}}_{(l)}^T) = \hat{\mathbf{W}} \hat{\Lambda} \hat{\mathbf{W}}^T, \quad (5.27)$$

where N_G is the number of gradient vector approximations. The procedure is explained in Algorithm 1.

Algorithm 1 Covariance Matrix Approximation by Elementary Effects

```
1:  $m$ : number of input variables
2:  $N_G$ : number of gradient vector approximations
3:  $\mathbf{e}_i$ : row vector with a one in  $i$ th element and zeros elsewhere.
4: for  $j = 1 : N_G$  do
5:    $\Delta_{1 \times m} \leftarrow [\Delta_1, \dots, \Delta_m]$             $\triangleright$  random sample or deterministic
6:    $\Delta_{1 \times m}^X \leftarrow F_{\Delta}^{-1}(F_{\Delta}(\Delta_{1 \times m}))$      $\triangleright$  transform to physical
7:    $\mathbf{q}_{1 \times m} \leftarrow [q_1, \dots, q_m]$             $\triangleright$  from normalized sample space
8:    $\mathbf{x}_{1 \times m} \leftarrow F_{\mathbf{X}}^{-1}(F_{\mathbf{Q}}(\mathbf{q}_{1 \times m}))$      $\triangleright$  transform to physical
9:   for  $i = 1 : m$  do
10:     $d_i = \frac{Z(\mathbf{x} + \Delta_i^X \mathbf{e}_i) - Z(\mathbf{x})}{\Delta_i}$ 
11:   end for
12:    $\hat{\mathbf{G}}(*, j) = [d_1, \dots, d_m]^T$ 
13: end for
14: return  $\hat{\mathbf{C}} = \hat{\mathbf{G}} \hat{\mathbf{G}}^T$ 
```

5.6.4 Polynomial Chaos Expansion in a Reduced Dimension Space

It is challenging to build an accurate surrogate model when a QoI is defined in a high-dimensional input space. We may need a large number of samples to obtain meaningful statistics of the high-dimensional input variables; otherwise we miss some information and it can lead to inaccurate surrogate modeling. We can benefit from the use of coordinate rotation to build an accurate surrogate model even with a small number of samples.

Building a PCE model in a reduced dimension space implies expressing the QoI as an expansion of orthogonal polynomials involving all of the selected uncertain model parameters following an Askey scheme [2]. These model parameters are the “active” variables, \mathbf{Y}_1 . Appropriate orthogonal polynomials needed for the expansion are selected according to the probability distribu-

tions of the auxiliary random variables to which \mathbf{Y}_1 must be mapped [21]. For example, Hermite polynomials can be used if \mathbf{Y}_1 is mapped to a standard normal random variable vector, \mathbf{Q} .

After establishing the polynomial basis functions and assuming that all the variables in \mathbf{Y}_1 have finite variance, the QoI can be expressed as a series involving these basis functions:

$$Z(\mathbf{Y}_1) = \sum_{i=0}^{\infty} c_i \Psi_i(\mathbf{Q}) = \sum_{i=0}^{\infty} c_i \Psi_i(T(\mathbf{Y}_1)), \quad (5.28)$$

where c_i are the coefficients to be estimated, $\Psi_i(\cdot)$ represents the i th multivariate orthogonal polynomial function expressed in terms of \mathbf{Q} , and $T(\cdot)$ describes the mapping from the variable space of \mathbf{Y}_1 to the independent associated variable space of \mathbf{Q} .

The i th multivariate orthogonal polynomial function is constructed in terms of a product of associated univariate polynomials as follows:

$$\Psi_i(\mathbf{Q}) = \prod_{l=1}^m \bar{\Psi}_{\alpha_{il}}(Q_l), \quad (5.29)$$

where $\bar{\Psi}(\cdot)$ is a univariate orthogonal polynomial, α_{il} is an index of $\bar{\Psi}(Q_l)$ to make up for the i th multivariate orthogonal polynomial, and m is the number of the derived active variables. Orthogonality of the selected basis functions implies that:

$$\mathbb{E}[\Psi_i \Psi_j] = \delta_{ij} \mathbb{E}[\Psi_i^2], \quad (5.30)$$

where δ_{ij} is the Kronecker delta, equal to unity when $i = j$ and zero otherwise; $\mathbb{E}[\Psi_i^2]$ is available in closed form for all i .

A truncated PCE on the active subspace (AS-PCE) for Z that involves polynomials up to order p can be represented as:

$$Z(\mathbf{Y}_1) \approx Z^{\text{AS-PCE}}(\mathbf{Y}_1) = \sum_{i=0}^{N-1} c_i \Psi_i(T(\mathbf{Y}_1)), \quad (5.31)$$

where $N = \binom{m+p}{m}$ denotes the number of unknown PCE coefficients (or basis functions). The next step is to estimate the coefficients. Several methods such as spectral projection, stochastic collocation, and linear regression can be employed. Spectral projection and linear regression have both been employed on high-dimension problems for extreme response prediction of various offshore structures [14, 10].

In the present study, we use linear regression for PCE coefficient estimation; accordingly, the coefficients are computed by minimizing the sum of the squared residuals between the truncated AS-PCE and the truth system:

$$\mathbf{c} = \arg \min_{c_i} \sum_{j=1}^{N_E} \left[Z(\mathbf{y}_1^{(j)}) - \sum_{i=0}^{N-1} c_i \Psi_i(T(\mathbf{y}_1^{(j)})) \right]^2, \quad (5.32)$$

where N_E is the number of simulations performed in the truth system as part of the linear regression; the j th drawn sample is obtained by $\mathbf{y}_1^{(j)} = \mathbf{W}_1^T \mathbf{x}^{(j)}$. Typically, $N_E = 2 \times N$ or $3 \times N$ is required for accuracy.

5.7 Numerical Examples

We demonstrate the proposed method for the extreme response prediction of various offshore structures. For illustration, simple analytical functions with an offshore analogy are examined first.

5.7.1 Simple Quadratic Model

Consider a toy example function as follows:

$$Z_{\mathbf{Q}}(\mathbf{q}) = c_1 q_1^2 + c_2 q_2 + c_3 q_3 + c_4 q_4, \quad (5.33)$$

where Z is assumed to be the extreme response in terms of four standard normal variables with a mapping, $\mathbf{Q} = T(\mathbf{X})$, where $\mathbf{X} = [H_s, T_p, a_1, \theta_1]^T$. We assume that the extreme comes from only four sources (environment and wave train variables) although they typically involve hundreds or thousands. The other assumptions are: (1) a mapping from \mathbf{X} to \mathbf{Q} is always possible, and (2) generalized dependence in \mathbf{X} is mapped to independent \mathbf{Q} . Now, it is convenient to consider different levels of variability in \mathbf{Q} .

The total variance of the function is given as follows:

$$\sigma_Z^2 = 2c_1^2 + c_2^2 + c_3^2 + c_4^2. \quad (5.34)$$

The importance of long-term and short-term uncertainties due to the associated variables can be defined in terms of variances:

$$\sigma_L^2 = \frac{2c_1^2 + c_2^2}{\sigma_Z^2}, \quad (5.35)$$

$$\sigma_S^2 = \frac{c_3^2 + c_4^2}{\sigma_Z^2}. \quad (5.36)$$

We adjust $\{c_i\}_{i=1,\dots,4}$ to control these uncertainties. For the three cases shown in Table 5.1, the exact gradient vectors are used to obtain the covariance matrices; eigendecomposition of each covariance matrix reveals that the function only varies along two directions (there are two non-zero eigenvalues while the

others are zero). Consequently, AS-PCE models are built on the identified reduced dimension: $m = 2$.

Table 5.1: Three cases of different $\{c_i\}_{i=1,\dots,4}$ values in the simple quadratic model

Case	Description	c_1	c_2	c_3	c_4	σ_L^2	σ_S^2
1	Long-term Uncertainty “Dominant”	0.2	0.05	0.01	0.01	0.998	0.002
2	Long-term Uncertainty “Important”	0.2	0.05	0.10	0.10	0.805	0.195
3	Long-term Uncertainty “Less Important”	0.2	0.05	0.20	0.20	0.508	0.492

In Fig. 5.1, probability density functions (pdfs) and exceedance probability curves are estimated using 10 sets of MCS and AS-PCE models (order-2) for the three cases. Eighteen random samples are used as part of the linear regression for the PCE coefficient estimation: $N_E = 3 \times \binom{2+2}{2}$. The AS-PCE models estimate exceedance probabilities with no bias and variance error in the different uncertainty assumptions.

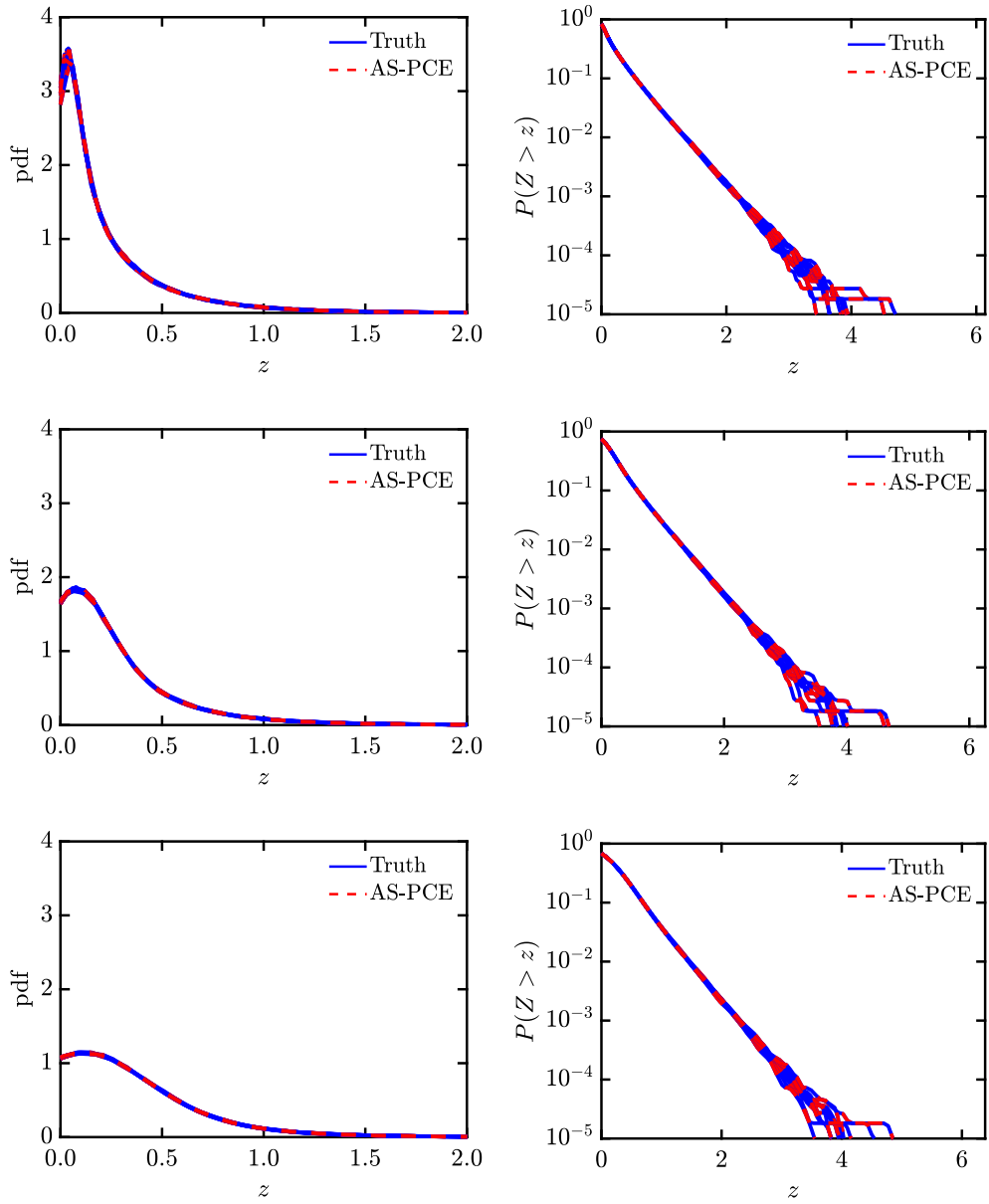


Figure 5.1: Estimation of pdfs (left column) and exceedance probabilities (right column) of the simple quadratic model by 10 sets of MCS and AS-PCE models for Cases 1 (top), 2 (middle), and 3 (bottom)

5.7.2 Quadratic Model with a Non-Polynomial Term

We study another simple analytical function and use its exact gradients for dimension reduction. The function with a non-polynomial term (oscillatory) is given as follows:

$$Z_{\mathbf{Q}}(\mathbf{q}) = c_1 q_1^2 + c_2 q_2 + c_3 q_3 + c_4 q_4 \sin q_4. \quad (5.37)$$

A total variance of the function is given as follows:

$$\sigma_Z^2 = 2c_1^2 + c_2^2 + c_3^2 + c_4^2 \left(\frac{1}{2} + \frac{3}{2e^2} - \frac{1}{e} \right). \quad (5.38)$$

Importance of long-term and short-term uncertainties due to the corresponding variables can be defined in terms of variances:

$$\sigma_L^2 = \frac{2c_1^2 + c_2^2}{\sigma_Z^2}, \quad \sigma_S^2 = \frac{c_3^2 + c_4^2 \left(\frac{1}{2} + \frac{3}{2e^2} - \frac{1}{e} \right)}{\sigma_Z^2}. \quad (5.39)$$

Table 5.2: Three cases of different $\{c_i\}_{i=1,\dots,4}$ values in the simple quadratic model with a non-polynomial term

Case	Description	c_1	c_2	c_3	c_4	σ_L^2	σ_S^2
1	Long-term Uncertainty “Dominant”	0.2	0.05	0.01	0.01	0.998	0.002
2	Long-term Uncertainty “Important”	0.2	0.05	0.10	0.10	0.861	0.139
3	Long-term Uncertainty “Less Important”	0.2	0.05	0.20	0.20	0.607	0.393

For each case shown in Table. 5.2, eigendecomposition of the covariance matrix results in three non-zero eigenvalues and, subsequently, AS-PCE models (order-2) are built on the reduced dimension: $m = 3$. The samples are

chosen randomly; to account for the oscillatory characteristics of the function, 60 samples are used for the PCE coefficient estimation: $N_E = 6 \times \binom{3+2}{2}$. In Fig. 5.2, results based on the AS-PCE models again show low bias and variance error in exceedance probability estimation even when the oscillation term is present.

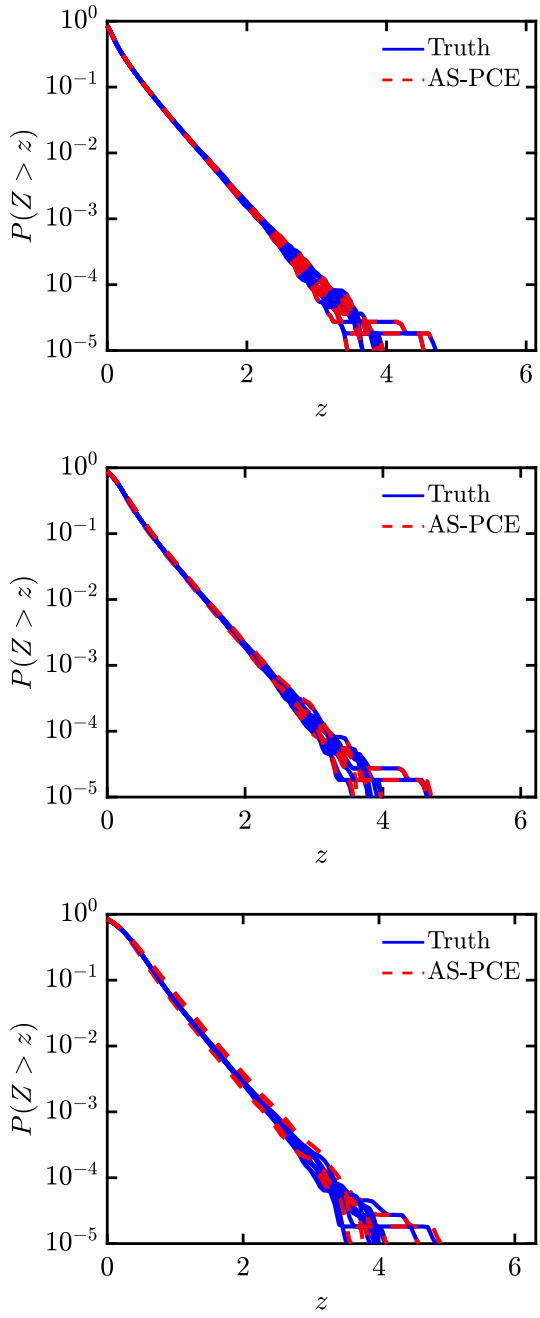


Figure 5.2: Exceedance probability estimation of the quadratic model with a non-polynomial term by 10 sets of MCS and AS-PCE models for Cases 1 (top), 2 (middle), and 3 (bottom)

5.7.3 High-Dimensional Linear Limit State Function

We study a high-dimensional linear limit state function as follows [16]:

$$g_{\mathbf{x}}(\mathbf{x}) = z - Z_{\mathbf{x}}(\mathbf{x}), \quad (5.40)$$

$$Z_{\mathbf{x}}(\mathbf{x}) = d + 3\sigma\sqrt{d} - \sum_{i=1}^d x_i, \quad (5.41)$$

where each X_i follows an independent lognormal distribution with a unit mean and standard deviation, and $\sigma = 0.2$. For surrogate limit state modeling with dimension reduction, we use the exact gradients. For example, the covariance matrix of Z when $d = 3$ can be calculated as follows:

$$\begin{aligned} \mathbf{C} &= \mathbf{W}\Lambda\mathbf{W}^T \\ &= \begin{bmatrix} 1 & 1 & 1 \\ 1 & 1 & 1 \\ 1 & 1 & 1 \end{bmatrix} \\ &= \begin{bmatrix} 0.41 & 0.71 & 0.58 \\ 0.41 & -0.71 & 0.58 \\ -0.82 & 0.00 & 0.58 \end{bmatrix} \begin{bmatrix} 0 & 0 & 0 \\ 0 & 0 & 0 \\ 0 & 0 & 3 \end{bmatrix} \begin{bmatrix} 0.41 & 0.71 & 0.58 \\ 0.41 & -0.71 & 0.58 \\ -0.82 & 0.00 & 0.58 \end{bmatrix}^T. \end{aligned} \quad (5.42)$$

The sole non-zero eigenvalue indicates that Z is a univariate function with respect to the new variable, $\mathbf{y} = \mathbf{W}_1^T \mathbf{x}$, where $\mathbf{W}_1 = [0.58, 0.58, 0.58]^T$.

For the three cases ($d = 20$, 50, and 100), AS-PCE models (order-1) built in one dimension show accurate prediction of $P[Z > z]$ for various z values, as shown in Fig. 5.3. The samples are randomly selected by using $N_E = 3 \times \binom{1+1}{1} = 6$. Eigenvectors, $\mathbf{W}_1 = [1, \dots, 1]^T / \sqrt{d}$, are used for the surrogate modeling in the reduced dimension.

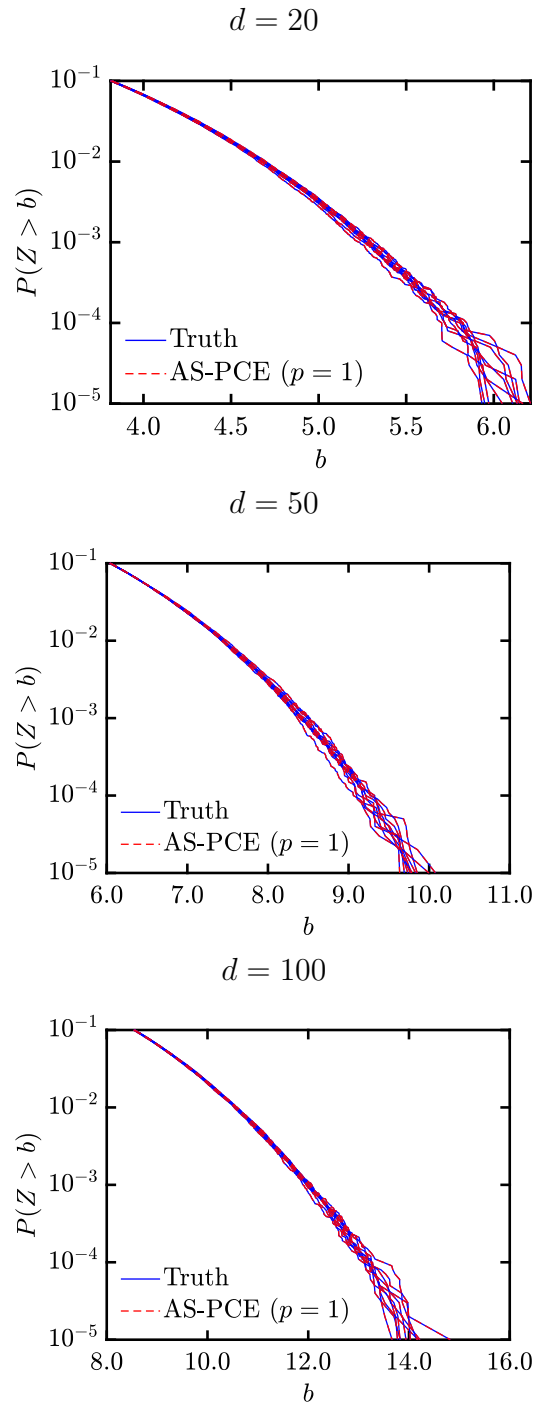


Figure 5.3: Probabilities of exceedance of G by 10 sets of MCS and AS-PCE models when $d = 20$ (top), 50 (middle), and 100 (bottom)

5.7.4 High-Dimensional Nonlinear Limit State Function

We consider a high-dimensional nonlinear limit state function as follows [23]:

$$g_{\mathbf{x}}(\mathbf{x}) = z - Z_{\mathbf{x}}(\mathbf{x}), \quad (5.43)$$

$$Z_{\mathbf{x}}(\mathbf{x}) = 3 - x_d + 0.01 \sum_{i=1}^{d-1} x_i^2, \quad (5.44)$$

where each X_i follows the independent standard normal distribution.

Surrogate modeling following dimension reduction is carried out using the exact gradients. For the three cases ($d = 100$, 150, and 200), AS-PCE models (order-1) built in one dimension reveal accurate exceedance probability prediction of Z for various z values, as shown in Fig. 5.4. The number of samples used for surrogate model building in each case is $N_E = 3 \times \binom{1+1}{1} = 6$, $4 \times \binom{1+1}{1} = 8$, and $5 \times \binom{1+1}{1} = 10$, respectively.

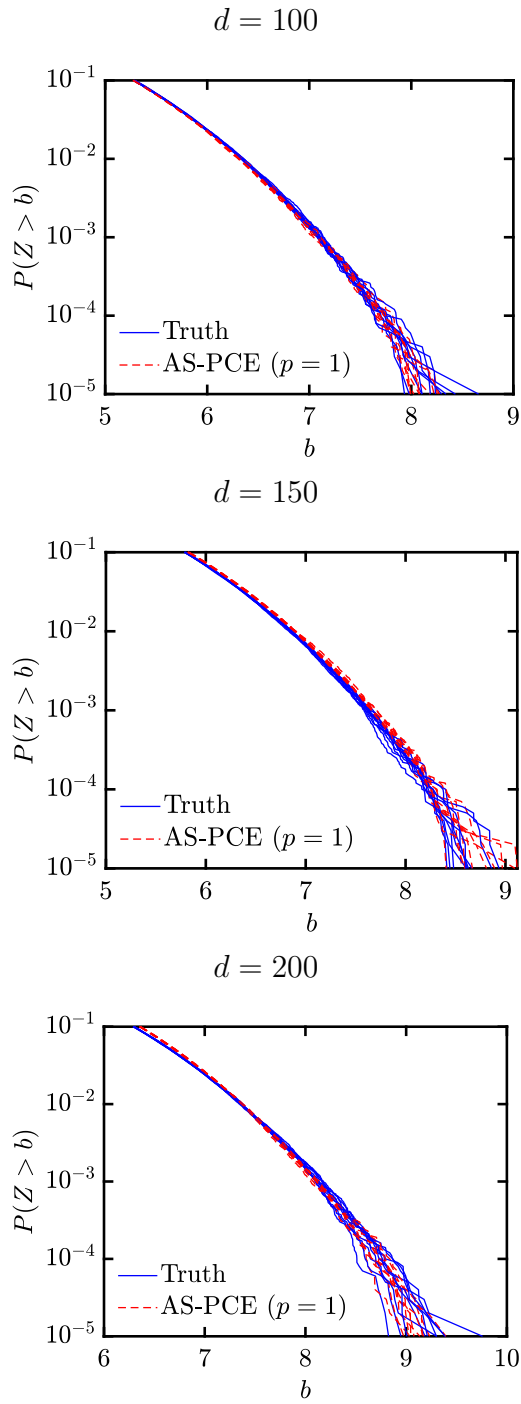


Figure 5.4: Probabilities of exceedance of G by 10 sets of MCS and AS-PCE models when $d = 100$ (top), 150 (middle), and 200 (bottom)

5.7.5 Extreme Wave Elevations at Different Sites of Interest

We study different sites of interest for demonstration of the proposed method in the prediction of the extreme wave elevation. The JONSWAP spectrum is used for the three sites: in the North Sea, at National Data Buoy Center (NDBC) Station 46022, and in the Barent Sea. The jpdfs of H_s and T_p have their own characteristics as summarized in Table 5.3.

Table 5.3: Joint PDFs of H_s and T_p at selected sites of interest

Sites	Marginal H_s	Conditional T_p (fitting for mean and variance)
North Sea	Lognormal & Weibull (LONOWE)	lognormal conditional on H_s (power curve and exponential)
NDBC Station 46022	2-parameter Weibull	lognormal conditional on H_s (polynomial)
Barent Sea	3-parameter Weibull	lognormal conditional on H_s (power curve and exponential)

5.7.5.1 Site I: North Sea

Model order reduction is carried out before building surrogate models for prediction of the maximum wave elevation in the North Sea. The jpdf of H_s and T_p for this site is employed [8, 7, 11]. The QoI is defined as the maximum wave elevation in the time series:

$$Z = \max\{\eta(t); 0 \leq t \leq T\}. \quad (5.45)$$

A severe sea state resulting from a high H_s value of low occurrence probability is chosen for the model order reduction: $H_s = 12.6$ m and $T_p = 15.0$ s. This sea

state's variance (total area of a wave spectrum) is divided equally by N_ω . Each centroid of the masses is then selected as the frequency for the model order reduction, as shown in Fig. 5.5. The spectral ordinates at these frequencies are scaled to keep the wave elevation variance of the sea state unchanged.

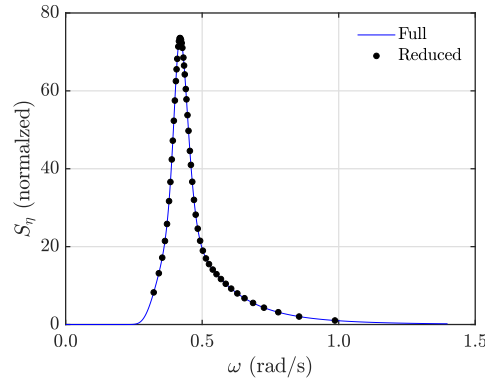


Figure 5.5: Frequencies ($N_\omega = 51$) selected by model order reduction for prediction of the maximum wave elevation in the North Sea

Reduced order modeling by $N_\omega = 51$ shows accurate estimation of exceedance probabilities of the extreme wave elevation, as shown in Fig. 5.6. Ten sets of MCS with the reduced model show small mean and variance errors, compared against the full model ($R = 1, 120$). The variability at low $P[Z > z]$ ranges in the reduced models is consistent with the full model. As seen in Fig. 5.7, accuracy in the prediction is better at low $P[Z > z]$ ranges because the selected frequencies are distributed near the peak of the chosen wave spectrum; hence, the reduced models barely miss the important frequencies needed to obtain the high extreme response values.

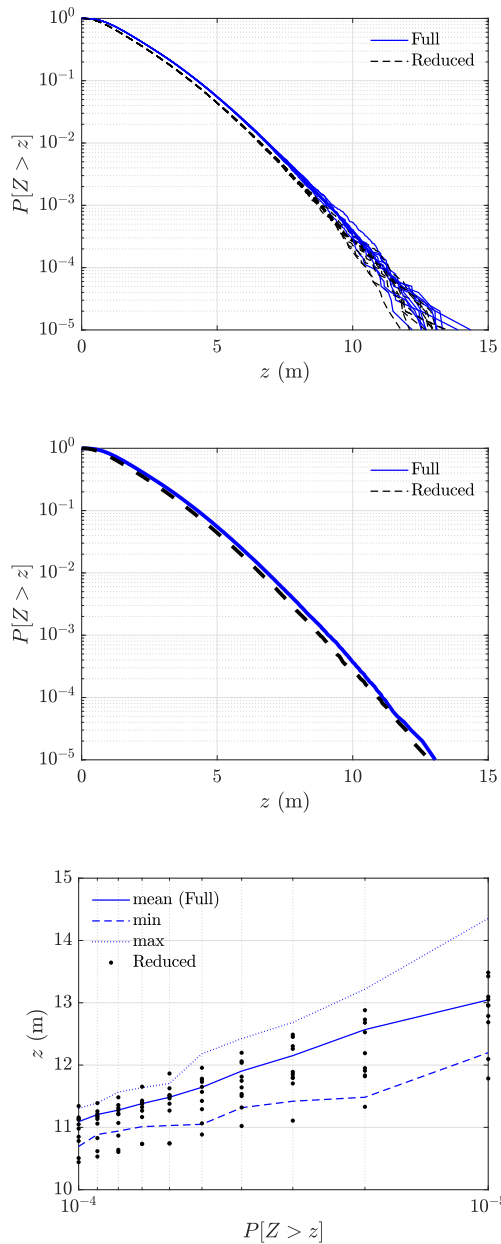


Figure 5.6: Exceedance probabilities (top), mean exceedance probabilities (middle), confidence intervals of low occurrence probability responses (bottom) by 10 sets of full and reduced wave elevation models in the North Sea

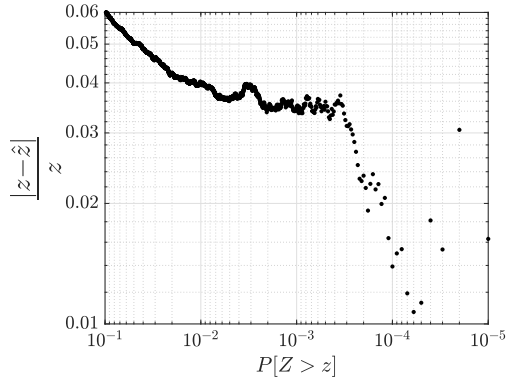


Figure 5.7: Errors in the mean quantile values (z) satisfying $10^{-5} < P[Z > z] < 10^{-1}$ based on 10 sets of full and reduced wave elevation models in the North Sea

Surrogate models are built in the reduced dimension space comprised of the new variables. The active subspace approach uses reduced model's gradients (by the elementary effects) to find the rotated coordinates where the extreme response varies significantly. A converged covariance matrix is obtained by multiple realizations of the gradient vector with $N_G = 29$ and a fixed $\Delta_i = 0.1$. Eigendecomposition of the matrix reveals two important directions where more than 85% of the output's variability is accounted for. Two variable AS-PCE models (order-2) shown in Fig. 5.8 accurately predict exceedance probabilities of the maximum wave elevation in the North Sea; $2 \times \binom{2+2}{2} = 12$ random samples are used for the surrogate models.

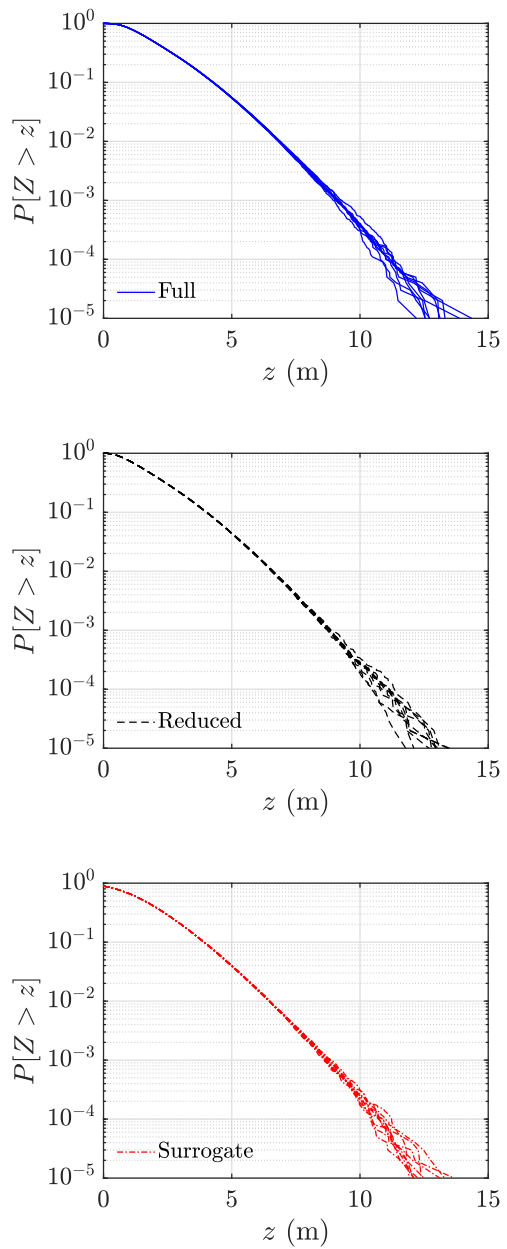


Figure 5.8: Exceedance probabilities of the extreme wave elevation in the North Sea by 10 sets of full (top), reduced, (middle), and PCE surrogate models (bottom)

5.7.5.2 Site II: National Data Buoy Center Station 46022

We use the proposed method for the prediction of the maximum wave elevation at the NDBC Station 46022. This site, which is located 17 nautical miles west-southwest of Eureka in California, was studied for deployment of wave energy converters (WECs) and their extreme response prediction [14]. Prediction of the extreme wave elevation at this site by the full and reduced model ($N_\omega = 45$) shows good agreement; the chosen sea state for the model order reduction is $H_s = 7.7$ m and $T_p = 16.7$ s. The covariance matrix is obtained by multiple realization of the gradient vector with $N_G = 19$ and a fixed $\Delta_i = 0.1$. Eigendecomposition of the matrix reveals two important directions. Ten sets of two variable AS-PCE models (order-2) show accurate prediction of the extreme wave elevation, as seen in Fig. 5.9. The number of samples is $2 \times \binom{2+2}{2} = 12$.

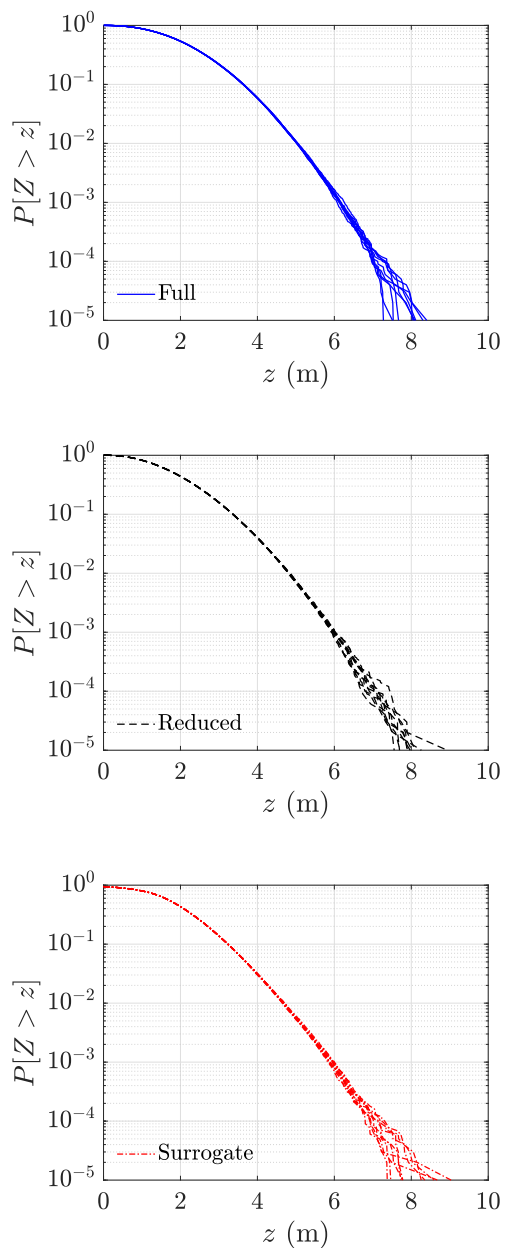


Figure 5.9: Exceedance probabilities of the extreme wave elevation in the National Data Buoy Center Station 46022 by 10 sets of full (top), reduced, (middle), and PCE surrogate models (bottom)

5.7.5.3 Site III: Barent Sea

Prediction of maximum wave elevation in the Barent Sea is carried out by using the same two-step dimension reduction method; the jpdf of H_s and T_p for this site is employed [15]. The chosen sea state for the reduced order modeling is $H_s = 13.3$ m and $T_p = 17.4$ s; the reduced order model by $N_\omega = 51$ is used for the active subspace calculation. For approximation of the covariance matrix, we use random step sizes for the gradient approximation; the samples are drawn from the standard normal distribution. The computed covariance matrix with $N_G = 15$ reveals three important new variables that account for more than 90% of the output's variability. Shown in Fig. 5.10, ten sets of AS-PCE models (order-3) built on the reduced dimension ($m = 3$) show small bias and variance error, relative to the full model; the number of samples is $2 \times \binom{3+3}{3} = 40$.

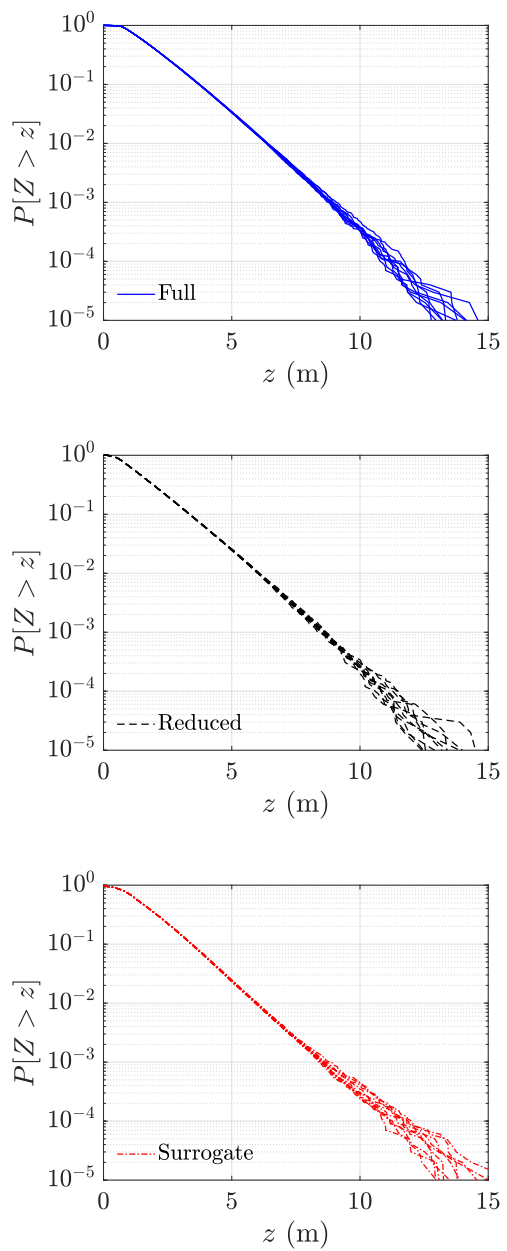


Figure 5.10: Exceedance probabilities of the extreme wave elevation in the Barent Sea by 10 sets of full (top), reduced, (middle), and PCE surrogate models (bottom)

5.7.6 Extreme Response of Various Offshore Structures

An implicit performance function for offshore structure design can be given as follows:

$$g(\mathbf{x}) = z - Z_T(\mathbf{x}), \quad (5.46)$$

where z represents a threshold value and Z_T is the T -year long-term extreme response of a structure.

5.7.6.1 Type I: Long Natural Period

We apply the proposed dimension reduction method to extreme response prediction of a linear SDOF system, where $M = 70.36$ kg, $\zeta = 0.01$, and $K = 10$ N/m; the natural frequency is 0.38 rad/s. For simplicity, the frequency-dependent linear transfer function, $T(\omega)$, is assumed to be unity. For model order reduction, we use the following sea state: $H_s = 12.6$ (m) and $T_p = 15.0$ (sec). The selected frequencies show accurate exceedance probability prediction for the extreme responses, as seen in Fig. 5.11; ten sets of the reduced-order models show small bias and variance error, relative to ten sets of the full models. The reduced order models with $N_\omega = 36$ show small error in the range, $10^{-5} < P[Z > z] < 10^{-4}$, as seen in Fig. 5.12.

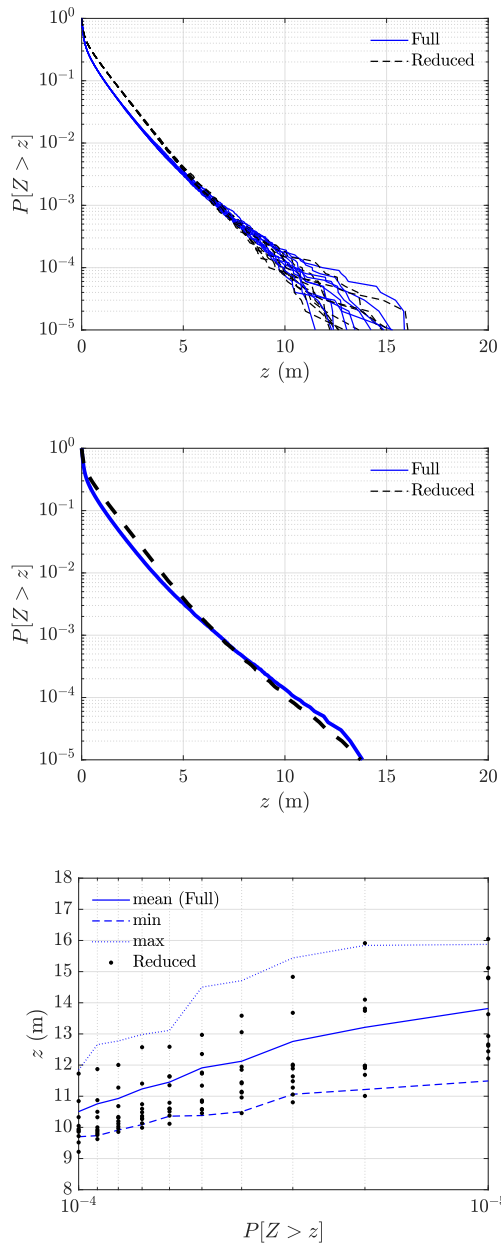


Figure 5.11: Exceedance probabilities (top), mean exceedance probabilities (middle), confidence intervals of low occurrence probability responses (bottom) by 10 sets of full and reduced response models (Type I) in the North Sea

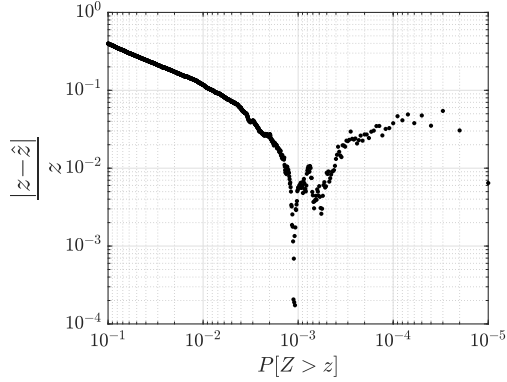


Figure 5.12: Error in the mean quantile values (z) satisfying $10^{-5} < P[Z > z] < 10^{-1}$ based on 10 sets of full and reduced response models (Type I) in the North Sea

Eigendecomposition of the computed covariance matrix with $N_G = 13$ and a fixed $\Delta_i = 0.1$ reveals two important directions where the extreme response changes significantly. Shown in Fig. 5.13, AS-PCE models (order-3) are then built on the reduced dimension ($m = 2$). They show small mean and variance error, relative to the full model; the number of samples is $2 \times \binom{3+2}{2} = 20$.

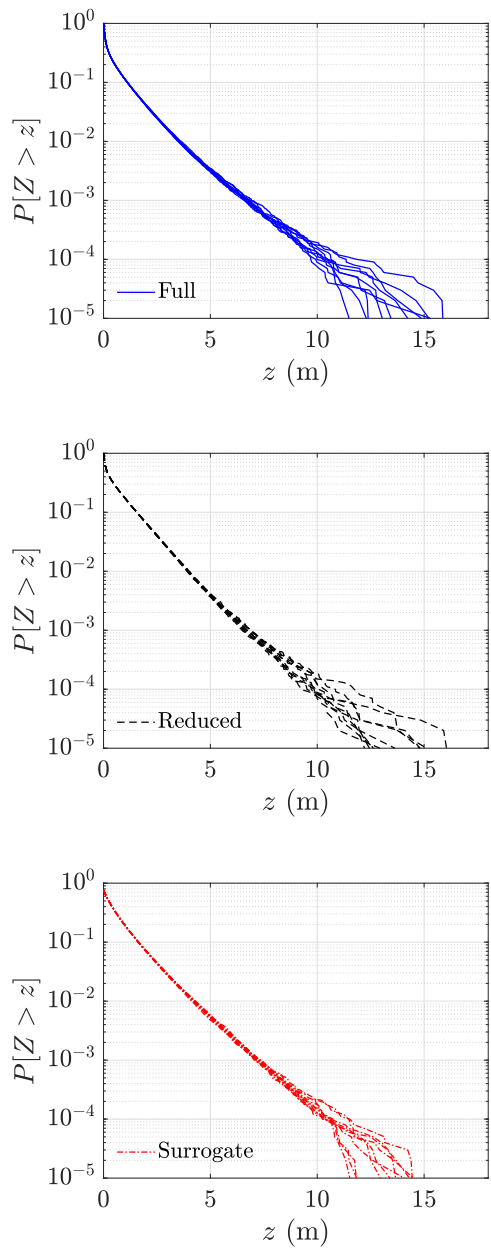


Figure 5.13: Exceedance probabilities of the extreme structural response (Type I) in the North Sea by 10 sets of full (top), reduced, (middle), and PCE surrogate models (bottom)

5.7.6.2 Type II: Short Natural Period

A SDOF system with a relatively short natural period (0.75 rad/s) compared to the Type I system is considered: $M = 17.59$ kg, $\zeta = 0.01$, and $K = 10$ N/m. Equally spaced frequencies in the range from 0.39 to 0.84 rad/s are selected for the model order reduction. Eigendecomposition of the computed covariance matrix with $N_G = 7$ in the reduced order model with $N_\omega = 150$ reveals a few important direction ($m = 11$). Ten sets of order-1 PCE models built in the reduced dimension space show small mean and variance errors in exceedance probability prediction, as can be seen in Fig. 5.14. The number of samples for the AS-PCE models is $2 \times \binom{1+11}{1} = 24$.

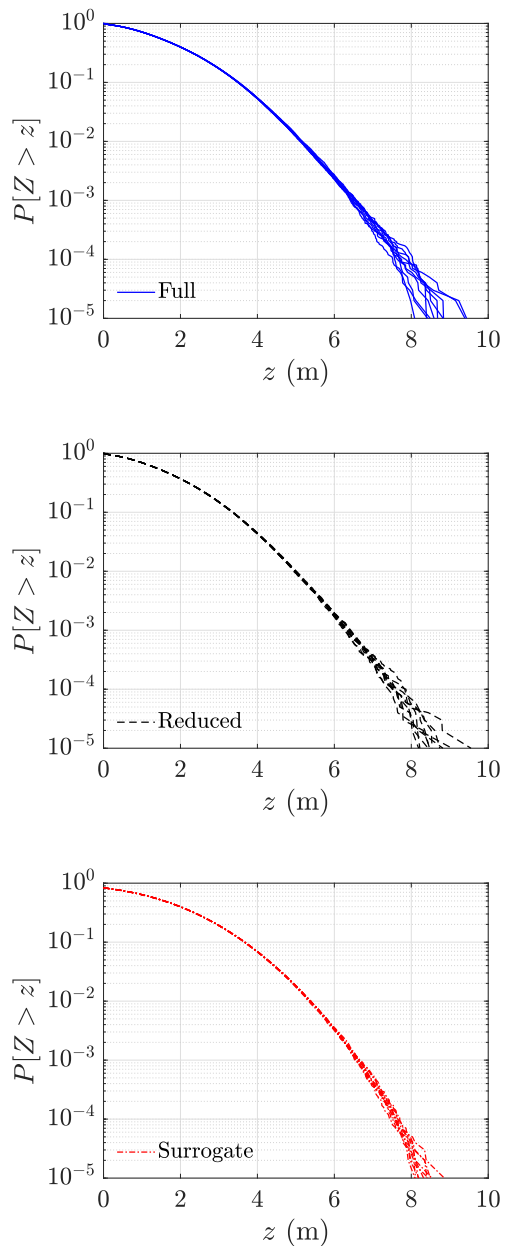


Figure 5.14: Exceedance probabilities of the extreme structural response (Type II) in the North Sea by 10 sets of full (top), reduced, (middle), and PCE surrogate models (bottom)

5.8 Conclusions

In this study, we propose a two-step dimension reduction method to help build surrogate models for the long-term extreme response prediction of offshore structures. The proposed method includes (1) model order reduction in the frequency domain to describe the irregular wave processes and (2) gradient-based stochastic dimension reduction on the reduced order model. For the irregular wave processes, we choose a small number of frequency harmonic components and scale their power spectrum ordinates to keep the variance consistent with the original model. With the active subspace calculation in the reduced order model, we select a subset in the reduced input space that accounts for most of the response's variability. Then, we build PCE surrogate models on the reduced dimension. Results confirm that AS-PCE surrogate building is efficient and accurate for exceedance probability prediction of various offshore structural responses subjected to uncertain environmental loading.

Bibliography

- [1] Puneet Agarwal and Lance Manuel. On the modeling of nonlinear waves for prediction of long-term offshore wind turbine loads. *Journal of Offshore Mechanics and Arctic Engineering*, 131(4), 2009.
- [2] George E Andrews and Richard Askey. Classical orthogonal polynomials. In *Polynômes orthogonaux et applications*, pages 36–62. Springer, 1985.
- [3] Nigel DP Barltrop. *Floating structures: a guide for design and analysis*, volume 1. Oilfield Publications Incorporated, 1998.
- [4] Paul G Constantine. *Active subspaces: emerging ideas for dimension reduction in parameter studies*, volume 2. SIAM, 2015.
- [5] Roger G Ghanem and Pol D Spanos. *Stochastic finite elements: a spectral approach*. Courier Corporation, 2003.
- [6] Klaus Hasselmann. Measurements of wind wave growth and swell decay during the joint north sea wave project (JONSWAP). *Deutches Hydrographisches Institut*, 8:95, 1973.
- [7] Sverre Haver. On the prediction of extreme wave crest heights. *International Workshop on Wave Hindcasting and Forecasting*, 2002.

- [8] Sverre Haver and Kjell A Nyhus. A wave climate description for long term response calculations. *OMAE. International Symposium*, 4:27–34, 1986.
- [9] HyeongUk Lim, Lance Manuel, and Ying Min Low. On efficient long-term extreme response estimation for a moored floating structure. *ASME. International Conference on Offshore Mechanics and Arctic Engineering*, 2018.
- [10] HyeongUk Lim, Lance Manuel, Ying Min Low, and Narakorn Srinil. Uncertainty quantification of riser fatigue damage due to VIV using a distributed wake oscillator model. *ASME. International Conference on Ocean, Offshore and Arctic Engineering*, 2017.
- [11] Ying Min Low and Xiaoxu Huang. Long-term extreme response analysis of offshore structures by combining importance sampling with subset simulation. *Structural Safety*, 69:79–95, 2017.
- [12] Max D Morris. Factorial sampling plans for preliminary computational experiments. *Technometrics*, 33(2):161–174, 1991.
- [13] Andre Nataf. Determination des distribution don t les marges sont donnees. *Comptes Rendus de l Academie des Sciences*, 225:42–43, 1962.
- [14] Phong TT Nguyen, Lance Manuel, and Ryan G Coe. On the development of an efficient surrogate model for predicting long-term extreme loads

- on a wave energy converter. *Journal of Offshore Mechanics and Arctic Engineering*, 141(6):061103, 2019.
- [15] Adekunle P Orimolade and Ove T Gudmestad. On weather limitations for safe marine operations in the barents sea. *Materials Science and Engineering Conference Series*, 276(1):012018, 2017.
 - [16] Rüdiger Rackwitz. Reliability analysis—a review and some perspectives. *Structural Safety*, 23(4):365–395, 2001.
 - [17] Murray Rosenblatt. Remarks on a multivariate transformation. *The Annals of Mathematical Statistics*, 23(3):470–472, 1952.
 - [18] Korn Saranyasoontorn and Lance Manuel. A comparison of wind turbine design loads in different environments using inverse reliability techniques. *Journal of Solar Energy Engineering*, 126(4):1060–1068, 2004.
 - [19] Korn Saranyasoontorn and Lance Manuel. On assessing the accuracy of offshore wind turbine reliability-based design loads from the environmental contour method. *International Journal of Offshore and Polar Engineering*, 15(2):132–140, 2005.
 - [20] Christian Soize and Roger Ghanem. Physical systems with random uncertainties: chaos representations with arbitrary probability measure. *SIAM Journal on Scientific Computing*, 26(2):395–410, 2004.
 - [21] Bruno Sudret. Meta-models for structural reliability and uncertainty quantification. *arXiv preprint arXiv:1203.2062*, 2012.

- [22] Det Norske Veritas. *Environmental conditions and environmental loads*. Recommended Practice, DNV-RP-C205, Norway, 2010.
- [23] Jun Xu and Fan Kong. A new unequal-weighted sampling method for efficient reliability analysis. *Reliability Engineering & System Safety*, 172:94–102, 2018.

Bibliography

- Puneet Agarwal and Lance Manuel. On the modeling of nonlinear waves for prediction of long-term offshore wind turbine loads. *Journal of Offshore Mechanics and Arctic Engineering*, 131(4), 2009.
- George E Andrews and Richard Askey. Classical orthogonal polynomials. In *Polynômes orthogonaux et applications*, pages 36–62. Springer, 1985.
- Richard Askey and James A Wilson. *Some basic hypergeometric orthogonal polynomials that generalize Jacobi polynomials*, volume 319. American Mathematical Society, 1985.
- Siu-Kui Au and James L Beck. Estimation of small failure probabilities in high dimensions by subset simulation. *Probabilistic Engineering Mechanics*, 16(4):263–277, 2001.
- Nigel DP Barltrop. *Floating structures: a guide for design and analysis*, volume 1. Oilfield Publications Incorporated, 1998.
- Géraud Blatman and Bruno Sudret. An adaptive algorithm to build up sparse polynomial chaos expansions for stochastic finite element analysis. *Probabilistic Engineering Mechanics*, 25(2):183–197, 2010.

Géraud Blatman and Bruno Sudret. Efficient computation of global sensitivity indices using sparse polynomial chaos expansions. *Reliability Engineering & System Safety*, 95(11):1216–1229, 2010.

Christian G Bucher. Adaptive sampling – an iterative fast Monte Carlo procedure. *Structural Safety*, 5(2):119–126, 1988.

Christian G Bucher and Ulrich Bourgund. A fast and efficient response surface approach for structural reliability problems. *Structural Safety*, 7(1):57–66, 1990.

Robert H Cameron and William T Martin. The orthogonal development of non-linear functionals in series of Fourier-Hermite functionals. *Annals of Mathematics*, pages 385–392, 1947.

Seung-Kyun Choi, Ramana V Grandhi, and Robert A Canfield. Structural reliability under non-gaussian stochastic behavior. *Computers & Structures*, 82(13-14):1113–1121, 2004.

Paul G Constantine. *Active subspaces: emerging ideas for dimension reduction in parameter studies*, volume 2. SIAM, 2015.

Armen Der Kiureghian and Pei-Ling Liu. Structural reliability under incomplete probability information. *Journal of Engineering Mechanics*, 112(1):85–104, 1986.

Charles F Dunkl and Yuan Xu. *Orthogonal polynomials of several variables*. Number 155. Cambridge University Press, 2014.

Roger G Ghanem and Pol D Spanos. *Stochastic finite elements: a spectral approach*. Courier Corporation, 2003.

Abraham M Hasofer and Niels C Lind. Exact and invariant second-moment code format. *Journal of the Engineering Mechanics division*, 100(1):111–121, 1974.

Klaus Hasselmann. Measurements of wind wave growth and swell decay during the joint north sea wave project (JONSWAP). *Deutches Hydrographisches Institut*, 8:95, 1973.

Sverre Haver. On the prediction of extreme wave crest heights. *International Workshop on Wave Hindcasting and Forecasting*, 2002.

Sverre Haver and Kjell A Nyhus. A wave climate description for long term response calculations. *OMAE. International Symposium*, 4:27–34, 1986.

Chao Hu and Byeng D Youn. Adaptive-sparse polynomial chaos expansion for reliability analysis and design of complex engineering systems. *Structural and Multidisciplinary Optimization*, 43(3):419–442, 2011.

Tsutomu Ishigami and Toshimitsu Homma. An importance quantification technique in uncertainty analysis for computer models. *International Symposium on Uncertainty Modeling and Analysis*, pages 398–403, 1990.

Mourad Ismail, JJ Foncannon, and Osmo Pekonen. Classical and quantum orthogonal polynomials in one variable. *The Mathematical Intelligencer*, 30(1):54–60, 2008.

Bin Liang and Sankaran Mahadevan. Error and uncertainty quantification and sensitivity analysis in mechanics computational models. *International Journal for Uncertainty Quantification*, 1(2), 2011.

HyeongUk Lim, Lance Manuel, and Ying Min Low. On efficient long-term extreme response estimation for a moored floating structure. *ASME. International Conference on Offshore Mechanics and Arctic Engineering*, 2018.

HyeongUk Lim, Lance Manuel, Ying Min Low, and Narakorn Srinil. Uncertainty quantification of riser fatigue damage due to VIV using a distributed wake oscillator model. *ASME. International Conference on Ocean, Offshore and Arctic Engineering*, 2017.

Pei-Ling Liu and Armen Der Kiureghian. Multivariate distribution models with prescribed marginals and covariances. *Probabilistic Engineering Mechanics*, 1(2):105–112, 1986.

Pei-Ling Liu and Armen Der Kiureghian. Optimization algorithms for structural reliability. *Structural Safety*, 9(3):161–177, 1991.

Ying Min Low. A new distribution for fitting four moments and its applications to reliability analysis. *Structural Safety*, 42:12–25, 2013.

Ying Min Low and Xiaoxu Huang. Long-term extreme response analysis of offshore structures by combining importance sampling with subset simulation. *Structural Safety*, 69:79–95, 2017.

Ying Min Low and Robin S Langley. A comparison of methods for the coupled analysis of floating structures. *ASME. International Conference on Offshore Mechanics and Arctic Engineering*, pages 249–258, 2007.

Ying Min Low and Narakorn Srinil. Sensitivity study of wake oscillator parameters influencing the fatigue damage of a riser undergoing VIV. *ASME. International Conference on Ocean, Offshore and Arctic Engineering*, 2015.

Ying Min Low and Narakorn Srinil. VIV fatigue reliability analysis of marine risers with uncertainties in the wake oscillator model. *Engineering Structures*, 106:96–108, 2016.

Henrik O Madsen, Steen Krenk, and Niels C Lind. *Methods of structural safety*. Courier Corporation, 2006.

Chu V Mai, Minas D Spiridonakos, Eleni N Chatzi, and Bruno Sudret. Surrogate modeling for stochastic dynamical systems by combining nonlinear autoregressive with exogenous input models and polynomial chaos expansions. *International Journal for Uncertainty Quantification*, 6(4), 2016.

Lance Manuel, Phong TT Nguyen, Jarred Canning, Ryan G Coe, Aubrey C Eckert-Gallup, and Nevin Martin. Alternative approaches to develop environmental contours from metocean data. *Journal of Ocean Engineering and Marine Energy*, 4(4):293–310, Nov 2018.

Milton A Miner. Cumulative damage in fatigue. *Journal of Applied Mechanics*, 12(3):159–164, 1945.

Yasuhiro Mori and Bruce R Ellingwood. Time-dependent system reliability analysis by adaptive importance sampling. *Structural Safety*, 12(1):59–73, 1993.

Max D Morris. Factorial sampling plans for preliminary computational experiments. *Technometrics*, 33(2):161–174, 1991.

Habib N Najm. Uncertainty quantification and polynomial chaos techniques in computational fluid dynamics. *Annual Review of Fluid Mechanics*, 41:35–52, 2009.

Andre Nataf. Determination des distribution don t les marges sont donnees. *Comptes Rendus de l Academie des Sciences*, 225:42–43, 1962.

John N Newman. Second-order, slowly-varying forces on vessels in irregular waves. *Marine Vehicles*, pages 182–186, 1974.

Phong TT Nguyen, Lance Manuel, and Ryan G Coe. On the development of an efficient surrogate model for predicting long-term extreme loads on a wave energy converter. *ASME. International Conference on Offshore Mechanics and Arctic Engineering*, 2018.

Phong TT Nguyen, Lance Manuel, and Ryan G Coe. On the development of an efficient surrogate model for predicting long-term extreme loads on a wave energy converter. *Journal of Offshore Mechanics and Arctic Engineering*, 141(6):061103, 2019.

Sergey Oladyshkin and Wolfgang Nowak. Data-driven uncertainty quantification using the arbitrary polynomial chaos expansion. *Reliability Engineering & System Safety*, 106:179–190, 2012.

Adekunle P Orimolade and Ove T Gudmestad. On weather limitations for safe marine operations in the barents sea. *Materials Science and Engineering Conference Series*, 276(1):012018, 2017.

Rüdiger Rackwitz. Reliability analysis—a review and some perspectives. *Structural Safety*, 23(4):365–395, 2001.

Rüdiger Rackwitz and Bernd Flessler. Structural reliability under combined random load sequences. *Computers & Structures*, 9(5):489–494, 1978.

Malur R Rajashekhar and Bruce R Ellingwood. A new look at the response surface approach for reliability analysis. *Structural Safety*, 12(3):205–220, 1993.

Murray Rosenblatt. Remarks on a multivariate transformation. *The Annals of Mathematical Statistics*, 23(3):470–472, 1952.

Korn Saranyasoontorn and Lance Manuel. A comparison of wind turbine design loads in different environments using inverse reliability techniques. *Journal of Solar Energy Engineering*, 126(4):1060–1068, 2004.

Korn Saranyasoontorn and Lance Manuel. On assessing the accuracy of offshore wind turbine reliability-based design loads from the environmental

contour method. *International Journal of Offshore and Polar Engineering*, 15(2):132–140, 2005.

Chen Shi and Lance Manuel. Non-parametric prediction of the long-term fatigue damage for an instrumented top-tensioned riser. *Applied Ocean Research*, 82:245 – 258, 2019.

Chen Shi, Lance Manuel, and Michael A Tognarelli. Empirical procedures for long-term prediction of fatigue damage for an instrumented marine riser. *Journal of Offshore Mechanics and Arctic Engineering*, 136(3):031402, 2014.

Chen Shi, Lance Manuel, and Michael A Tognarelli. A comparison of empirical procedures for fatigue damage prediction in instrumented risers undergoing vortex-induced vibration. *Applied Sciences*, 8(11), 2018.

Richard A Skop and Sathish Balasubramanian. A new twist on an old model for vortex-excited vibrations. *Journal of Fluids and Structures*, 11(4):395–412, 1997.

Christian Soize and Roger Ghanem. Physical systems with random uncertainties: chaos representations with arbitrary probability measure. *SIAM Journal on Scientific Computing*, 26(2):395–410, 2004.

Narakorn Srinil. Multi-mode interactions in vortex-induced vibrations of flexible curved/straight structures with geometric nonlinearities. *Journal of Fluids and Structures*, 26(7):1098–1122, 2010.

Narakorn Srinil. Analysis and prediction of vortex-induced vibrations of variable-tension vertical risers in linearly sheared currents. *Applied Ocean Research*, 33(1):41–53, 2011.

Narakorn Srinil, Pierre-Adrien Opinel, and Francesca Tagliaferri. Empirical sensitivity of two-dimensional nonlinear wake–cylinder oscillators in cross-flow/in-line vortex-induced vibrations. *Journal of Fluids and Structures*, 83:310–338, 2018.

Narakorn Srinil, Marian Wiercigroch, and Patrick O’Brien. Reduced-order modelling of vortex-induced vibration of catenary riser. *Ocean Engineering*, 36(17):1404–1414, 2009.

Bruno Sudret. Uncertainty propagation and sensitivity analysis in mechanical models—contributions to structural reliability and stochastic spectral methods. *Habilitationa diriger des recherches, Université Blaise Pascal, Clermont-Ferrand, France*, 2007.

Bruno Sudret. Meta-models for structural reliability and uncertainty quantification. *arXiv preprint arXiv:1203.2062*, 2012.

Bruno Sudret, Marc Berveiller, and Maurice Lemaire. A stochastic finite element procedure for moment and reliability analysis. *European Journal of Computational Mechanics/Revue Européenne de Mécanique Numérique*, 15(7-8):825–866, 2006.

Det Norske Veritas. *Environmental conditions and environmental loads. Recommended Practice*, DNV-RP-C205, Norway, 2010.

Norbert Wiener. The homogeneous chaos. *American Journal of Mathematics*, 60(4):897–936, 1938.

Jeroen AS Witteveen and Hester Bijl. Modeling arbitrary uncertainties using Gram-Schmidt polynomial chaos. *AIAA. Aerospace Sciences Meeting and Exhibit*, page 896, 2006.

Dongbin Xiu and George Em Karniadakis. The Wiener–Askey polynomial chaos for stochastic differential equations. *SIAM Journal on Scientific Computing*, 24(2):619–644, 2002.

Jun Xu and Fan Kong. A new unequal-weighted sampling method for efficient reliability analysis. *Reliability Engineering & System Safety*, 172:94–102, 2018.

Xufang Zhang and Mahesh D Pandey. Structural reliability analysis based on the concepts of entropy, fractional moment and dimensional reduction method. *Structural Safety*, 43:28–40, 2013.

Yan-Gang Zhao and Tetsuro Ono. Moment methods for structural reliability. *Structural Safety*, 23(1):47–75, 2001.

Vita

HyeongUk Lim was born in South Korea. He graduated from Suwon High School in 2006. He obtained a Bachelor of Engineering degree with the highest honor in Civil Engineering from Kyung Hee University in 2012 and he had his mandatory military service as a military engineer in the 3rd infantry division from 2007 to 2009. He received a Master of Science degree in Civil and Environmental Engineering from Korea Advanced Institute of Science and Technology (KAIST) in 2014. He worked at Korea Institute of Civil Engineering and Building Technology (KICT) as a research intern from 2014 to 2015. He joined the doctoral program in the Department of Civil, Architectural and Environmental Engineering at the University of Texas at Austin in 2015.

E-mail: hyeonguklim@gmail.com

This dissertation was typeset with L^AT_EX[†] by the author.

[†]L^AT_EX is a document preparation system developed by Leslie Lamport as a special version of Donald Knuth's T_EX Program.